

LEABHARLANN CHOLÁISTE NA TRÍONÓIDE, BAILE ÁTHA CLIATH | TRINITY COLLEGE LIBRARY DUBLIN
Ollscoil Átha Cliath | The University of Dublin

Terms and Conditions of Use of Digitised Theses from Trinity College Library Dublin

Copyright statement

All material supplied by Trinity College Library is protected by copyright (under the Copyright and Related Rights Act, 2000 as amended) and other relevant Intellectual Property Rights. By accessing and using a Digitised Thesis from Trinity College Library you acknowledge that all Intellectual Property Rights in any Works supplied are the sole and exclusive property of the copyright and/or other IPR holder. Specific copyright holders may not be explicitly identified. Use of materials from other sources within a thesis should not be construed as a claim over them.

A non-exclusive, non-transferable licence is hereby granted to those using or reproducing, in whole or in part, the material for valid purposes, providing the copyright owners are acknowledged using the normal conventions. Where specific permission to use material is required, this is identified and such permission must be sought from the copyright holder or agency cited.

Liability statement

By using a Digitised Thesis, I accept that Trinity College Dublin bears no legal responsibility for the accuracy, legality or comprehensiveness of materials contained within the thesis, and that Trinity College Dublin accepts no liability for indirect, consequential, or incidental, damages or losses arising from use of the thesis for whatever reason. Information located in a thesis may be subject to specific use constraints, details of which may not be explicitly described. It is the responsibility of potential and actual users to be aware of such constraints and to abide by them. By making use of material from a digitised thesis, you accept these copyright and disclaimer provisions. Where it is brought to the attention of Trinity College Library that there may be a breach of copyright or other restraint, it is the policy to withdraw or take down access to a thesis while the issue is being resolved.

Access Agreement

By using a Digitised Thesis from Trinity College Library you are bound by the following Terms & Conditions. Please read them carefully.

I have read and I understand the following statement: All material supplied via a Digitised Thesis from Trinity College Library is protected by copyright and other intellectual property rights, and duplication or sale of all or part of any of a thesis is not permitted, except that material may be duplicated by you for your research use or for educational purposes in electronic or print form providing the copyright owners are acknowledged using the normal conventions. You must obtain permission for any other use. Electronic or print copies may not be offered, whether for sale or otherwise to anyone. This copy has been supplied on the understanding that it is copyright material and that no quotation from the thesis may be published without proper acknowledgement.

Visualisation of abnormal morphological development and molecular mechanisms that give rise to tracheo-oesophageal malformations and other VACTERL anomalies in an Adriamycin treated Mouse Model

Piotr Hajduk, MD

A thesis submitted to the University of Dublin in partial fulfilment of the requirements for the degree of

Doctor of Philosophy

January 2012

Supervisors

Dr. Paula Murphy

Prof. Prem Puri

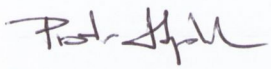
TRINITY COLLEGE
25 SEP 2012
LIBRARY DUBLIN

Thesis 9603

Declaration

I declare that I am the sole author of the thesis and that the work presented in it, unless otherwise referenced, is entirely my own. I also declare that the work has not been submitted, in whole or in part, to any other university as an exercise for a degree or other qualification.

I agree that the library of Trinity College Dublin may lend and copy this thesis upon request.



Piotr Hajduk

July 2011

Summary

Oesophageal atresia/Tracheo-oesophageal fistula (OA/TOF) are relatively common malformations of the foregut in humans (Spitz, 2007). They require urgent corrective surgery after birth and have an impact on the future health of the individual (Tomaselli *et al.*, 2003). These abnormalities are mimicked by exposure of rat and mouse embryos *in utero* to the drug adriamycin. The causes of OA/TOF during human development are not known. However, a number of mouse mutants where different signalling pathways are directly affected, show similar abnormalities, implicating multiple and complex signalling mechanisms. The similarities in developmental outcome seen in human infants and in the Adriamycin Mouse Model (AMM) underline its use to unravel early embryological events and provide insight into our understanding of the disturbances that lead to such abnormalities. The objective of this thesis was to explore the morphological and molecular alterations in the AMM using a combination of 3D imaging Optical Projection Tomography (OPT) and molecular probes. Additionally, this thesis aimed to address the hypothesis that anomalies observed in the AMM could be a result of fundamental defects in the notochord leading to abnormal delamination and ectopic placement of this potent signalling tissue during crucial stages of foregut development.

The development of the mouse foregut and its associated structures, including the notochord, were captured using the OPT. Foregut development was monitored between embryonic days (E) 9 and E12 using wholemount immunohistological staining with an endoderm marker (HNF3β) to visualize foregut and lung bud morphology in control and adriamycin treated embryos. These data provided a framework for further comparative analysis of morphology between control and adriamycin treated embryos and allowed the detailed description of the range of foregut malformations induced. Seven morphological alterations of the foregut, including OA and TOF, and abnormal notochord branching were noted, and the frequencies of occurrence were established. This analysis also revealed a close spatial relationship between notochord branch position and thickness and certain foregut malformations, indicating for the first time a causative link between abnormalities in these neighbouring tissues.

The expression of candidate regulatory genes *Shh*, *Foxf1*, *Nkx2.1*, *Sox2*, *Tbx4*, *Fgf10*, *Noggin*, *BMB4*, *Wnt2* and *Wnt7b* were investigated by wholemount *in situ* hybridisation in

control and adriamycin treated mouse embryos. The molecules encoded by these genes are known to play vital roles in regulating foregut separation and lung branching morphogenesis (Morrisey and Hogan, 2010). Ectopic signalling from the displaced notochord branches in the AMM and was verified here to express *Shh* and *Noggin*, corresponded with abnormal dorsoventral (D/V) patterning of the foregut shown by altered *Shh*, *Foxf1*, *Sox2* and *Noggin* gene expression across the foregut at the level of the branches. This correspondence between abnormal notochord delamination and gene expression supports the hypothesis that abnormal notochord signalling affected D/V patterning of the foregut and indicates that notochord abnormalities may have a causative effect on the foregut abnormalities seen in the AMM. Additionally, in terms of the origin of TOF in the AMM, this work confirmed previous findings that the fistula expressed the *Nkx2.1* gene, which is well known as a respiratory marker. In addition, the detection of *Wnt2* gene transcripts reinforces the hypothesis that the fistula is of respiratory origin and implicates Wnt signalling in this ectopic tissue.

Given the findings that foregut abnormalities show a close spatial relationship to ventrally displaced notochord branches in the AMM, I proposed that the notochord may be a primary target of adriamycin treatment with foregut abnormalities arising from abnormal signalling from the displaced notochord. To explore this hypothesis I examined the position and structure of the notochord at early stages following adriamycin treatment. It was observed that the application of adriamycin not only affected the position of the notochord, but that it also appeared to impact on the structure of the tissue as indicated by changes in the extracellular matrix (ECM) in treated embryos. The ECM was investigated by immunohistochemical techniques to visualise E-cadherin and laminin in control and treated embryos comparing the cellular organization and position of the notochord with respect to the foregut endoderm within a defined development period when delamination of the notochord normally occurs. The observed changes in notochordal properties supported the hypothesis that the notochord may be the primary target of disruption resulting in abnormal patterning of the foregut.

The work presented in this thesis provides new insights into the regulation of embryonic foregut development in the mouse as well as the effects of adriamycin treatment. The use of 3D imaging enabled direct comparison of gene expression and foregut

development both across developmental time and between control and treated embryos. This work demonstrates the integral role that the notochord plays in the development of the foregut.

Acknowledgements

Firstly, I would like to thank my supervisors Dr Paula Murphy and Prof. Prem Puri for all their support, expertise and patience over the course of the last three years. This has been a truly wonderful experience and I am indebted to both of them for giving me this opportunity to do laboratory based research towards my dream of becoming an academic paediatric surgeon. I would like to thank Paula for introducing me to the wonderful world of developmental biology and Prof Prem Puri to giving me the opportunity to present my work internationally in my field of interest of Paediatric Surgery. I would like to thank all the members of the Murphy and Puri groups past and present for all their help: Kristen, Suzanne, Karen, Audrey, Celine, Alison, Antonia, Hide, Takashi, Reshma and Anne-Marie.

I would like to thank the staff of the Department of Zoology and the National Children's Research Centre. I particularly want to thank Prof. Celia Holland, Dr Colby Tanner, Dr Yvonne Williams, Dr Michael Wride, Allison Boyce, Vanessa Woods and Sylvia Harding for their help.

I would particularly like to thank my wonderful parents for their endless words of encouragement and support.

Finally I want to thank Iwona. You have given me so much support over the last years. Your belief in me kept me going. Thank you so much. I dedicate this thesis to our son Jan, the most wonderful person I have ever met.

This work was supported by the National Children's Research Centre.

Publications and presentations resulting from this study

Hajduk P., May A., Puri P., Murphy P., "The effect of Adriamycin exposure on the notochord of mouse embryo", accepted to *Birth defects Part B: Developmental and Reproductive Toxicology.*

Hajduk P., Sato H., Puri P., Murphy P., "Abnormal notochord branching is associated with foregut abnormalities in an adriamycin treated mouse model", *PloS One*, 2011; 6(11): e27635.

Hajduk P., Murphy P., Puri P., "A role for Wnt2 gene in the pathogenesis of tracheoesophageal fistula in the adriamycin mouse model", In *Proceeding of the Young Investigator Award Session, 12th European Congress of Paediatric Surgery*, Barcelona, Spain, 2011 [Presented June 16th 2011, Barcelona, Spain].

Hajduk P., Murphy P., Puri P., "Altered Sox2 gene expression in the foregut in the Adriamycin Mouse Model", In *Proceeding of the 3rd World Congress of Pediatric Surgery*, New Delhi, India [Presented on October 21st 2010, New Delhi, India].

Hajduk P., Piazzesi A., Murphy P., Puri P., "Increased Noggin gene in abnormal branches of the notochord in the adriamycin mouse model", In *Proceeding of the Irish Society of Paediatric Surgeons*, Dublin, Ireland [Presented on June 26th 2010, Dublin, Ireland].

Hajduk P., Piazzesi A., Murphy P., Puri P., "Increased Noggin gene in abnormal branches of the notochord in the adriamycin mouse model", In *Proceeding of the 11th European Congress of Paediatric Surgery,* Berne, Switzerland [Presented on June 3rd 2010, Berne, Switzerland].

Hajduk P., Murphy P., Puri P., "Mesenchymal expression of Tbx4 gene in not altered in Adriamycin Mouse Model", *Pediatric Surgery International*, 2010, Vol. 26(4), pp. 407-11.

Hajduk P., Murphy P., Puri P., "Fgf10 gene expression is delayed in the embryonic lung mesenchyme in the adriamycin mouse model". *Pediatric Surgery International,* 2010, Vol. 26(1), pp. 23-27.

Hajduk P., Puri P., Murphy P., "Morphological and gene expression analysis in a mouse model of congenital foregut abnormalities", In *Proceeding of the 13th meeting of Irish Network of Developmental Biologist*, Galway, Ireland [Presented on December 15th 2009, Galway, Ireland].

Hajduk P., Murphy P., Puri P., "Morphological abnormalities in analysis of adriamycin treated mouse model", In *Proceeding of the American Academy of Pediatrics*, Washington, USA [Presented on October 16th 2009, Washington, USA].

Hajduk P., Murphy P., Puri P., "Fgf10 gene expression is delayed in the embryonic lung mesenchyme in the adriamycin mouse model", 1st Aesculap Prize, In *Proceeding of the 22nd*

International Symposium on Paediatric Surgical Research, Genova, Italy [Presented on September 16th 2009, Genova, Italy].

Hajduk P., Puri P., Murphy P., "Investigating the basis of foregut and lung abnormalities in a mouse model of human congenital malformations", In *Proceeding of the 16th International Society of Developmental Biologists Congress*, Edinburgh, Scotland [Presented on September 7th 2009, Edinburgh, Scotland].

Hajduk P., Murphy P., Puri P., "Mesenchymal expression of Tbx4 gene is not altered in adriamycin mouse" In *Proceeding of the 56th annual international congress British Association of Paediatric Surgeons and European Paediatric Surgeons Association*, Graz, Austria [Presented on June 18th 2009, Graz, Austria].

Hajduk P., Sato H., Giles S., Bannigan J., Puri P., Murphy P., "Tbx4 gene expression in a mouse model of congenital abnormalities of the foregut and lungs" In *Proceeding of the 12th meeting of Irish Network of Dewelopmental Biologists*, Dublin, Ireland [Presented on November 13th 2008, Dublin, Ireland].

Hajduk P., Sato H., Murphy P., Puri P., "HNF3β gene expression in the embryonic gut using optical projection tomography", In *Proceeding of the 15th International colorectal club meeting*, Salamanca, Spain [Presented on July 1st 2008, Salamanca, Spain].

Contents

1 Introduction **1**

1.1 Embryogenesis 4

1.1.1 Early foregut development 4

1.1.2 Foregut separation 6

1.1.3 Lung branching morphogenesis 8

1.1.4 Notochord development 9

1.2 The molecular basis of early foregut patterning 12

1.2.1 Endoderm cell specification 12

1.2.2 Tracheo-oesophageal patterning 14

1.2.3 Activation of lung bud morphogenesis 25

1.2.4 The molecular basis of lung branching morphogenesis 27

1.3 Etiology of OA/TOF in humans 31

1.3.1 Environmental factors 31

1.3.2 Genetic factors 32

1.4 Adriamycin rat/mouse models of OA/TOF 35

1.5 Objective of the thesis 41

2 Materials and Methods **44**

2.1 Embryo collection and fixation 44

2.2 *In situ* Hybridisation 45

2.2.1 Probe preparation 45

2.2.2 Fixation and pre-treatment of the embryos 47

2.2.3 Hybridisation, washing and detection of probe in whole mount preparations 49

2.3 Immunolocalisation 50

2.3.1 Incubation with primary antibody 50

2.3.2 Incubation with secondary antibody 51

2.4 Preparation and imaging of whole embryos using OPT 52

2.4.1 Analysis of 3D digital data 53
2.4.2 Analysis of gene expression patterns 53
2.5 Embryo collection, fixation and processing for cryosectioning 54
2.7.1 Cryostat sectioning 56
2.6 Immunohistochemistry 56
2.7 Imaging using Laser Scanning Confocal Microscopy 57
2.7.1 Image analysis 58
2.7.2 Overview of specimens investigated 58
2.7.3 Scoring criteria used in the investigation of notochord position 59
2.7.4 Scoring used in investigation of E-cadherin localisation 59
2.8 Statistical analysis 60

3 Abnormal notochord branching is associated with foregut abnormalities in an Adriamycin treated Mouse Model 61

3.1 Introduction 62
3.2 Results 66
3.2.1 Delayed development in adriamycin treated embryos 66
3.2.2 A spectrum of foregut abnormalities are caused by adriamycin treatment 67
3.2.3 Abnormal notochord branching in adriamycin treated embryos is associated with the location and severity of foregut abnormalities 71
3.2.4 Patterning of the foregut is disturbed at the site of abnormal notochord branches 74
3.2.5 Tracheal separation and lung branching in adriamycin treated embryos 81
3.3 Discussion 84

4 Temporospatial gene expression analysis during the critical period of separation of the trachea and oesophagus in normal and adriamycin treated embryo 92

4.1 Introduction 93
4.2 Results 96
4.2.1 *Tbx4* gene expression in control embryos and the effect of adriamycin treatment on gene expression patterns 96
4.2.2 *Fgf10* expression in control embryos and the effect of adriamycin treatment on *Fgf10* gene expression patterns 100

4.2.3 The effect of adriamycin treatment on noggin gene expression 103
4.2.3.1 *Noggin* gene expression in control embryos 103
4.2.3.2 Effect of adriamycin treatment on *Noggin* gene expression 104
4.2.4 The effect of adriamycin treatment on *Bmp4* gene expression 108
4.2.4.1 *Bmp4* gene expression in control embryos 108
4.2.4.2 Effect of adriamycin treatment on *Bmp4* gene expression across the stages from E10-E12 109
4.2.5 The effect of adriamycin treatment on *Wnt2* gene expression 112
4.2.5.1 *Wnt2* gene expression in control embryos 112
4.2.5.2 Effect of adriamycin treatment on *Wnt2* gene expression 113
4.2.6 The effect of adriamycin treatment on *Wnt7b* gene expression 114
4.2.6.1 *Wnt7b* gene expression in control embryos 114
4.2.6.2 Effect of adriamycin treatment on *Wnt7b* gene expression 115
4.3 Discussion 116
4.3.1 Overview of findings 117
4.3.2 Expression of *Fgf10* expression is delayed in the ventral mesoderm of the anterior foregut of treated embryos: implication for lung primordial outgrowth 118
4.3.3 Ectopic *Noggin* gene expression in the notochord and posterior wall of the foregut in adriamycin treated embryos: implication for foregut separation 121
4.3.4 *Wnt* signalling in Adriamycin Mouse Model 125

5 Notochord position and cellular organization in Adriamycin Mouse Model 129
5.1 Introduction 129
5.2 Results 133
5.2.1 Notochord position 133
5.2.2 Laminin localisation in control embryos 136
5.2.3 Laminin localisation in adriamycin treated embryos 139
5.2.4 E-cadherin localisation in control embryos 140
5.2.5 E-cadherin localisation and position of the notochord in adriamycin treated embryos 142
5.3 Discussion 144

5.3.1 Overview of findings 144
5.3.2 Abnormal delamination of the notochord in adriamycin treated embryos: implication for notochord structure 145
5.3.3 E-cadherin is abnormally expressed in the notochord of treated embryos: implication for notochord structure and signalling 147
5.3.4 The possible impact of altered notochord architecture on the foregut endoderm: possible role in endodermal anomalies 150

6 General Dicsussion and Future Directions **153**
6.1 Summary of the findings and conlusions 153
6.2 Significance of the findings and future studies 157
6.2.1 Impact of notochord on foregut patterning and development 158
6.2.2 Adriamycin influences the physical characteristics of the notochord tissue: the significance of E-cadherin expression 160
6.2.3 Identification of further molecular role players 163
6.3 Impact of our understanding of human OA/TOF; clinical implications 164

Bibliography **168**

List of Figures

1.1 The normal anatomical relationship between the oesophagus and trachea and five anatomical variances seen in OA/TOF according to the Gross classification 3

1.2 Formation of the gut tube 6

1.3 Foregut division forming the oesophagus and trachea in mouse embryos 7

1.4 Early *Nkx2.1* gene expression in the ventral foregut, in the region of the prospective thyroid and lungs 15

1.5 Dorso-ventral patterning of the foregut during separation of the trachea from the oesophagus 19

1.6 The role of Gli transcription factors in mammalian Shh signal transduction 22

1.7 A/P patterning of the ventral foregut and precise specification of the future lung primordia through *Nkx2.1* gene expression 24

3.1 Theiler staging of adriamycin and control embryos revealed a significant delay in development following adriamycin treatment 67

3.2 Morphological analysis of the spectrum of effects of adriamycin treatment on foregut and notochord development 70

3.3 Association between notochord branching and foregut abnormalities in 6 Adriamycin treated embryos 74

3.4 *Shh* gene expression in the branched notochord and disturbed *Shh* gene expression in the foregut following adriamycin treatment 76

3.5 Expression of *Foxf1* gene in adrimycin treated and control embryos 78

3.6 *Sox2* gene expression and *Nkx2.1* gene expression in control and adriamycin treated embryos at embryonic days 10 and 11 80

3.7 Abnormal trachea-oesophageal separation and lung morphogenesis in adriamycin treated embryos 83

3.8 Schematic representation summarising the observed effects of adriamycin treatment on dorso-ventral patterning of the foregut, specifially in the vicinity of a ventral notochord branch 84

4.1 The expression of the *Tbx4* gene at E11 97

4.2 *Tbx4* gene expression in control and adriamycin treated mouse embryos at embryonic days E9 - E12 following whole mount in situ hybrydization 99

4.3 *Fgf10* gene expression in TS17 and TS18 control embryos 101

4.4 *Fgf10* gene expression in TS18 adriamycin treated embryos 102

4.5 *Fgf10* gene expression at E13 in the dissected embryonic trunk of control and adriamycin treated embryos 103

4.6 *Noggin* gene expression in control embryos 104

4.7 *Noggin* gene expression in virtual sections of control and adriamycin treated embryos at E10-E11 106

4.8 *Noggin* gene expression in virtual sections of control and adriamycin-treated embryos at E12 107

4.9 *Bmp4* gene expression in control embryos 109

4.10 *Bmp4* gene expression in virtual sections of control and adriamycin treated in E10 embryos 110

4.11 *Bmp4* gene expression in virtual sections of control and adriamycin treated embryos

at E10 and E11 111

4.12 *Bmp4* gene expression in virtual sections of control and adriamycin treated embryos at E12 112

4.13 *Wnt2* gene expression in the mesenchyme on the ventral aspect of the developing foregut and around the lung buds 114

4.14 *Wnt7b* gene expression in the developing foregut and lung in control and adriamycin treated embryos at E11 and E12 116

4.15 Diagramatic summary of candidate gene expression analysis in control and adriamycin treated transverse sections of developing notochord and foregut during separation of the trachea from the oesophagus 128

5.1 Example of five different positions of the notochord in relation to the dorsal wall of the foregut and floor plate in progressively more advanced control embryos 134

5.2 Graphical representation of recordings of notochord position along the dorsoventral axis in the thoracic region, comparing control and adriamycin treated embryos 135

5.3 Laminin and Brachyury distribution in transverse sections through the thoracic region of control and Adriamycin treated embryos at progressively more advanced developmental stages 138

5.4 Detection of E-cadherin and Brachyury in transverse sections through the thoracic region of control and Adriamycin treated embryos at progressively more advanced developmental stages 141

5.5 Integrating observations on abnormal notochord position and relative intensity of abnormal E-cadherin detection in the notochord of adrimaycin treated embryos across stage groups 144

List of Tables

1.1 Summary of gene inactivation studies affecting trachea-oesophageal development. 25

2.1 Summary of cDNA clones used to generate RNA in situ probes 47

2.2 Length of time embryos were permeabilisied in 10 μg/ml Preteinase K 48

2.3 Summary of the antibody used in immunodetection 51

2.4 Staging of control and adriamycin treated embryos into designated groups based on somite number 55

2.5 Number of embryo specimens analysed for each of the sets of markers of the extra-cellular matrix according to stage group 59

3.1 The spectrum of adriamycin induced abnormalities observed showing % incidence at each embryonic day 71

3.2 Scoring of notochord branching and co-incidence of specific foregut abnormalities in 50 E10 and E11 adriamycin treated embryos 73

3.3 Extent of foregut in which dorso-ventral localised expression of either *Shh* or *Foxf1* gene was disturbed in individual Adriamycin treated embryos at either E10 or E11 79

Nomenclature

AEG Anophtalmia, Oesophageal atresia, Genital anomalies

AMM Adriamycin Mouse Model

ARM Adriamycin Rat Model

BCIP 5-bromo-4chloro-3-indyl-phosphate

Bmp Bone morphogenetic protein (gene locus)

BMP Bone morphogenetic protein (protein product)

BMS Bristol Meyers Squibb

Ci Cubitus interruptus

CNS Central Nervous System

CHAPS 3-[(3-Cholamidopropyl) dimethylammonio] -2hydroxy-1-propanesulfonate

CHARGE Coloboma, Heart anomalies, Atresia chonae , Retarded growth, Genital and Ear anomalies

DES Diethylstilbestrol

Dig digoxigenin

DNA Deoxyribonucleic acid

E-cadherin Endothelial cadherin

ECM Extracellular matrix

EDTA Ethylenediamine tetraacetic acid

EMAP Edinburgh Mouse Atlas Project

ENU N-ethyl-N-nitrosurea

Fgf Fibroblast growth factor (gene locus)

FGF Fibroblast growth factor (protein product)

Fgfr FGF receptor

Foxf1 Forkhead box protein F1

Hesx1 Homeobox expressed in embryonic stem cells 1

Hh Hedgehog

Hip Hedgehog-interacting inhibitory protein

IFABP Intesinal fatty binding protein

Isl1 Insulin gene enhancer protein 1

LMP Low melting point

LTEC Total LaryngoTrache-oEsophageal Cleft

mRNA messenger Ribonucleic acid

NBT 4-nitro blue tetrazolium chloride

Nkx2.1 Neurokinin 2 homeobox 1

OA Oesophageal atresia

OPT Optical projection tomography

Otx1 orthodenticle homeobox 1

PBS Phosphate Buffered saline

Pdx1 Pancreatic and duodenal homeobox 1

PFA Paraformaldehyde

Pitx2 Pituitary homeobox 2

Raldh2 Retinaldehyde dehydrogenase 2

RA Retinoid acid

RAR Retinoid acid receptor

RNA Ribonucleic acid

RXR Retinoid X receptor

Shh Sonic hedgehog

SSC Saline-sodium citrate buffer

Tbx T-box transcription factor

TGF Transforming Growth Factor

TOF Tracheo-oesophageal fistula

TUNEL Terminal deoxynucleotidyl transferase dUDP nick and labeling

UV Ultraviolet

VACTERL Vertebral, Anorectal, Cardiac, Tracheoesophageal, Renal and Limb defects

VTK Visualisation Toolkit

Chapter 1

Introduction

Congenital malformations of the foregut are common birth defects in humans and represent a challenge to the paediatric surgeon both in terms of surgical repair and the management of long term morbidity (Holland *et al.*, 2009; Tomaselli *et al.*, 2003). Oesophageal atresia (OA) encompasses a group of congenital anomalies that involve interruption of the continuity of the oesophagus with or without a persistent communication with the trachea called tracheo-oesophageal fistula (TOF). The most common manifestation is known as OA with distal TOF. Affected babies have a cranial oesophagus that ends in a blind sac and a connection or fistula between the trachea and the stomach (Brunner and Bokhoven, 2005; Clark, 1999; Gross, 1953; Spitz, 2007). Less common related malformations such as isolated TOF are also described in recent reviews (Gross, 1953; Spitz, 2007). Different anatomical classifications of OA/TOF were proposed but the most frequently used, and of greatest practical value to the paediatric surgeon, are those proposed by Gross (Gross, 1953) based on the frequency of each anomaly (Figure 1.1). Associated anomalies occur in 50% of cases, the majority involving one or more of a set of associations known as VACTERL (vertebral, anorectal, cardiac, tracheoesophageal, renal and limb defects) (Shaw-Smith, 2006). The continuity of the oesophagus and the pathological connection that persists between the digestive and respiratory tracts requires urgent

surgery and further long-term medical follow up due to late complications. These conditions were first described by Durston in 1670 (Myers, 1986), although at this time they were not treatable. The first attempts for surgical correction of the anomalies were undertaken by Charles Steel in 1888 (Myers, 1986; Zhou *et al.*, 1999). The baby died after surgery, however this study gave an indication that the abnormality was potentially treatable. The first described successful operative treatment for isolated OA was performed by Donovan in 1935 (Myers, 1986). Since that time improvements in neonatal intensive care, anaesthesia and surgical techniques have brought a steady decline in overall mortality due to the primary foregut malformation. However mortality still remains high for babies with low birth weight and other associated major cardiac anomalies (Spitz, 2006). The etiology of these foregut malformations still remains largely unknown.

A good knowledge of the mechanisms underlying normal development of the foregut in mammalian embryos is essential to uncover the origin of OA/TOF. In normal development, the respiratory and digestive tubes are derived by division of a single foregut tube that is surrounded by splanchnic mesoderm (Cardoso and Lu, 2006). The first evidence of this in mice is the formation of lung primordia from the ventral foregut endoderm at embryonic day (E) 9.5 (Cardoso and Lu, 2006; Morrisey and Hogan, 2010). From E10.5 the laryngo-tracheal groove begins to separate the trachea ventrally and oesophagus dorsally (Morrisey and Hogan, 2010). Both tubes elongate, bronchial stalks extend to form the main bronchi and stereotypic branching and budding occurs as the bronchial and bronchiolar tubules form between approximately E11 and E16 (Maeda *et al.*, 2007). In humans the process of foregut division starts from 28 days post fertilization (Carnegie stage 13). This is a complex process in which

tissues and organs undergo an intricate sequence of movements relative to each other, controlled by interaction through diffusible signalling molecules. While the normal mechanisms driving proper foregut development are still not clear, investigating abnormal foregut development is even more challenging.

A valuable animal model reproducing OA and TOF was developed in the rat (Diez-Pardo *et al.*, 1996; Merei *et al.*, 1999) following the discovery that treatment of pregnant females with the drug Adriamycin led to similar malformations (Thompson *et al.*, 1978). However, given that the mouse is the developmental biologists mammal of choice, providing greater availability of molecular tools and techniques, and transferable knowledge from mutant mice, Adriamycin treated mouse models displaying OA/TOF were developed (Dawrant *et al.*, 2007a; Ioannides *et al.*, 2002). Also a number of mouse mutants replicate aspects of OA/TOF shown in the adriamycin model indicating that complex signalling events are involved in normal foregut development and disturbed in OA/TOF, lending some valuable information about the possible mechanisms that might be disturbed in these foregut anomalies.

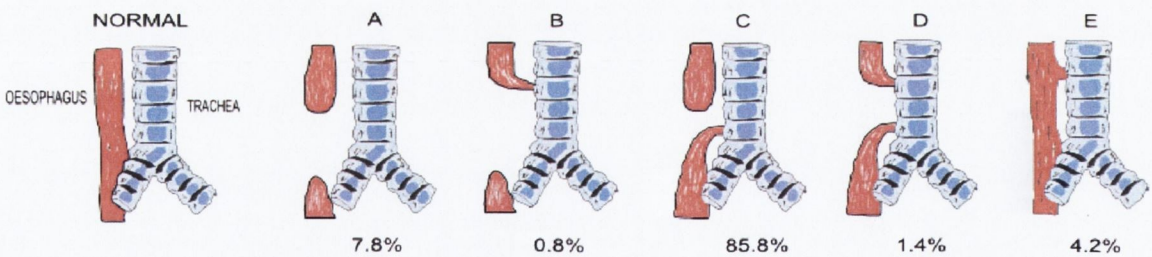


Figure 1.1: The normal anatomical relationship between the oesophagus and trachea (normal) and five anatomical variances seen in OA/TOF according to the Gross classification (Gross, 1953) with the percentage of occurance of each in newborn infants. Adapted from Gross, 1953.

In this chapter, I review the literature in order to outline current knowledge on early foregut and notochord embryogenesis (section 1.1), our understanding of the molecular basis of

normal foregut development and theories explaining tracheal separation and lung branching morphogenesis (section 1.2). I also outline the state of current knowledge regarding the possible aetiology of the OA/TOF malformations in humans (section 1.3) and I review current hypotheses relating to the molecular mechanisms leading to formation of OA/TOF in mammals based on observations from the adriamycin model, reproducing OA/TOF in rodents (section 1.4). Finally I set out the aims and objectives of this research in the context of current knowledge (section 1.5).

1.1 Embryogenesis

1.1.1 Early foregut development

During gastrulation, a layer of undifferentiated cells (the epiblast) forms three germ layers; the ectoderm, mesoderm and endoderm. Differentiation of the precursor endodermal and mesodermal cells occurrs during cell migration through the primitive streak, a region in which several genes involved in cell fate specification are expressed (Wells and Melton, 1999). At E 7.5 in the mouse, the endoderm forms a one cell-layer thick sheath that underlies the mesoderm and ectoderm of the embryo, which is cup shaped. The most anterior endoderm that involutes from the most anterior part of the primitive streak (Lawson *et al.*, 1986), forms the proximal foregut adjacent to the developing heart and organs such as the the liver and ventral part of the pancreas. The mid region gives rise to distal foregut and midgut and contributes to formation of the stomach, pancreas, duodenum, and the part of the intestine. The most

posterior part of the endoderm forms the hindgut and contributes to the large intestine and colon (Lawson *et al.*, 1991; Wells and Melton, 1999).

Through a series of morphogenetic processes within the next 24 hours (E7.5 - E8.5) the endoderm sheath folds into a tube (Figure 1.2). The anterior endoderm folds over posteriorly to form a diverticulum called the foregut pocket while the most posterior endoderm folds anteriorly to form the hindgut diverticulum. The posterior migration of the anterior foregut pocket and the anterior migration of the hindgut, in combination with ventral folding during the turning of the embryo on the anterior to posterior axis, closes the midgut and forms a primitive gut tube by E9 (Wells and Melton, 1999) (Figure 1.2). Initially the endoderm is in very close proximity to the notochordal plate but from about E9 the notochord delaminates from the endoderm in the mid regions of the embryo and by about E9.5 it is separated from the anterior foregut by mesenchyme, becoming more closely associated dorsally with the neural folds/neural tube (Jurand, 1974) where it is well known to contribute to dorso-ventral (DV) patterning of the developing Central Nervous System (CNS) and laterally to patterning of the somites. Signals from the notochord are also important in patterning the foregut and its associated mesenchyme ventrally (Cleaver and Krieg, 2001).

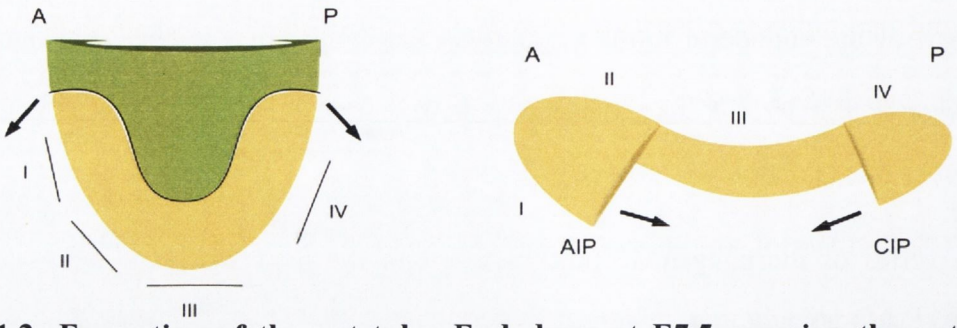


Figure 1.2: Formation of the gut tube. Endoderm at E7.5 covering the outside of the embryo (left diagram). Gut endoderm is yellow and visceral endoderm is green. Roman numbers I-IV represent regions of the endoderm at E7.5 that fate map to regions I-IV of the E8.5 gut tube (shown on the right) (Wells and Melton, 1999). The foregut tube forms as region I folds over region II and migrates in a posterior direction. The hindgut tube forms by folding of region IV and migration in the anterior direction (right diagram). The midregion forms a tube by ventral folding. AIP, anterior intestinal porta; CIP, posterior intestinal porta. Adapted from Wells and Melton, 1999.

1.1.2 Foregut separation

Both the respiratory and digestive anlagen arise from the foregut, the trachea forming ventrally and the oesophagus dorsally. The first morphological evidence of this is at E9.5 in mice (22 somite stage in mice, 28 days in human) with the appearance of two ventrolateral bulges which subsequently elongate to form the bronchi and lung buds, in conjunction with surrounding mesenchyme (Cardoso and Lu, 2006; Morrisey and Hogan, 2010) (Figure 1.3). The location of the lung primordia along the antero-posterior (A-P) axis of the foregut is determined by localized expression of the *Nkx.2.1* gene in the ventral wall of the foregut endoderm (Morrisey and Hogan, 2010). Anterior to this, the single foregut diverticulum septates laterally by formation of a local constriction (folds or ridges) that moves towards the centre of the lumen and contacts in the midline to separate the trachea and oesophagus (Cardoso and Lu, 2006; Morrisey and Hogan, 2010; Qi and Beasley, 2000). There is some disagreement in the literature about how the process of septation progresses. Recent work

measuring the respective lengths of the undivided and divided regions of the foregut overtime indicates that septation progresses anteriorly from an initial point (Ioannides *et al.*, 2010). However, similar work from another group concluded that progressive separation is achieved through posterior elongation from the point of septation (Williams *et al.*, 2003). It is possible that these two processes occur simultaneously and a combination of both are important during the process of separation (Morrisey and Hogan, 2010).

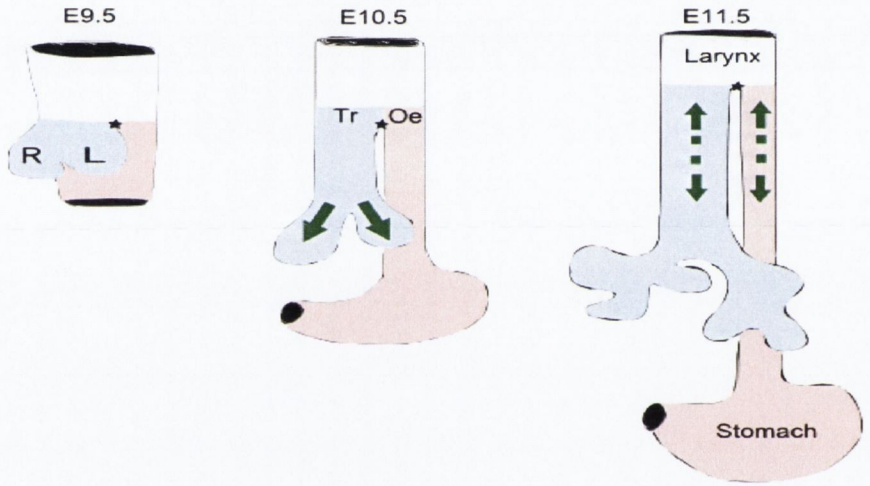


Figure 1.3: Foregut division forming the oesophagus and trachea in mouse embryos. At E9.5 lung primordia appear on the ventrolateral surface of the foregut. The point of foregut separation, marked by a star, moves anteriorly (progressive septation) while at the same time the oesophagus and tracheal tubes elongate. At E11.5 the lung buds undergo branching morphogenesis. Adapted from Morrisey and Hogan, 2010.

Although some progress has been made towards understanding foregut separation, there is still little known about the cellular mechanisms involved in dynamic coordinated changes to the shape and alignment of the cells in the foregut epithelium, at the level of tracheal separation. Formation of the lateral epithelial folds were investigated using scanning electron microscopy by Kluth et al. (Kluth *et al.*, 1987) in chick embryos. Rapid endodermal cellproliferation was described at the region of separation of the primitive foregut into trachea and oesophagus. Qi

and Beasley (Qi and Beasley, 1998) described increased cell death at the site of foregut separation in rats at E12. This process was investigated in detail by another group (Orford *et al.*, 2001) by comparing normal separation of the foregut in rats and adriamycin treated animals where separation was not seen. This group using the TUNEL technique for detection of cell death showed apoptosis in the lateral epithelial folds (the prospective site of tracheoeophageal separation) of the foregut in control animals and the absence of apoptosis in treated embryos displaying no separation. This suggested that programmed cell death contributes to the formation and morphogenesis of the middline fusion point. However this finding was refuted in a recent study by Ioannides et al, where the authors examined foregut separation in embryos at E10.5 and E11.5, comparing normal events with a mutant in which no apoptosis takes place (*Apaf1/CED-4/ARK* null) (Ioannides *et al.*, 2010). Apoptosis was detected using an antibody for activted caspase-3 on transverse sections of the foregut. Results confirmed increased programmed cell death at the point of foregut separation at E11.5 but in *Apaf1* null embryos, with drammatically reduced activation of caspase 3 and complete supression of apoptosis, foregut separation occurred properly showing that programmed cell death is not essential for foregut separation.

1.1.3 Lung branching morphogenesis

Simultaneous with the process of tracheal separation, development of the lung primordia progresses with extension of the bronchial stalks and stereotypic branching and budding as the bronchial and bronchiolar tubules form between approximately E9.5 and E16.5 (Maeda *et al.*, 2007; Morrisey and Hogan, 2010). The bronchial tree develops by branching of the airway

epithelium into the surrounding mesenchyme. Initially the primary lung buds grow ventrally and posteriorly, and initiate lateral branches at invariant positions at E10.5. In this way, five secondary buds are generated, four on the right side and one on the left side, leading to the formation of four right lobes and one left lobe of the mature lung in mice. In addition to lateral branching, dichotomous branching occurrs at the tip of each duct. This leads to expansion of the lung epithelium. After the branching process is accomplished, from E16.5 - E17.5, terminal buds become narrower and then from E18.5 to postnatal day 5, they develop numerous small sacs that are the precursors of the alveoli (Morrisey and Hogan, 2010).

1.1.4 Notochord development

The notochord is an axial structure of mesodermal origin that arises during gastrulation, directly from the cells of the primary organiser. The presence of the notochord during development defines members of the Chordate phylum and is a common characteristic of all vertebrate embryos (Jurand, 1974). During development of vertebrates it is present only in early stages of embryonic life although in some lower chordates the notochord persists throughout life and acts as a structural support for the entire organism (Jurand, 1974).

As described in section 1.1.1, in the mouse embryo at E7.5 the future anterior foregut endoderm consists of epithelial cells blanketing the ectoderm and mesoderm (Wells and Melton, 1999). The formation of the notochord is first detected at E8, at the cranial end of the primitive streak. These early chordomesoderm cells are embedded in the endoderm sheath although they are more columnar than the endoderm cells (Jurand, 1974). From E9.5 the two

distinct cell types start to separate and the notochord delaminates in the dorsal direction. The notochord becomes a slender flattened rod adhering dorsally to the endoderm and lying ventral to the neural tube. The notochord detaches from the foregut endoderm first at the level of the cardiac primordium and then gradually progresses in anterior and posterior directions. At E11 the entire central portion of the notochord contacts with the ventral surface of the neural tube and only the most cranial and caudal ends are still attached to the endoderm (Jurand, 1974). By E12 mesenchymal cells have penetrated between the notochord and neural tube and the notochord becomes a uniform cylindrical rod surrounded by mesenchyme extending from Rathke's pouch to the end of the tail. From E13 the mesenchyme lateral to the notochord, which is segmented into the somites, undergoes cartilage condensation forming the pre vertebrae (Jurand, 1974). Then the notochord fragments and becomes ossified in specific regions forming the vertebral bodies and contributes to the centre of the intervertebral discs in a structure called the nucleus pulposis (Linsenmayer *et al.*, 1986; Smits and Lefebvre, 2003).

The fundamental roles of the notochord are to provide the cranio-caudal orientation of the embryonic axis and act as a primary organizer for adjacent embryonic organs (Cleaver and Krieg, 2001). The rigidity of the notochord maintains alignment of embryonic tissues during development and allows axis elongation (Adams *et al.*, 1990). As well as a structural function, many studies have shown the importance of the notochord in patterning of surrounding ectoderm and mesodermal tissues. Perhaps the best characterised is the role of the notochord in patterning of the neural tube. In chick embryos, grafting of the notochord next to the lateral part of the neural tube results in the appearance of floor plate-cells, characteristic of the ventral neural tube, in the adjacent neural epithelium, indicating that the notochord induces formation

of the floor plate (van Straaten *et al.*, 1985a; van Straaten *et al.*, 1988; van Straaten *et al.*, 1985b). In addition, in chick embryos in which the notochord was extirpated *in ovo*, the spinal cord appeared reduced in size and lacked a floor plate (van Straaten, 1991). The notochord also patterns the somites, for example in zebrafish mutants *ntl* and *flh*, which both lack a notochord, somites are fused with disruption of the characteristic chevron formation and the lack of muscle pioneer cells (Halpern *et al.*, 1993). In the chick embryo, removal of the notochord results in the failure of sclerotome formation and enlargement of the dermamyotome (Goulding *et al.*, 1994). These mutants also show the importance of the notochord for formation of the dorsal aorta (Fouquet *et al.*, 1997). There is also evidence that the notochord is involved in assignment of left-right asymmetry. For example in Xenopus embryos, when the notochord is experimentally ablated by UV irradiadion or surgically removed, *nodal*, which is normally expressed on the right side of the lateral plate mesoderm, is expressed bilaterally leading to cardiac reversal (Danos and Yost, 1995; Lohr *et al.*, 1997). Similar results were seen in mouse embryos when the node was surgically ablated and the notochord failed to form or was disrupted (Davidson *et al.*, 1999). The notochord appears to act as a barrier to diffusion of molecules localized to one side. As a result the *Pitx2* gene, encoding a regulatory transcription factor in the laterality pathway, was no longer restricted to the left side but was found on both sides of the body or was completely absent from the lateral plate mesoderm (Davidson *et al.*, 1999).

In terms of patterning of the endoderm by the notochord there is less evidence in the literature, although these structures are in very close contact during development. In chick embryos removal of the notochord just prior to the time when pancreas fate is specified prevents

expression of *Isl1* and *Pdx1* genes, which are crucial for pancreas development (Kim *et al.*, 1997). *In vitro* growth of isolated endoderm from the dorsal pancreatic anlage with adjacent notochord shows that the notochord can induce expression of early pancreas genes (Kim et al., 1997). Moreover grafting of the notochord in chick embryo repress *Shh* expression in the foregut endoderm and removal of the notochord results in ectopic *Shh* expression in the pancreatic anlage and inhibits pancreatic endodermal differentiation (Hebrok *et al.*, 1998). These experiments demonstrate that notochord signals are necessary for dorsal pancreas development and show the important role of the notochord in patterning of the endoderm.

1.2 The molecular basis of early foregut patterning

1.2.1 Endoderm cell specification

Mesoderm and endoderm cells both arise from the epiblast and then migrate (involute) through the primitive streak (Lawson *et al.*, 1991). It is not clear if cell fate is determinated prior or during the migration through the primitive streak. Several soluble factors including members of the fibroblast growth factor (*FGF*), transforming growth factor (*TGF β*) and *Wnt* families, as well as the morphogen retinoic acid are expressed in the region of the primitive streak and are widely known to influence cell fate and may act to induce mesoderm and endoderm, although a direct role of specific molecules in endoderm differentiation in not known (Wells and Melton, 1999).

At the end of gastrulation gut endoderm is a sheet of approximately 500 cells that extends from the anterior headfold to the primitive streak. Fate-mapping experiments suggest that endoderm cells have A-P identity by this stage (Lawson *et al.*, 1986). The headfold is adjacent to mesendoderm cells that involute and migrate anteriorly, while the cells forming posterior endoderm leave the primitive streak later in gastrulation (Lawson and Pedersen, 1987). Regional expression of certain genes indicate anterior–posterior specification of the endoderm at a very early stage. For example expression of *Cerberus* (Bouwmeester *et al.*, 1996), *Otx1* (Rhinn *et al.*, 1998) and *Hesx1* (Thomas and Beddington, 1996) is restricted to the anterior endoderm and the Intesinal Fatty Acid Binding Protein gene (*IFABP*) (Green *et al.*, 1992) and *Cdx2* (Beck *et al.*, 1995) to the posterior endoderm. As the endoderm tube forms, cells condense into the epithelium and start de novo expression of several genes including *Pdx1*, *NeuroD* and *Somatostatin*, and mark specific regions of endoderm which will give rise to stomach, pancreas, and duodenum (Wells and Melton, 2000). *Somatostatin* expression extends to the more posterior gut tube, the future small intestine. *IFABP* expression is strong in the posterior region, the future hindgut (Wells and Melton, 2000). Futhermore endoderm coculture experiments with mesoderm/ectoderm show that the endoderm receives inductive signals from mesoderm and ectoderm for expression of these genes, that the A-P nature of the endoderm is not irreversibly determined by E7.5 and can be altered by changing the spatial source of the signal (Wells and Melton, 2000). The same study showed that notochord cocultured with E7.5 endoderm does not induce *Pdx1*, *Somatostatin*, *NeuroD* and *IFAB* expression and therefore it is possible that early signals from measoderm/ectoderm make the endoderm competent to respond to subsequent notochord and mesenchyme signals (Wells and Melton, 2000). This signalling between germ layers is mediated by soluble factors. For example *FGF4*, which is

expressed by the primitive streak at the posterior part of the embryo induces *NeuroD* and *Somatostatin* expression in the endoderm in a concentration-dependent manner. Higher concentrations of *FGF4* promote expression of *Somatostatin* in the posterior endoderm while lower expression of *FGF4* promotes expression of *NeuroD* in more anterior endoderm, further away from the source of *FGF4* (Wells and Melton, 2000).

1.2.2 Tracheo-oesophageal patterning

A key step in division of the respiratory and digestive tracts is patterning of the foregut tube into ventral (respiratory) and dorsal (digestive) territories and a large number of regulatory molecules, working within several pathways, have now been implicated in this process. From lineage tracing studies in mice we know that cells that give rise to the distal regions of the respiratory tract (distal airway epithelium) and proximal regions (trachea, proximal airway) have different origins (Perl *et al.*, 2002).

The mechanisms leading to specification of the respiratory progenitors in vertebrates are starting to be elucidated. Initial specification of the foregut endoderm cells into the respiratory system starts before the lung primordium can be identified; by E9 the ventral foregut in the thoracic region is characterized by localized *Nkx.2.1* gene expression (Desai *et al.*, 2004; Morrisey and Hogan, 2010). The specific expression of *Nkx2.1* expression by respiratory progenitors has been described across multiple species including Xenopus (Small *et al.*, 2000), chick (Sakiyama *et al.*, 2003), rat (Lazzaro *et al.*, 1991), mouse (Kimura *et al.*, 1996) and human (Hösgör *et al.*, 2002). *Nkx2.1* is also known as thyroid transcription factor 1 and is first

expressed by thyroid progenitors in the foregut endoderm more anterior to the lung primordium from E8.5 in mice (Desai *et al.*, 2004). Moreover it is expressed in the lung buds, hypothalamic area of the diencepahalon, and infundibulum of the developing brain in rats (Lazzaro et al., 1991). Analysis of *Nkx2.1* knockout mice revealed that *Nkx2.1* is essential for the embryonic differentiation of the thyroid, the lung, and the ventral areas of the forebrain and the pituitary (Kimura *et al.*, 1996). Null mutations in *Nkx2.1* result in failure of separation of the trachea and oesophagus with a single lumen of the foregut composed of both tracheal and oesophageal components (Kimura *et al.*, 1999).

Expression of *Nkx2.1* in the ventral foregut endoderm was shown to be dependent on the concentration of *FGF* signals from the adjacent cardiac mesoderm (Serls *et al.*, 2005). *FGF2* from the cardiac mesoderm co-cultured with ventral foregut endoderm promoted expression of *Nkx2.1* (Serls *et al.*, 2005) and it could be inhibited by blocking the *FGFR4* endoderm receptor (Serls *et al.*, 2005). However *in vivo*, mice lacking *FGF2* and *FGF4* are viable and have no major abnormalities suggesting functional redundancy in *FGF* signalling (Figure 1.4).

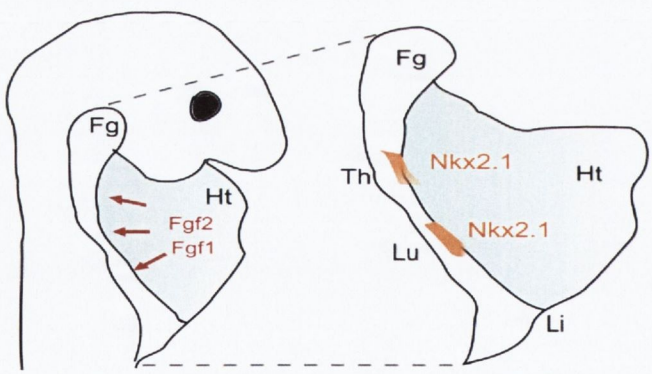


Figure 1.4: Early *Nkx2.1* expression in the ventral foregut, in the region of the prospective thyroid and lungs, responds to *FGF* signalling from the adjacent heart mesoderm. Model proposed by Serls *et al.* (2005) where foregut endoderm (Fg) is specified by *FGF* signalling from adjacent cardiac mesoderm (Ht). Distinct territories of liver (Li), lung (Lu) and thyroid (Th) are indicated. Adapted from Cardoso and Lu, 2006.

Retinoic acid (RA) is a metabolite of vitamin A (retinol) that mediates the requirements of vitamin A for growth and development. Fetuses from rat dams reared on a vitamin A deficient diet exhibit severe congenital malformations including lung agensis and undivided foregut (Dickman *et al.*, 1997; Wilson *et al.*, 1953). *Nkx2.1* is markedly reduced in the presumptive respiratory region of the foregut in these embryos at E13 (Desai *et al.*, 2004). There are two families of retinoic acid nuclear receptors (*RARs* and *RXRs*) that act as transcriptional transducers of the retinoid signals during pregnancy. There are three *RAR* encoding genes (*RAR α, β* and *γ*) each producing a number of isoforms. The majority of knockout out mice for different combinations of genes encoding subtypes of retinoic receptors, display similar abnormal morphology of the trachea and oesophagus to vitamin A deficient pups (Luo *et al.*, 1996; Mendelsohn et al., 1994). In particular, *RAR* double mutant fetuses, $RAR\alpha^{(-/-)}$, $RAR\beta2^{(-/-)}$, have been described to have an absence of an oesophagotracheal septum (Mendelsohn *et al.*, 1994). Endogenous RA synthesis and utilization throughout the foregut including the preasumptive lung field begins at E8 in mice (Malpel *et al.*, 2000; Rossant *et al.*, 1991). Foregut explants from E8.5 mice cultured with pan-retinoic acid receptor (pan-RAR) antagonist BMS493 (Bristol Meyers Squibb), show no lung bud formation after 3 days of incubation. *Nkx2.1* expression was significantly reduced in the presumptive respiratory field of the ventral foregut endoderm (Desai *et al.*, 2004). Genetic deletion of retionaldehyde dehydrogenase 2 (*Raldh2),* an enzyme essential for RA synthesis in mouse embryos, also leads to absence of lung buds and significantly reduced *Nkx2.1* expression in the endoderm of the prospective lung region in E9 embryos (Desai *et al.*, 2006). Microarrary analysis on RNA isolated from the foregut of BMS493 treated and *Raldh2* $^{-/-}$ mutant mice revealed a striking over expression of *Tgfβ* signalling pathway-related genes and abnormal hyperactivity of the

Tgfβ pathway in developing foregut (Chen *et al.*, 2007). *Tgfβ* protein applied directly to foreguts, blocked induction of lung bud formation and reduced expression of *Nkx2.1* in foregut endoderm (Chen *et al.*, 2007). These results suggest that endogenous RA signalling maintains an early program of differentiation in the lung endodermal progenitor cells including expression of *Nkx2.1* and is necessary to initiate bud morphogenesis in the lung field, acting at least in part by opposing *Tgfβ* signalling.

Wnt2 and *Wnt2b* are expressed in the mesoderm surrounding the ventral aspect of the foregut endoderm from E9 in mice (Goss *et al.*, 2009). *Wnt2/2b* double knock-out mutants display complete lung agenesis without foregut separation (Goss *et al.*, 2009). *Nkx2.1* expression is absent in such embryos in the anterior foregut endoderm at the level of lung primordial at E9.5. *B-catenin* is an intracellular protein required to transmit a canonical Wnt signal and when this gene was conditionally deleted in cells of the anterior foregut that normally express *Shh* (*Ctnnb1*$^{flox/flox}$*:Shh-cre*), the *Wnt2/2b* double knockout phenotype was replicated, lacking lung specification and tracheal budding and demonstrating that *Wnt2/Wnt2b* acts in the *β-catenin* dependent canonical Wnt pathway, which is required to specify lung endoderm progenitors (Goss *et al.*, 2009). This conditional inactivation of *β-catenin* inhibits foregut separation (Goss *et al.*, 2009; Harris-Johnson *et al.*, 2009) and investigation of undivided foreguts showed that E10.5 mutant embryos lose *Nkx2.1* expression and expand *Sox2* gene expression, which is normally restricted to the ventral endoderm of the foregut in this region (Harris-Johnson *et al.*, 2009).

There is strong evidence that a balance between the respiratory (trachea/lung) and digestive (oesophagus/stomach) progenitors is maintained through D/V regulation of expression of *Nkx2.1* and *Sox2* genes. *Sox2* is a member of a family of evolutionary conserved transcription factors containing an Sry-related HMG box. From E9.5, *Sox2* gene expression is localized in all endoderm cells of the undivided foregut. Protein levels are higher dorsally, in the future oesophagus, and lower ventrally, in the future trachea (Que *et al.*, 2007). The high expression of *Sox2* in dorsal foregut is reciprocal to that of *Nkx2.1* ventrally (Que *et al.*, 2007). Hypomorphic $Sox2^{EGFP/COND}$ mutant mice display an undivided foregut with ectopic *Nkx2.1* expression and reduced *Sox2* in the dorsal foregut endoderm (Que et al., 2007). Upregulation of the *Sox2* gene was seen in the undivided foregut endoderm of *Nkx2.1* null mutant mice (Que *et al.*, 2007). Explants of foregut from normal E10 embryos treated by addition of *Fgf10*, blocked separation of the oesophagus and trachea, implicating FGF signalling in dorso-ventral patterning. In addition *Sox2* gene expression is significantly reduced in the endoderm of these explants and the *Nkx2.1* gene is upregulated leading to the conclusion that *FGF10* signalling from the ventral mesoderm regulates the reciprocal expression patterns of these two genes (Que *et al.*, 2007) (Figure 1.5).

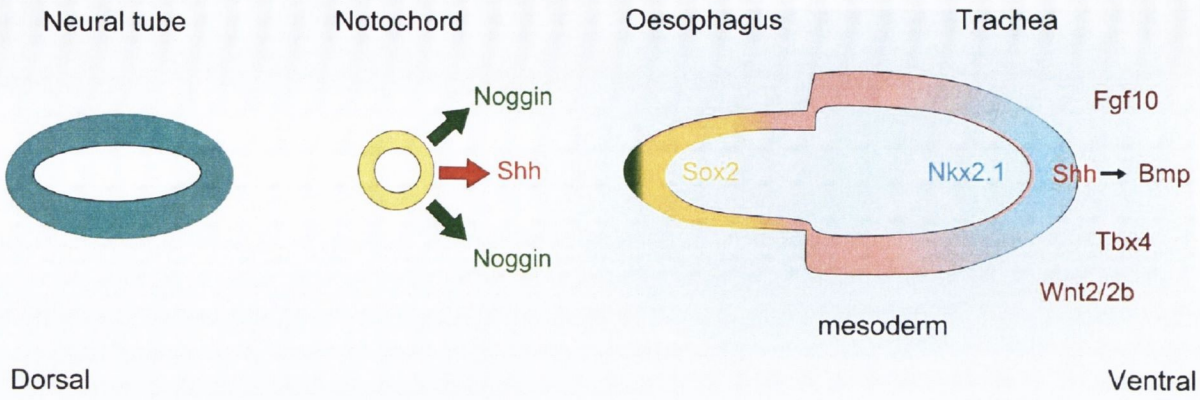


Figure 1.5: Dorso-ventral patterning of the foregut during separation of the trachea from the oesophagus. Ventral expression of *Nkx2.1*, regulated through signaling from the ventral mesoderm *(Wnt2/2b, Fgf10, and Bmp*) determines the future trachea. Higher *Sox2* expression in the dorsal foregut endoderm establishes the future oesophagus. D/V patterning of the foregut is modified through *Noggin* secretion from the notochord, most probably by inhibiting the action of *Bmps* in the dorsal foregut endoderm. *Shh* from the notochord and ventral foregut endoderm induces mesodermal *Bmp* expression. Experimental evidence reviewed in section 1.2.2. Adapted from Morrisey and Hogan, 2010.

Tbx4 is a member of the T-box transcription factor gene family. It is expressed in the ventral mesoderm surrounding the lung primordia in chicks and has also been reported in early mouse lung development (Chapman *et al.*, 1996; Sakiyama *et al.*, 2003). In normal development *Fgf10* and *Tbx4* are co-expressed in the visceral mesoderm of the lung primordia, coinciding with endodermal *Nkx2.1* expression in the ventral foregut (Sakiyama *et al.*, 2003). Ectopic *Tbx4* expression produced by in ovo electroporation in the prospective oesophagus-respiratory mesoderm region in chick embryos induced ectopic lung bud formation in the foregut, by activating the expression *Nkx2.1* in the corresponding ventral endoderm and *Fgf10* in the visceral mesoderm indicating that *Tbx4* facilitates the necessary signalling cascades (Sakiyama *et al.*, 2003). Ectopic *Fgf10* expression introduced into the visceral mesoderm alone induced ectopic budding of the foregut and caused ectopic mesodermal *Tbx4* expression around anterior foregut. These findings indicate the presence of a feedback loop between *Tbx4* and *Fgf10* (Sakiyama *et al.*, 2003). Misexpression of *Tbx4* or *Fgf10* in the visceral mesoderm

posterior to lung primordia, result in posterior expansion of *Nkx2.1* gene expression (Sakiyama *et al.*, 2003). In addition, some of these embryos result in failure of separation of the trachea from the oesophagus (Sakiyama *et al.*, 2003). This suggests that a *Tbx4-Fgf10* system acts as a signaling component of the inductive interactions specific to lung primordium mesoderm and that altered boundaries of expression can affect tracheo-oesophageal separation. In chick, interference (inactivation) of *Tbx4* function in the visceral mesoderm repressed *Fgf10* expression in corresponding mesoderm and led to failure of lung bud formation (Sakiyama *et al.*, 2003). However in mice inactivation of the *Tbx4* gene does not prevent lung bud formation (Naiche and Papaioannou, 2003). Overlapping expression of *Tbx2, Tbx3, Tbx4* and *Tbx5* during foregut development suggests possible functional redundancy of these genes during lung morphogenesis in mice (Chapman *et al.*, 1996); multiple Tbx genes are also present in humans.

Sonic hedgehog (*Shh*) is a secreted glycoprotein morphogen that is fundamental to a large spectrum of developmental processes in both vertebrates and invertebrates (Hooper and Scott, 2005). Most of the components of Hedgehog (*Hh*) signal transduction were first revealed by genetic studies in *Drosophila* embryos (Nusslein-Volhard and Wieschaus, 1980). Two transmembrane proteins Patched (*Ptch*) and Smoothened (*Smo*) function as the *Hh* binding receptor complex (Alcedo and Noll, 1997; Chen and Struhl, 1996; Stone *et al.*, 1996). *Ptch* has been shown to bind both *Hh* and *Smo* (Marigo *et al.*, 1996; Stone *et al.*, 1996). In the absence of *Ptch*, *Smo* constitutively activates the *Hh* signaling pathway (Alcedo *et al.*, 1996). In the absence of *Hh* signal, *Ptch* will inhibit the activity of *Smo* (Denef *et al.*, 2000). Downstream of *Smo* is a multi-protein complex known as the Hedgehog signaling complex which compromise

the zinc-finger-containing transcription factor Cubitus interruptus (*Ci*) necessary to activate *Hh* targets (Alexandre *et al.*, 1996; Dominguez *et al.*, 1996). In mammals there are three Hedgehog genes, Sonic, Indian and Desert Hedgehog, two *Ptch* genes (*Ptch1* and *Ptch2*) and three *Ci* homologues; *Gli1, Gli2* and *Gli3*. *Gli1* posssesses only an activator function, whereas *Gli2* and *Gli3* are bi-functional, acting as both activators and repressors of transcription. In the absence of a *Hh* signal, *Gli2* and *Gli3* exibit a repressor function while in response to *Hh* signal they are converted into activators (Dai *et al.*, 1999; Ruiz i Altaba, 1999; Sasaki *et al.*, 1997; Sasaki *et al.*, 1999; Wang *et al.*, 2000) (Figure 1.6).

During foregut development *Shh* gene expression is spatially restricted to the ventral aspect of the foregut endoderm from E9 (Litingtung *et al.*, 1998; Sato *et al.*, 2008). *Shh* signaling acts as a positive regulator of *Ptch* expression in the lung mesenchyme (Bellusci *et al.*, 1997a). *Shh*-null mutants ($Shh^{-/-}$) are highly malformed (Chiang *et al.*, 1996; Litingtung *et al.*, 1998). Development of the lung buds is delayed for at least half a day, appearing by E10.5 and the trachea fails to separate from the oesophagus (Litingtung *et al.*, 1998). $Shh^{-/-}$ mutant lung are hypoplastic and in the older stages (E17.5) the trachea and oesophagus are connected to the stomach as a common tube (Litingtung *et al.*, 1998). *Ptch* and *Gli3* expression is downregulated and *Gli1* expression is undetectable in the mesenchyme adjacent to the lung buds at E11.5 (Litingtung *et al.*, 1998). *Nkx2.1* expression in the mutant embryos at E10.5 is well defined and restricted to the ventral endoderm of the foregut, resembling that of wild type embryos (Ioannides *et al.*, 2010). $Shh^{-/-}$ mutants have overlaping phenotypes with *Gli2* knockout ($Gli2^{-/-}$) mice and $Gli2^{(-/-)}$, $Gli3^{(+/-)}$ double mutants. $Gli2^{(-/-)}$ mutants have foregut defects with tracheal and oesophageal stenosis, as well as hypoplasia of the lungs (Motoyama

et al., 1998). Consistent with the notion that *Gli2*$^{(-/-)}$ mutant lungs have reduced response to the *Shh* signal, the expression of *Ptch* and *Gli1* is diminished. Double mutant embryos lacking both copies of *Gli2* and one copy of the *Gli3* gene, *Gli2*$^{(-/-)}$, *Gli3*$^{(+/-)}$, have an undivided foregut connected to the stomach, with a single undivided hypoplastic lung (Motoyama *et al.*, 1998). Mutants lacking both copies of *Gli2* and *Gli3* have even more severe defects lacking a trachea, oesophagus and lungs following degeneration of the undivided foregut during development (Motoyama *et al.*, 1998). Similar abnormalities seen in the *Shh* and *Gli* mutant mice including hypoplastic lungs and lobulation defects, oesophageal and tracheal stenosis, or oesophageal atresia and tracheo-oesophageal fistula have been reported in heterozygous *Foxf1*$^{(+/-)}$ mutant mice (Mahlapuu *et al.*, 2001). The *Shh* target gene *Ptch* shows an expression pattern complementary to *Foxf1* in the mesenchyme surrounding the distal epithelium of the lung buds (Bellusci *et al.*, 1997a; Mahlapuu *et al.*, 2001). *Foxf1* expression can be activated by ectopic *Shh* secretion in in vitro cultered lung mesenchyme and *Foxf1* expression is absent in the mesenchyme surrounding the trachea and lung buds in *Shh*$^{-/-}$ mutants (Mahlapuu *et al.*, 2001). *Therefore Shh, Gli and Foxf1* are likely to be part of the same pathway and *Foxf1* a downstream target of *Shh*.

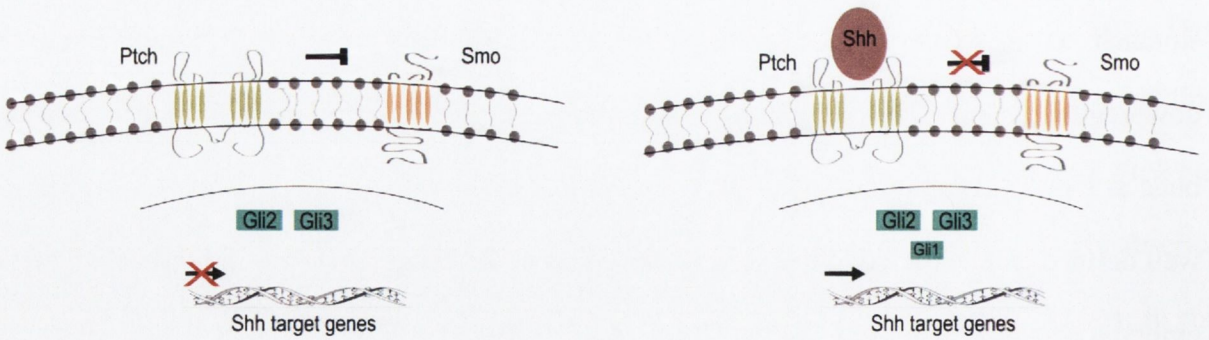


Figure 1.6: The role of *Gli* transcription factors in mammalian *Shh* signal transduction. In the absence of a *Shh* signal (left) the transcription factors *Gli2* and *Gli3* act as negative regulators of pathway target genes. When a *Shh* signal is received (right) *Gli2* and *Gli3* together with *Gli1* act as transcription activators.

The canonical *BMP* signalling pathway is activated by secreted ligands (e.g. *Bmp4*) interacting with a complex of type I and type II transmembrane receptors. This initiates signal transduction by phosphorylation of intracellular proteins called *Smads*; *Smad 1/5/8*, which interact with a co-Smad (*Smad4*) to regulate downstream target genes (Miyazono *et al.*). The role of *BMP* signalling is still unclear in the initial specification of foregut primordia. Although *Bmps* are expressed in the ventral foregut mesoderm and endoderm (Li *et al.*, 2008b; Weaver *et al.*, 2000) and *Bmp4* knockout mice display tracheal agenesis, *Nkx2.1* gene expression domain appeared to be normal in the foregut of knockout embryos. Therefore, *Bmp4* is not required for the initial specification of the respiratory bud; rather, it plays a vital role in tracheal outgrowth and elongation which was severely impaired in *Bmp4* knockout mice (Li *et al.*, 2008b). *Bmp4* may be also involved in development of the dorsal foregut, its separation and elongation. *BMP* signalling is modulated by extracellular antagonists, including *noggin*, *chordin* and *follistatin* that interfere with effective binding to its receptors (Massague *et al.*, 2005). The *Noggin* gene is expressed in mice from E7.5 along the entire length of the notochord, the floor plate of the neural tube and in a single cell layer of the dorsal foregut endoderm (McMahon *et al.*, 1998; Que *et al.*, 2006). It was suggested from the observation made in *Noggin* knockout mice, which display lack of separation of the foregut, that the noggin gene expressed from the notochord may protect dorsal foregut endoderm by inhibiting action of *Bmp4* in promoting intercellular adhesion (Que *et al.*, 2006). This is proposed to allow the cells from the dorsal foregut to reorganise, detach from the future trachea and elongate properly. Mesodermal expression of *Bmp4* is induced by *Shh* from the endoderm through mesodermal transcription factors *Foxf1*, *Gli1* and *Gli3* (Weaver *et al.*, 2003). It was also shown that *Shh* up-regulates *noggin* expression in the mesoderm (Weaver *et al.*, 2003)

and *Foxf1*, *Gli2* and *Gli3* knockout mice display overlapping phenotypes and display lack of foregut separation (Litingtung *et al.*, 1998; Mahlapuu *et al.*, 2001; Motoyama *et al.*, 1998) therefore interaction between *Bmp4/noggin* and *Shh* pathways is critically important for tracheoesophageal separation.

The signalling pathways and transcription factor interactions implicated in tracheo-oesophageal patterning reviewed in this section are summarized in Figure 1.7. The genes suggested to be involved in abnormal trachea-oesophageal separation are summarised in Table 1.1.

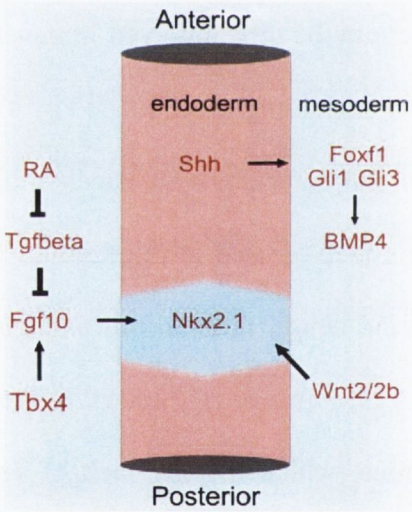


Figure 1.7: A/P patterning of the ventral foregut and precise specification of the future lung primordia through *Nkx2.1* gene expression (ventral view). *Shh* in the endoderm regulates *Bmp4* in the mesoderm through *Foxf1, Gli1* and *Gli3*. Expression of *Fgf10* in the mesoderm drives outgrowth of the lung buds and is modified by *RA* and *Tgfβ* pathways. In chicks *Fgf10* is a downstream target of the *Tbx4* transcription factor. The evidence for these molecular interactions is given in the text. Adapted from Morrisey and Hogan, 2010.

Table 1.1: Summary of gene inactivation studies affecting tracheo-oesophageal development.

Gene	Mutant phenotype	Human homologue	Human locus	References
Shh$^{(-/-)}$	OA; TOF; lungs form rudimentary sacs	*SHH*	7q36	Litingtung et al., 1998
Rara$^{(-/-)}$,*Rarβ*$_2^{(-/-)}$ or *Rara*$_1^{(-/-)}$,*Rarβ*$^{(-/-)}$	TOF; lung hypoplasia or agenesis	*RARα, RARβ*	RARα:17q21.1 RARβ:3p24	Mendelsohn et al., 1994; Luo et al., 1996
Gli2$^{(-/-)}$; *Gli3*$^{(+/-)}$ *Gli2*$^{(-/-)}$; *Gli3*$^{(-/-)}$	OA; TOF; severe lung phenotype No formation of the oesophagus, trachea and lungs	*GLI2, GLI3*	GLI2: 2q14; GLI3: 7p13	Motoyama et al., 1998
Foxf1$^{(-/-)}$ *Foxf1*$^{(+/-)}$	Lethal before embryonic day 10; extra-embryonic defects OA; TOF; lung immaturity/hypoplasia; lobulation defect	*FOXF1*	16q24.1	Mahlapuu et al., 2001
Ttf1$^{(-/-)}$	TOF; rudimentary peripheral lung primordial	*TTF1*	14q13	Kimura et al., 1999
Hypomorphic *Sox2*$^{EGFP/COND}$ mutant	OA; TOF; lung branching defect	*SOX2*	3q26.2-q27	Que et al., 2007
Noggin$^{(-/-)}$	OA; TOF; lung branching defects; abnormal notochord morphogenesis	*NOG*	17q22	Que et al., 2006
Pcsk5 C470R mutant[a]	Abnormal tracheoesophageal septation; hypoplastic lungs	*PCSK5*	9q21.3	Szumska et al., 2008
Hoxc4$^{(-/-)}$	Partially or completely blocked oesophageal lumen; disruption of oesophageal musculature	*HOXC4*	12q13.3	(Boulet and Capecchi, 1996)
Tbx4 misexpression	TEF	*TBX4*	17q21-q22	Sakiyama et al., 2003

[a]Ethylnitrosourea (ENU)-induced mouse mutation
Adapted from de Jong *et al.*, 2010.

1.2.3 Activation of lung bud morphogenesis

Once the respiratory field is established in the ventral foregut endoderm, outgrowth and extension of the lung primordia into surrounding mesenchyme starts from E9.5. Studies in

different species including chick and mouse have shown that this process is entirely dependent on the localized expression of *Fgf10* in the mesenchyme overlying the tips of the primary lung buds and expression of the receptor *Fgfr2b* in the endoderm of the foregut (De Moerlooze *et al.*, 200; Sakiyama *et al.*, 2003; Sekine *et al.*, 1999). *Fgf10* activates *Fgfr2b* signalling in a subset of *Nkx2.1* expressing endodermal cells, triggering an *Fgf*-mediated program of proliferation and migration. In mutants lacking *Fgf10*, the trachea separates although no lung bud extension occurs indicating that the lung progenitor cells require *Fgf10* for survival (Minoo *et al.*, 1999; Sekine *et a*l., 1999). It was shown that *Fgf9*, which is also expressed in the mesenchyme of the lung, induces expansion of the lung mesenchyme in culture and triggers *Fgf10* expression most probably through upregulation of *Tbx4* and *Tbx5*, so *Fgf10* expression appears to be regulated by *Fgf9* signalling (del Moral *et a*l., 2006).

Expression of *Fgf10* is reduced in *Wnt2/Wnt2b* double knock-out mutants, suggesting that it acts downstream of canonical *Wnt* signalling in the anterior foregut (Goss *et al.*, 2009). However, when *β-catenin* is conditionally inactivated in the ventral foregut endoderm, *Fgf10* and *Fgfr2b* expression is unaltered suggesting that *β-catenin* is not required for *Fgf10/Fgfr2b* expression during lung initiation (Harris-Johnson *et al.*, 2009).

Foregut explants from E8.5 mice cultured with the pan-*RAR* antagonist *BMS493*, show absence of *Fgf10* expression in the mesoderm, near where the lung buds are expected to form, while endodermal *Fgfr2b* expression is not affected (Desai *et al.*, 2004). *Fgf10* mesodermal gene expression is also significantly reduced in vivo, in vitamin A deficient rat embryos (Desai *et al.*, 2004). As previously mentioned, inhibition of *RA* signaling in *BMS493* treated

and *Raldh2* $^{-/-}$ mutant mice leads to hyperactivation of *Tgfβ* signalling. *Tgfβ* protein applied directly to foregut explants result in marked downregulation of *Fgf10* providing additional support for a critical role of *RA* in the regulation of *Fgf10* expression during initial lung bud outgrowth (Chen *et al.*, 2007).

Shh is part of an epithelial network of regulators that restrict expression of *Fgf10* in the mesenchyme around the lung bud (Bellusci *et al.*, 1997b; Lebeche *et al.*, 1999). Downregulation of *Fgf10* was seen in the study in which *Shh* was upregulated in mice lung explants cultured with trans-retinoic acid or in the presence of recombinant *Shh* (Bellusci *et al.*, 1997b; Lebeche *et al.*, 1999). The widespread upregulation of *Fgf10* expression in the lung mesenchyme seen in *Shh*$^{-/-}$ mutants strongly suggests that the level of *FGF10* expression is negatively regulated by *Shh* expression (Litingtung *et al.*, 1998; Pepicelli *et al.*, 1998).

1.2.4 The molecular basis of lung branching morphogenesis

Ultimately the basic pattern of the respiratory tree has to be established. In mice this consists of four lobes on the right and one on the left. This process is driven by localized expression of *Fgf10* in distal mesoderm acting through *Fgfr2b* in the endoderm (De Moerlooze *et al.*, 200; Morrisey and Hogan, 2010). The D/V and A/P position of localized *Fgf10* expression is probably genetically determinate through local patterning genes acting in each segment (Ackerman *et al.*, 2005; Ackerman *et a*l., 2007; Morrisey and Hogan, 2010). Localized sources of *Fgf10* at the tip of the lung bud mesoderm become critical components of distal organizers and signalling centers. *Fgf10* expression is modified through several groups of

evolutionary conserved signalling pathways including *Bmps/Tgfβ, Wnts, Shh, Notch* and *RA* (Cardoso and Lu, 2006; Tsao *et al.*, 2008), which coordinate reciprocal interaction between the epithelium and mesoderm and drive repetitive cycles of bud elongation, cessation of outgrowth, expansion of the tip and bifurcation (Metzger *et al.*, 2008).

Two important features of the distal signaling network are crucial to drive lung branching morphogensis. First it involves multiple antagonists and complex feedback loops that limit or refine the range, magnitude and duration of mitogenic and morphogenetic signals. It can be illustrated by the mechanisms that control the *Shh* pathway or *Fgf10-Fgfr2* expression respectively. Epithelial *Shh* signalling regulates mesenchymal *Fgf10* expression during branching morphogenesis (Bellusci *et al.*, 1997b; Lebeche *et al.*, 1999). It was proposed that *Fgf10* expression is inhibited by a *Shh* signal within the interbud region. In the tip of the lung buds, although epithelial *Shh* expression is high, *Fgf10* expression is maintained and drives budding. This is possibly by inhibiting *Shh* signalling through sequestration of the *Shh* protein by increased levels of *Ptch1* and *Hip1* (Chuang *et al.*, 2003). Both *Ptch1* and *Hip1* are membrane-bound proteins that directly bind *Shh*, can transduce the *Shh* signal but not on their own and are positively regulated by *Shh*. *Spry2* gene expression was detected by whole-mount *in situ* hybridization in the epithelium of the actively growing tips of lung buds from E10.5 (Mailleux *et al.*, 2001). In cultured lungs, *FGF10*-coated beads strongly induced *Spry2* expression in adjacent lung epithelium and caused decreased epithelial proliferation and branching morphogenesis (Mailleux *et al.*, 2001). *Spry2* inhibits *Fgf10-Fgfr2* signalling in distal respiratory epithelial cell culture and reducing *Spry2* activity in lung culture results in increased branching (Tefft *et al.*, 2002; Tefft *et al.*, 1999). These two examples were proposed

as part of the mechanism controling the size of the lung bud and branching morphogensis itself. Second is that different signalling pathways cross-regulate one other. *Shh* stimulates *Wnt2* and *Bmp4* in the mesenchyme (Pepicelli *et al.*, 1998), *Wnt7b/beta-catenin* signaling promotes the expression of *Bmp4* and *Fgfr2* in the epithelium (Rajagopal *et al.*, 2008; Shu *et al.*, 2005) and *Fgf9* promotes the expression of *Fgf10* in the distal mesoderm (del Moral *et al.*, 2006).

The roles of *BMP* and *Wnt* signalling during lung branching morphogenesis are still unclear. At E10.5 in mice, when the cranial bud first appears near the tip of the right primary bud, *Bmp4* expression is low and *Fgf10* is expressed in the mesenchyme around the tip. As the cranial bud extends, driven by high mesenchymal *Fgf10* expression, *Bmp4* expression is upregualted in the endoderm. During dichotomous branching *Bmp4* declines in the region between the two new buds but is maintained in their tips. Similar patterns of restriction of *Bmp4* expression is seen during further branching morphogenesis (Weaver *et al.*, 2000). The precise role of *Bmp4* in the developing lung *in vivo* remains unclear. *In situ* hybridisation analysis in mesenchyme-free lung epithelial cultures shows that recombinant *Fgf10* induces budding and *Bmp4* expression, while recombinant *Bmp4* inhibits *Fgf10*-mediated budding in these cultures (Lebeche *et al.*, 1999; Weaver *et al.*, 2000). Other authors show that when recombinat *Bmp4* is administered to intact lung explants in which both epithelium and mesenchyme are present, branching is enhanced (Bragg *et al.*, 2001). Therefore it was proposed that when *Bmp4* signalling is activated in the epithelium (autocrine fashion), proliferation is inhibited. In intact lungs with the presence of mesenchyme, *Bmp4* from the epithelium may activate *Bmp* signalling in adjacent mesenchyme (paracrine fashion) and then

induce a currently unknown distal mesenchyme signal that enhances proliferation of distal epithelial buds (Bragg *et al.*, 2001).

Several *Wnt* ligands, frizzled receptors and components of the Wnt canonical pathway, including *β-catenin*, are present in the developing lung (Warburton *et al.*, 2005). In the early mouse lung at E12.5, *Wnt7b* is expressed in the lung epithelium with a more intense expression distally and *Wnt2* is highly expressed in the distal mesenchyme (De Langhe *et al.*, 2005; Warburton *et al.*, 2005). Inactivation of *Wnt7b* in mice resulted in perinatal death due to respiratory failure and lung hypoplasia (Shu *et al.*, 2002). Activation of canonical *Wnt* signalling can be monitored by detection of nuclear translocated of *β-catenin* and activation of the transcription of *Wnt* target genes (Nelson and Nusse, 2004). Nuclear-localized of *β-catenin* is increased in the distal lung epithelium, the sites that are actively branching (Okubo and Hogan, 2004). Disruption of the canonical Wnt pathway by targeted deletion of *β-catenin*, or by targeted expression of the *Wnt* inhibitor dickkopf 1 in vivo prevents distal lungs from forming by affecting branching morphogenesis (De Langhe *et al.*, 2005; Mucenski *et al.*, 2003). Contrary to these findings, two other studies showed increased branching morphogenesis as a consequence of disrupted *Wnt* signaling. *Wnt5a*, a noncanonical *Wnt* which is able to inhibit canonical *Wnt* signalling (Topol *et al.*, 2003; Westfall *et* al., 2003), is expressed at low levels in lung mesenchyme and epithelium at E12.5 and is highest around the trachea and pharynx. Mice that lack the *Wnt5a* gene revealed increased branching morphogenesis (Li *et al.*, 2002). Similar results were reported after lung explants were treated with morpholino oligonucleotides against *β-catenin* (Dean *et al.*, 2005). In both studies *Fgf10* expression was locally increased in the lungs.

1.3 Etiology of OA/TOF in humans

OA/TOF are common malformations of the foregut in humans affecting 1:3500 live births (Depaepe, 1993) (Figure 1.1). In approximately 50% of the cases (syndromic oesophageal atresia), there are other associated anomalies, with cardiac anomalies being the most common (Shaw-Smith, 2009). The best known association of anomalies is VACTERL (Vertebral, Anal, Cardiac, Tracheo-Oesophageal, Renal, Limb) found in around 10% - 30% of the infants with OA/TOF (Chittmittrapap *et al.*, 1989; de Jong *et al.*, 2010; Quan and Smith, 1973; Temtamy and Miller, 1974). In the other 50% of cases OA/TOF occurs in isolation (non-syndromic oesophageal atresia) (Robert *et al.*, 1993). OA/TOF is thought to be a multifactorial complex disease and various isolated reports indicate environmental and/or genetic factors in the aetiology of the malformation, although in the majority of cases, the etiology of the malformations remains unknown.

1.3.1 Environmental factors

Several environmental factors have been suggested as risk factors for development of tracheoesophageal anomalies and a number of examples are given below. It was suggested from several studies that maternal exposure to methimazole, medication used as a treatment of hyperthyroidism, given during the first trimester, may cause OA with TOF (Clementi *et al.*, 1999; Di Gianantonio *et al.*, 2001). A retrospective study which was based on a questionnaire sent to mothers of children with OA/TOF who were members of the Dutch parents association of children with OA/TOF, showed increased prevalence of OA/TOF in babies born after

maternal *in utero* exposure to diethylstilbestrol (DES), a synthetic estrogen used for the prevention of miscarriage between 1938 and 1975 (Felix *et al.*, 2007a). The authors hypothesised that exposure to DES might cause genetic or epigenetic (imprinting) changes in primordial oocytes of female embryos in utero, with effects which were not seen until the birth of the offspring of these exposed embryos, 2 generations later. Exposure to progestagen and oestrogen (exogenous sex hormones) during the first trimester of pregnancy were also reported to be associated with increased risk of OA/TOF in new born babies (Goujard and Rumeau-Rouquette, 1977; Nora *et al.*, 1976). Periconceptional exposure to maternal alcohol consumption and smoking was reported to cause increased risk of OA/TOF in newborns (Wong-Gibbons *et al.*, 2008). It was suggested from a study carried out in Finland that microbial infection may be an aetiological factor for oesophgeal atresia (Kyyrönen and Hemmink, 1988). However, while a number of environmental insults have been connected with a predisposition to OA/TOF, no consistent predominant teratogen has been identified and supported in multiple studies.

1.3.2 Genetic factors

The association of OA/TOF with a number of human syndromes indicates genetic mechanisms lying behind the pathogenesis of foregut malformations or at least predisposing the occurance. OA/TOF is found in around 0.5% - 1% of children with trisomy 21 (Dawn syndrome) and up to 25% of children with trisomy 18 (Edwards syndrome). Foregut malformation was also reported in several other structural chromosomal abnormalities (Felix *et al.*, 2007b). Mutation and deletion of the MYCN gene on chromosome 2p24.1 was shown to cause Feingold

syndrome where 30 – 40% of the patients have OA/TOF (van Bokhoven *et al.*, 2005). It is the most common cause of familial syndromic gastrointestinal atresia. The *MYCN* gene is a direct target of the *SHH* pathway (Kenney *et al.*, 2003), however, the literature only reports one patient with OA/TOF having a deletion encompassing one copy of the *SHH* gene (Speleman *et al.*, 1992).

About 10% of patients with CHARGE (coloboma, heart anomalies, choanal atresia, growth and/or mental retardation, genital and ear anomalies) syndrome display OA/TOF. It is associated with mutation of the *CHD7* gene on chromosome 8q12 which is important for early embryonic development, affecting epigenetic regulation by chromatin organization and euchromatic gene expression (Vissers *et al.*, 2004).

Deletions and mutation of the *SOX2* gene are causative for the AEG (anophtalmia/optic nerve hypoplasia, oesophageal atresia, and/or genital anomalies) syndrome that includes oesophageal atresia (Williamson *et al.*, 2006) and this corresponds with studies from mutant mice that provide evidence of the importance of the *Sox2* gene during early foregut development (Que *et al.*, 2009).

Mutations of *GLI3* cause Pallister-Hall syndrome (Johnston *et al.*, 2005) which includes bifid epiglottis, hypothalamic hamartoblastoma, postaxial polydactyly, anal atresia and laryngeal cleft. Although OA/TOF are only occasionally part of the syndrome, severe foregut anomalies reported in *Gli2/Gli3* knockout mice imply an important role for these genes in foregut development (Motoyama *et al.*, 1998). OA/TOF as also reported as part of Opitz G syndrome,

associated with mental retardation and agenesis of the corpus callosum and mutation of the *MID1* gene (De Falco *et al.*, 2003). This gene is involved in the establishment of the right-left axis during chick development and has been shown to be positively regulated by *Bmp4* and negatively regulated by *Shh* during this process (Granata and Quaderi, 2003).

Gastrointestinal malformation including duodenal atresia, anorectal malformation and OA/TOF were found in 14% of patients with Fanconi Anemia due to mutation in *FANCA, FANCB, FANCC, FANCD1, FANCD2* and *FANCG* genes causing the disease (Auerbach, 2009).

Deletions of several chromosomal loci were also reported in some cases of OA/TOF (Digilio *et al.*, 1999; Felix *et al.*, 2007b; Puusepp *et al.*, 2009; Stankiewicz *et al.*, 2009; Walsh *et al.*, 2001). Some of the deleted loci include important genes that cause the pathogenesis of OA/TOF like phenotypes in mutant mice. The 17q21.3-q24.2 region includes the *Noggin* gene (*NOG*), known to cause OA/TOF when inactivated in mice(Felix *et al.*, 2007b; Que *et al.*, 2006), the *TBX4* gene involved in proper foregut formation in chick (Felix *et al.*, 2007b; Sakiyama et al., 2003) and the *RARα* gene known from mutant mice to be involved in foregut development (Mendelsohn *et al.*, 1994). The 16q24.1 locus includes the *FOXF1* gene and haploinsufficiency of the *Foxf1* in mouse embryos leads to OA/TOF (Mahlapuu *et al.*, 2001; Stankiewicz *et al.*, 2009).

Use of the mutagen ENU (N-ethyl-N-nitrosurea) to delete exon 1 of the Proprotein convertase subtilisin/kexin type 5 (*Pcsk5*) gene in mouse was recently reported to recapitulate many

aspects of VACTERL association malformations (Szumska *et al.*, 2008). All of the mutant mice had abnormal tracheoesophageal separation and resulted in abnormal expression of several *Hox* genes. In human patients the *PCSK5* mutation was found in association with VACTERL (Szumska *et al.*, 2008).

OA/TOF may occur as an isolated anomaly, it may be part of a complex of congenital defects or it may develop within the context of a known syndrome or association defects. Genetic factors are most likely to play a role in the etiology of OA/TOF in the last two groups (Felix *et al.*, 2007b). While a number of genetic lesions have been assocaited with individual incidences of human OA/TOF, no common genetic basis has been found indicating that the condition may result from altering any of several complex pathways at multiple points.

1.4 Adriamycin rat/mouse models of OA/TOF

In 1978 Adriamycin, a chemotherapy agent, was found through teratogenic studies to cause birth defects in rats that resemble the VACTERL anomalies, along with other gastrointestinal atresias (Thompson *et al.*, 1978). Adriamycin is an antibiotic of the anthracycline group commonly used for treatment of cancers such as lymphomas, leukemias, neuroblastoma and breast cancer. It enters the nucleus, intercalates into DNA (causes DNA adducts) and causes protein associated single and double strand DNA breaks (Cullinane *et al.*, 1994). It was suggested that the major mechanism of adriamycin involves formation of interstrand cross-links with DNA, interfering with DNA replication and transcription, through inhibiting nucleic

acid synthesis (Cullinane *et al.*, 2000; Meriwether and Bachur, 1972). The direct action of adriamycin in causing the defects were not known, however, the potential of this teratogen to create a reproducible model in which to study the pathogenesis of these birth defects was realised in 1996 (Diez-Pardo *et al.*, 1996). The first step in creating the model was to optimise the dose of adriamycin, and the time frame for exposure to yield reproducible malformations, i.e. to produce a response curve between adriamycin dosage and birth defects (Orford and Cass, 1999; Qi *et al.*, 1996). Given that the mouse is the developmental biologists mammal of choice, providing greater availability of molecular tools and techniques, and transferable knowledge from mutant mice, adriamycin treated mouse models displaying OA/TOF were developed and was first described by Ioannides et al (Ioannides *et al.*, 2002) by administering a dose of 4mg/kg of Adrimycin to pregnant mice on days E7.5 and 8.5. This gave rise to a tracheo-oesophageal malformation in 47% of the fetuses. The tracheo-oesophageal malformation was a complete laryngotracheo-oesophageal cleft and the occurrence of oesophageal atresia was found to be rare. There was no description of the occurrence of any of the other VACTERL defects. Initial experience of the treatment regime described by Ioannides *et al* (Ioannides *et al.*, 2002) in the host group, gave rise to a very low rate of anomalies, with no tracheo-oesophageal malformations. Using the original protocol for the Adriamycin Mouse Model (AMM) as guidance, a dose response analysis of the teratogenicity of adriamycin in the mouse was carried out (Dawrant *et al.*, 2007a). This established that administering a dose of 6mg/kg of adriamycin on days E7 and 8 produces reproducible abnormalities similar to those described in the Adriamycin Rat Model (ARM) (Dawrant *et al.*, 2007a). On average, 43% of fetuses per litter had 3 or more VACTERL anomalies (including tracheo-oesophageal malformation in 29% of fetuses per litter) examined at E18. Adriamycin

was found to produce a spectrum of tracheo-oesophageal malformations: upper pouch oesophageal atresia, upper pouch oesophageal atresia with partial cleft larynx, complete laryngotracheo-oesophageal cleft, and tracheal agenesis. All of the fetuses with a tracheo-oesophageal malformation had a tracheo-oesophageal fistula. The spectrum of tracheo-oesophageal malformations produced in AMM were close to that seen in human (Dawrant *et al.*, 2007a). A histological study of the critical period of organogenesis of the tracheo-oesophageal malformations from day 9-13 was also carried out, confirming that many of the observations made in the ARM apply to the mouse (Dawrant *et al.*, 2007a). Similarity of the foregut malformations produced in AMM to that seen in human and easily reproducible method for range of congenital foregut anomalies provided great opportunity for further studying the embryology and molecular biology using this model. While certain knock-out mouse models show some of the anomalies see in OA/TOF, no single model reproduces the spectrum of OA/TOF malformations.

Initial studies on the development of OA/TOF in both the rat and mouse models focused on the mechanisms whereby the oesophagus becomes atretic. It was shown, in transverse histological sections through the foregut, that the fistula between the respiratory tract and the stomach was respiratory in origin, lined with ciliated respiartory epithelium emerging from the bifurcation of the trachea or from one of the main bronchii (Crisera *et al.*, 1999; Merei *et al.*, 1997) and the cells expressed the respiratory marker *Nkx2.1* (Crisera *et al.*, 2000a). The origin of the fistula was further elucidated in another study which confirmed neural and neuropeptide abnormalities in the distal oesophagus of adriamycin treated rats (Cheng *et al.*, 1997; Qi *et al.*, 1997). This could explain the oesophageal dysmotility found in some human patients after

surgery (Crisera *et al.*, 1999; Crisera *et al.*, 2000a; Possogel *et al.*, 1998). Although *Nkx2.1* positive, the fistula did not develop branches but was connected to the stomach (Crisera *et al.*, 2000a). This was addressed in another study where the *Fgf* signalling pathway was explored in the context of epithelial-mesenchymal signalling involved in the formation of TOF (Crisera *et al.*, 2000b). These authors found that respiratory epithelium and mesenchyme around the lung buds and fistula in adriamycin exposed embryos had a different capability to respond to signalling molecules *Fgf10* and *Fgf7*. The lung and fistula epithelium of the adrimaycin treated embryos cultured in the presence of *Fgf10* or *Fgf7* did not branch. Both *Fgf10* and *Fgf7* exlusively bind and signal through *Fgfr-IIIb* in the epithelium, therefore the authors suggested that absence or mutation of *Fgfr-IIIb* may affect branching morphogenesis in adriamycin treated embryos. Moreover normal lung epithelium didn't branch when cultured with the mesenchyme surrounding the fistula from the adriamycin exposed embryo suggesting that it must either actively inhibit branching or it may lack a critical branching morphogen (Crisera *et al.*, 2000b).

Recently it was found that a fistula arising from the dorsal part of the foregut is negative for *Nkx2.1* and a gradual extension of *Nkx2.1* expression into the fistula was suggested as a secondary and adaptive event converting the initially *Nkx2.1* negative trifurcation branch at E11.5 into the positive *Nkx2.1* fistula from E13.5 (Ioannides *et al.*, 2010).

One of the earliest and most striking features of the rodent models is the abnormality seen to occur in one of the early embryonic structures, the notochord. Many groups, including the present work, have reported that in the adriamycin model the notochord develops abnormal branches

extending toward the foregut, speculated to be a result of delayed separation from the endoderm (Gillick *et al.*, 2002; Gillick *et al.*, 2003; Williams *et al.*, 2001). Abnormal notochord branching was found in the AMM from day 9.5/10 (Dawrant *et al.*, 2007b). However abnormal notochord branches were not always found in embryos of later gestational age. On day 9.5 when the first evidence of failure of notochordal separation from the foregut was seen in histological sections, there was no indication of whether the foregut is going to maldevelop (Dawrant *et al.*, 2007b). In later stage embryos when there was evidence of abnormal tracheo-oesophageal development, the notochord and foregut have moved away from each other craniocaudally and dorsoventrally and the notochord was also undergoing a process of resorption (Possoegel *et a*l., 1999). Therefore, it remained unclear whether the notochord and foregut abnormalities have a cause and effect relationship or merely reflect two expressions of a profound disturbance of embryonic para-axial organisation (Possoegel *et al.*, 1999).

It was suggested before that the ventrally displaced notochord may be a source of ectopic *Shh* signalling and may have an effect on the distribution of *Shh* around the foregut endoderm (Orford *et al.*, 2001). Using whole mount in situ hybridization the host group showed the distribution of *Shh* transcripts to be restricted to the ventral endoderm of the laryngotracheal groove and lung primordia from E9 (Sato *et al.*, 2008). Orford *et al.* reported uniform distrubution of *Shh* transcripts around foregut endoderm in ARM embryos at the level of tracheal separation (Orford *et al.*, 2001). The loss of a normal ventral-to-dorsal shift in foregut endoderm expression of *Shh* was also reported in adriamycin exposed embryos by other groups (Arsic *et al.*, 2004; Ioannides *et al.*, 2003), although some of the treated embryos preserved the ventral pattern of *Shh* distribution (Arsic *et al.*, 2004). Despite *Shh* disruption, the patched receptor (*Ptch*) gene

expression pattern was not altered in the neural tube and mesenchyme surrounding the foregut (Orford *et al.*, 2001). Using immunoblotting and the ELISA quantification method, Arsic *et al.* reported initial high levels of *Shh* protein in the foregut endoderm of normal rat embryos which decreased with time as the embryos approach term (Arsić *et al.*, 2003). In the embryos exposed to adriamycin, *Shh* protein level remained low from the early stage (E10) and did not change with time in comaparison to control embryos. Authors suggested that adriamycin may affect the expression of this protein during early foregut development. The fistula tract extracted from the ARM and human neonates with OA/TOF showed reduced levels of mRNA for *Gli2*, which is a direct target gene of the *Shh* pathway, implicating the *Shh* pathway in the development of OA/TOF malformations (Spilde *et al.*, 2003a; Spilde *et al.*, 2003b).

Molecular aspects of foregut separation were also investigated in AMM. It was found that failure of foregut septation is not associated with generalised loss of dorso-ventral gene expression patterning in the foregut (Ioannides et al., 2010). Both *Nkx2.1* and *Sox2* genes showed appropriate patterning in adriamycin-induced OA/TOF malformed embryos suggesting that the balance between respiratory and gatrointestinal specification in the foregut is intact even though these two elements failed to separate (Ioannides *et al.*, 2002; Ioannides *et al.*, 2010).

The foregut defects in AMM were compared with the phenotypes of knock out mice for *Shh* and *Nkx2.1* that exibit foregut malformatios resembling human OA/TOF (Ioannides *et al.*, 2010). Interestingly the morphological and molecular features of abnormal foregut development were similar.

While analysis of abnormalities in the adriamysin treated mouse model has provided some insight into the etiology of OA/TOF, study to date has been limited either to describing abnormal morphology of the embryo in sections from a relatively small number of specimens, or single marker/candidate gene expression. Therefore, mechanisms that can lead to such malformations in the model are only partialy described.

1.5 Objectives of the thesis

Investigating the process of faulty foregut development and separation of the trachea from the oesophagus in AMM leading to formation of OA/TOF is important in order to elucidate the normal mechanisms that are impacted, which in turn could reveal the developmental processes disturbed in cases of human OA/TOF. The objective of this thesis was to explore the morphological and molecular alterations in the AMM using a combination of 3D imaging OPT and molecular probes. Additionally, this thesis aimed to address the hypothesis that anomalies observed in the AMM could be a result of fundamental defects in the notochord leading to abnormal delamination and ectopic placement of this potent signalling tissue during crucial stages of foregut development. The work presented in this thesis set out to further our understanding of the basis of the lesions that occur in an important mouse model of OA/TOF congenital abnormalities. The specific objectives of this thesis can be divided into three broad sets of aims:

- *To visualise and describe early foregut development and foregut malformations seen in AMM using Optical Projection Tomography, a 3D imaging technique designed for embryonic specimens.* This work tests the hypothesis that there is a causative link between notochord and foregut malformations seen in the AMM. This was designed to provide a detailed 3D dataset of abnormal morphogenesis and tissue differentiation in this model of tracheo-oesophageal malformations. The 3D approach using OPT gives more complete analysis of each individual embryo than was previously possible (Chapter 3) allowing a more comprehensive overview of the variety of malformations and any associations between different abnormalities.

- *To investigate the temperospatial expression of key candidate genes implicated in tracheaoesophageal development in detail using OPT during the critical period of separation of the trachea and oesophagus in normal and treated embryos and to relate any changes in gene expression patterns found to the abnormal morphology and developmental events observed in this model.* This work tests the hypothesis that specific regulatory genes are impacted in the AMM. Candidate genes were selected based on reported observations made in mutant mice where inactivation or activation of the candidate genes result in lack of separation of the foregut. The possible involvement of candidate regulatory genes in the abnormalities of the foregut was explored by comparing expression patterns in control and adriamycin treated embryos. Prior to this study, no detailed 3D analysis and comparison of expression of these genes was carried out in the mouse model (Chapter 3 and 4).

- *To investigate the structure of the notochord as a possible primary target of Adriamycin treatment.* This was designed to addresse the hypothesis that anomalies observed in AMM could be the result of defects in cellular organization of the notochord as an important organising tissue. This work therefore focused on the early stages following treatment, examining the cellular architecture and position of the notochord with respect to the foregut endoderm in normal and adriamycin treated mouse embryos. The early events in notochord delamination in control and treated embryos were examined using confocal miscroscopy and specific markers of ECM to explore the cause of the abnormal positioning and branching seen previously in the AMM (Chapter 5).

Chapter 2

Materials and Methods

2.1 Embryo collection and fixation

Male and female CBA/Ca mice (Harlan UK, Bicester, England), housed in the Biomedical Facility UCD, were accurately time-mated over a four-hour period starting at 8am. Finding a vaginal plug at the end of this mating period was taken to be the start of gestatation and was designated the start of day 0. Pregnant dams received two intraperitoneal injections, 24 hours apart, on days 7 and 8 of gestation at 10am. The Adriamycin treated dams received a dose of 6mg/kg of Adiamycin (Doxorubicin, EBEWE Pharma GmbH. Nfg.KG, A-4866 Unterach, Austria) in 0.9% Sodium Chloride. The control dams received an equivalent volume of 0.9% Sodium Chloride. The Adriamycin was prepared to a concentration of 0.3mg/ml just before the first injection and was stored in the dark at 2-8°C until the second injection was given. This means that there was a standard weight determined volume for the intraperitoneal injection given to the mice at 0.02ml/g. The dams were then humanely killed by swift cervical dislocation at 11am on embryonic days (E) 9 through 13. The uteri were dissected from the

mice, placed in ice cold PBS, and brought on ice to the Developmental Laboratory in Trinity College, where the embryos were removed from the uteri using RNase-free equipment, fixed in 4% paraformaldehyde in PBS overnight and dehydratated through a graded series of methanol/PBT (0.1% Triton X100 in PBS; 25%, 50%, 75% methanol; 1x10 minute) washes, followed by 2 x 10 minutes in 100% methanol and stored according to embryonic day in separate tubes at -20°C until needed.

All experiments were carried out in compliance with current European Union regulations for animal investigation (ED86/609/EC), with prior ethical approval under licence no. B100/4106 from the Department of Health, Ireland.

2.2 *In Situ* Hybridisation

2.2.1 Probe preparation

Plasmids carrying cDNA clones of candidate genes were obtained from a variety of sources (Table 2.1). To amplify and purify the plasmids, chemically competent *E. coli* (XL2-Blue, Ultracompetent Cells, Stratagene) were transformed by the standard heat-shock method (as recommended) and grown on Luria Bertoni (LB) agar plates (1% Tryptone, 0.5% Yeast Extract, 1% NaCl, 1.5% Agar, in dH_2O) supplemented with 100µg/ml ampicillan (Sigma-Aldrich, Germany). Details of the cDNA clones used to generate RNA probes are summarized in Table 2.1.

Plasmid DNA was extracted and purified from *E. coli* cultures expanded in LB broth (1% Tryptone, 0.5% Yeast Extract, 1% NaCl, in dH_2O) using a Maxiprep kit (Qiagen, UK). Plasmid DNA was sequenced to verify identity of the cDNA insert using vector primer sites flanking the insert. Sequences were analysed using tools provided by the National Centre for Biotechnology Information (http://www.ncbi.nlm.nih.gov). Plasmid DNA was linearised with appropriate restriction enzymes to produce template for in vitro transcription. Antisense and sense digoxigenin (dig)–labelled RNA probes were generated, according to vector and insert orientation in each case, from 1 µg linearised plasmid DNA using T7, T3 or SP6 promoter sites, as appropriate in each case (all reaction compononets from Roche, Germany) in a 20µl reaction volume at 37°C for 2 hours. RNA production and integrity was checked by running 1µl of the transcription reaction on a 1% agarose gel. In the case of sufficient RNA production, DNA template was degraded by incubation with 1µl RNase free DNase (Roche, Germany) for fifteen minutes at 37°C. The *in vitro* transcribed RNA was purified on G25 columns (Amersham bioscinces, USA) as per manufacturer's instructions, quantified by spectrophotometry absorbance at 260nm (Eppendorf Biophometer) and stored at -20°C in an equal volume of hybridization mix. Hybridisation buffer contained 2% blocking reagent (Roche, Germany), 50% formamide, 5 X saline-sodium citrate buffer (SCC), 0.5% 3-[(3-Cholamidopropyl) dimethylammonio] -2-hydroxy-1-propanesulfonate (CHAPS), 500ug/ml Heparin, 1 ug/ml Yeast RNA, 0.1% Tween 20 and 5mM ethylenediamine tetraacetic acid (EDTA).

Table 2.1: Summary of cDNA clones used to generate RNA in situ probes

Gene	Extent of Probe on Genbank Sequence	Source
Shh	Nucleotide 452 to 1097 on NM_009170.3	Prof. L. Lundh
Foxf1	Nucleotide 342 to 742 on NM_010426.1	Prof. L. Lundh
Nkx2.1	Nucleotide 65 to 563 on NM_009385.3	Dr L. Magno
Sox2	Nucleotide 31 to 778 on NM_011443.3	Prof. R. Lovell-Badge
Noggin	Nucleotides 291 to 1285 on NM_008711.2	Dr Richard Harland
BMP4	Nucleotides 6 to 1811 on NM_007554.2	Prof. Si Jen Lee
Wnt2	Nucleotides 35 to 1510 on NM_023653.4	Dr P. Murphy
Wnt5a	Nucleotides 576 to 2714 on NM_009524.2	Dr P. Murphy
Wnt7	Nucleotide 93 to 1581 on NM_009528.2	Dr P. Murphy
Tbx4	Nucleotide 526 to 1821 on NM_172798.1	Dr S.Bellusci
Fgf10	Nucleotide 686 to 1315 on NM_008002.4	Dr R. Kelly
RARα	Nucleotide 22 to 1160 on NM_001177303.1	Dr P. Dolle
RARβ	Nucleotide 63 to 1150 on NM_011243.1	Dr P. Dolle
Fgfr2b	Nucleotides 1816 to 1966 on NM_201601.2	Dr R. Kelly
Gli1	Nucleotides 967 to 2673 on NM_010296.2	Dr A. L. Joyner
Gli2	Nucleotides 1114 to 1943 on NM_001081125.1	Dr A.L. Joyner
Gli3	Nucleotides 384 to 2616 on NM_008130.2	Dr A.L. Joyner

2.2.2 Fixation and pre-treatment of embryos

For testing probes and preliminary analysis of expression patterns in the foregut and lung bud regions, whole mouse embryos (fixed and stored as per Section 2.1) at E10, E11, E12 and E13 were used. All embryos for wholemount *in situ* hybridisation (normal, control, adriamycin

treated) were processed as follows. Embryos were rehydrated through a graded series of methanol/PBT solutions (75%, 50%, 25% methanol; 1x10 minutes) at 4°C and subsequently washed 2x10 minutes in PBT. Embryos were then selected under an Olympus SZK-ILLD200 light microscope in ice cold PBT and dissected from any remaining membranes with RNase-free forceps. Specimens were then pierced through the eye and hindbrain with an RNase free needle to prevent the trapping of the probe in the brain vesicles. Embryos from E12 were dissected to include only the trunk region from the first branchial arch to the base of the liver to ensure penetration of RNA probes and antibodies. Embryos were then permeabilised by treatment with 10µg/ml proteinase K (Roche) in PBT, placed horizontally in 30ml tubes at room temperature with the mixture and spaced so as to ensure even digestion of the tissues., The length of digestion time depended on the age of the embryos (Table 2.2). Embryos were then refixed in 0.2% glutaraldehyde/ 4% PFA over 20 minutes and washed 3 times quickly in PBT at room temperature. Embryos were subsequently equilibrated with hybridisation buffer and then prehybridised with hybridisation buffer at 65°C overnight.

Table 2.2: Length of time embryos were permeabilised in 10µg/ml Preteinase K

Embryo age: Embryonic day (E)	Time required for permeabilisation
E9	10 minutes
E10	15 minutes
E11	60 minutes
E12	90 minutes
E13	120 minutes

2.2.3 Hybridisation, washing and detection of probe in whole mount preparations

The appropriate amounts of antisense and sense RNA probes were denatured at 80°C for 3 minutes and then diluted to a final concentration of 1µg/ml probe in hybridisation buffer. Embryos were incubated at 65°C in prewarmed hybridization buffer containing 1µg/ml digoxigenin-labeled riboprobes overnight. After hybridization the unhybridised probe was removed and stored at -20°C for reuse up to 3 times. Embryos underwent post-hybridization washes at 65°C, 1x5 minutes in posthybridisation wash solution (PWS) (50% formamide / 5 x SSC (Saline Sodium Citrate, Sigma-Aldrich) / 0.5% CHAPS (Sigma-Aldrich)), then three serial 30 minutes washes in decreasing concentrations of formamide, SSC and CHAPS (75% PWS/ 25% 2xSSC / 0.1 % CHAPS, 50% PWS/50% 2xSSC / 0.1 % CHAPS, 25% PWS/75% 2xSSC / 0.1 % CHAPS), culminating in 2x30 minutes wash in 2x SSC / 0.1% CHAPS and 2x30 minutes in 0.2x SSC / 0.1% CHAPS and 2x10 minutes in TNT (100 mM Tris, pH 7.5, 150 mM NaCl, 0.1% Triton X-100) at RT. After washing, the embryos were blocked in 10% goat serum overnight at 4°C followed by incubation with 1/3000 dilution of anti-digoxigenin Fab fragments conjucted with alkaline phosphatase (# 11 093 274 910, Roche, Germany) overnight at 4°C on a Stuart Scientific SSM4 mini see-saw rocker. The embryos were than washed 2 x 5 minutes and 4 x 1 hour in TNT with rocking at room temperature, then continued washing in TNT overnight at 4°C with rocking to remove unbound antibody. Following this the embryos were transferred to glass jars and washed 3 x 15 minutes in NMT (0.1M Tris ph9.5 / 0.1M NaCl / 0.05M $MgCl_2$). The chromogenic reaction was carried out in NMT containing 450µg/ml 4-nitro blue tetrazolium chloride (NBT; Roche Germany) and 175µg/ml 5-bromo-4-chloro-3-indolyl-phosphate (BCIP, Roche Germany) developed in the

dark at room temperature with rocking. The staining was monitored and once a strong signal had been produced (1-6 hours) the reaction was stopped by washing several times in PBT. The embryos were than fixed overnight in 4% PFA at 4°C. The stained embryos were examined and photographed under a microscope (Olympus SZX12 with attached camera) using normal light.

2.3 Immunolocalisation

Immunolocalisation of the endoderm marker HNF3β was used together with *in situ* hybridisation to visualize the notochord and foregut clearly, so that differences in morphology of the adriamycin treated embryos as well as the differences in gene expression could be analysed.

2.3.1 Incubation with Primary Antibody

Embryos were prepared for *in situ* hybridization, as per section 2.1 and the protocol for *in situ* hybridization was unchanged from section 2.2 until the incubation with 1/3000 dilution of anti-digoxigenin Fab fragments conjucted with alkaline phosphatase (Roche, Germany). When double staining was performed, HNF3β primary antibody (07-633 Upstate Cell Signaling Solution, Lake Placid, NY) was diluted 1/500 in 10% goat serum in TNT and exposed to the embryos together with anti-DIG for at least 4 days at 4°C with rocking. Embryos then were washed six times in TNT at room temperature while on a Stuart Scientific GYRO-ROCKER®

STR9 with 30 minute intervals between them, so as to remove any unbound antibody and then kept in TNT at 4°C overnight on the mini see-saw rocker.

2.3.2 Incubation with Secondary Antibody

The next morning, the embryos were incubated with Cy3 conjugated Goat anti-rabbit IgG (111-165-144 Jackson Immno Research) at 1/200 dilution in 10% goat serum in TNT overnight at 4°C. The specimens were then washed four times at room temperature in TNT on the rocker with 30 minute intervals, so as to remove any unbound secondary antibody. The subsequent NMT washes and NBT/BCIP staining protocol was unchanged from section 2.2.3. The stained embryos were than fixed overnight in 4% PFA/ PBS at 4°C, rinsed in PBS, examined under a microscope (Olympus SZX12 with attached camera) using normal and UV light and photographed. The primary and secondary antibodies used for immunohistochemistry throughout the thesis are summarized in Table 2.3.

Table 2.3: Summary of antibodies used in immunodetection

Antibody name	Supplier	Cat #	Dilution	Application
HNF3β rabbit polyclonal IgG	Upstate Cell Signaling	07-633	1:500	wholemount
Brochyury goat polyclonal IgG	R&D Systems	AF2085	1:200	section
E-catherin rat monoclonal IgG	Invitrogen	13-1900	1:200	section
Laminin rabbit polyclonal IgG	Sigma-Aldrich	L9393	1:50	section
Alexa Fluor 594 donkey anti-rat IgG	Invitrogen	A21209	1:200	section
Alexa Fluor 594 donkey anti-rabbit IgG	Invitrogen	A21207	1:200	section
Alexa Fluor 488 donkey anti-goat IgG	Invitrogen	A11055	1:200	section
Cy3 goat anti-rabbit IgG	Jackson ImmunoResearch	111-165-144	1:200	wholemount
DAPI	Invitrogen	P36931		section

2.4 Preparation and imaging of whole embryos using OPT

In situ hybridized and/or HNF3β immunostained embryos were rinsed briefly in water, and embedded in 1% low melting point agarose (Sigma-Aldrich, Germany) in dH_2O. Once set, the block of agarose was cut in the desired orientation for scanning and affixed to a metal mount. Specimens were then dehydrated overnight in 100% methanol, and cleared in BA:BB (1:2 benzyl alcohol : benzyl benzoate) for at least 5 hours. OPT works by measuring the amount of light transmitted (visible) or emitted (fluorescent) by an object when light is shone upon it (Sharpe, 2003; Sharpe et al., 2002). Specimens were scanned in a prototype OPT scanner built at the MRC Human Genetics Unit, Western General Hospital, Edinburgh, installed at Trinity College Dublin. Embryo blocks were inserted into the scanner and rotated through 360° and a series of 400 images were taken at different angles through a full rotation. At least two scans were performed for each specimen using UV light together with either a TXR filter (560/40nm excitation, 610LP nm emission), or GFP1 filter (425/60nm excitation, 480 nm emission) and, for colorimetric staining, the data were imaged using visible light together with a 700nm filter for very intense staining. Autofluoroesence from the tissue was captured to reconstruct embryo morphology. The raw data consisting of 400 images from each of the scans were loaded onto a Linux workstation and reconstructed using a set of programs provided by the Edinburgh Mouse Atlas Project (EMAP) (http://www.emouseatlas.org/emap/home.html). These programs used a back propagation algorithm to integrate the images and produce a 3D voxel based representation of the spacimen. This reconstruction could then be visualised as a 3D volume representation, a surface representation or as a number of virtual sections through any orientation using custom made software, MAPaint and MA3Dview provided by EMAP.

2.4.1 Analysis of 3D digital data

Surface rendering of the 3D data was carried out using a suite of Visualization Toolkit (VTK) scripts and software. This recreated the surface of the embryos, so that morphological characteristics such as the shape of the branchial arches or limbs could be used to attribute each embryo to a Theiler Stage (Theiler, 1989) to compare development rate in control and treated embryos and for more accurate comparisons. Staging allowed comparison of stage-matched embryos, in addition to embryos collected on the same embryonic day. Staging for each embryos was given by two independent investigators to avoid bias. 3D reconstructions of control and treated embryos following HNF3 β immunolocalisation and OPT scaning were analysed either by viewing 3D representations of HNF3 β stained tissue domains (using visualisation tool kit (vtk) software), or by virtually cutting sections through the 3D reconstructions to view the internal morphology of the developing tissues and staining patterns. Virtual sections through the 3D reconstructions in the appropriate planes which captured the morphological characteristics of the embryos and gene expression were selected and scored and/or measured. These sections from two different channels (Texas Red and Visible) were then merged with the IPLab software, in order to see the relationship between the expression patterns and the morphology.

2.4.2 Analysis of gene expression patterns

At least 5 and up to 8 specimens per stage per gene from each of control and adriamycin treated groups were assayed and all were subsequently analysed by OPT. Each embryo was

scanned using OPT to obtain 3D representations of the gene expression pattern and foregut morphology of the whole specimen. At least two scans were performed for each specimen using UV light with the TXR filter (560/40nm excitation, 610 nm emission) to visualise fluorescent staining (either autoflouresence from the tissue to view general morphology or immunoflouresence when embryos were stained for HNF3β localization) and visible light for colourometric stainining. These two scans, recorded on different channels, were reconstructed on a LINUX workstation using pogrammes provided by the EMAP. The 3D reconstructions were analysed in terms of gene expression pattern and morphology viewing virtual sections through any orientation using custom made software (MAPaint, MA3Dview). The morphology of the embryo were identified using images from the Atlas of Mouse Development (Kaufman, 1992). Gene expression patterns were compared visually between control and adriamycin treated groups, separately for each embryonic day from E9 to E13. Expression of Fgf10 was investigated from E10 to E13. All other genes were investigated from E10 to E12. The most representative sections were then edited as a .tif file for both channels and were merged using IPLAB software, to visualise gene expression together with morphological insight from the HNF3β marker.

2.5 Embryo collection, fixation and processing for cryosectioning

Male and female CBA/Ca mice (Harlan UK, Bicester, England) were mated and treated as per section 2.1. The dams were then humanely killed by swift cervical dislocation at embryonic days 9 or 10 at four hours intervals from 7am to produce embryos at a range of developmental

stages at each embryonic day. The uteri were dissected from the mice, placed in ice cold PBS and removed from the uteri, fixed in 4% paraformaldehyd in PBS for an hour and washed 2x5 minutes in PBS. Embryos were then transferred to a petri dish containing PBS and were observed under an Olympus SZX-ILLD200 stereo microscope at room temperature. The somites of each individual control and adriamycin treated embryo were counted and individual specimens were designated to 'stage groups' based on somite number (6-9, 14-18, 20-22, 24-28 somites) (Table 2.4) to facilitate comparison between control and adriamycin-treated embryos during precisely defined developmental periods. In total 46 treated embryos and 30 control embryos were analysed. Control embryos were collected from 12 independent litters and treated embryos form 16 independent litters. The embryos were then embedded in 1.5% agarose (Sigma-Aldrich, Germany), 30% sucrose solution in PBS, oriented appropriately and the solidified blocks trimmed with a straightedge blade so that when mounted in the cryostat, transverse sections could be cut. The blocks were then placed in 50ml tubes filled with 30% sucrose solution in PBS and left to equilibrate at 4°C overnight. On the next morning the agarose blocks were placed on metal foil on a dry ice bath (dry ice in ethanol) for slow freezing, wrapped and transferred to 50ml tubes according to number of somites and stored at -20°C until needed.

Table 2.4: Staging of control and adriamycin treated embryos into designated groups based on somite number.

Group	Somite Number
1	6-9
2	14-18
3	20-22
4	24-28

2.5.1 Cryostat Sectioning

Each embryo block was mounted using OCT freezing compound (Tissue-Tek® 4583 O.C.T™ Compound) on the chuck of the cryostat (Bright OTF, 5015) to obtain transverse sections from anterior to posterior. Serial 30μm sections of embryos were trimmed through the craniofacial region, monitored under a Olympus SZX-ILLD200 stereo microscope and discarded. The appropriate planes through the embryo were identified using images from the Atlas of Mouse Development (Kaufman, 1992). Once the anterior foregut endoderm had been reached, adjacent serial sections were cut and collected on three different slides (section 1 on slide 1, section 2 on slide 2 etc.) designated for visualising different sets of markers; E-cadherin & Brachyury, Laminin & Brachyury and F-actin & Brachyury. Once sections reached the hepatic process the sectioning procedure was ceased. Slides were stored at -20°C to preserve the tissue and to prevent thawing of sections until ready for immunohistochemistry.

2.6 Immunohistochemistry

Tissue sections were removed from the freezer and left to thaw at room temperature to ensure adhesion of the tissue to the slides. Sections underwent three one-hour washes in PBS with 0.5% Triton X-100 (Sigma-Aldrich) and 0.1% Tween 20 (Sigma-Aldrich) (PBTT), rocking on a Stuart Scientific GYRO-ROCKER STR9 at room temperature in a slide box wrapped in tinfoil. Sections were blocked in blocking solution contained 10% normal sheep serum in PBTT for one hour at room temperature in a humid chamber (each slide flooded with solution

(approx. 100µl), supported on struts in a closed box containing moist tissues). Slides were then flooded with the appropriate combination of primary antibodies according to the markers being assayed in each case (Table 2.3) in blocking solution (5% sheep serum in PBTT) and left overnight at 4° in the humid chamber. The combinations of antibodies used were E-cadherin (Invitrogen 13-1900) and Brachyury (Santa Cruz, SC 17743), a marker of notochord cells (Wilkinson et al., 1990) and Laminin (Sigma-Aldrich, L9393) and Brachyury. The antibodies used for immunohistochemistry throughout the thesis are detailed in Table 2.3. Following incubation in primary antibody, three one-hour washes in PBTT were carried out, followed by another one hour wash in 10% serum in blocking solution at room temperature. The secondary antibodies Alexa Fluor 594 donkey anti-rat (Invitrogen, A21209) for E-cadherin detection, Alexa Fluor 594 donkey anti-rabbit (Invitrogen, A21207) for Laminin detection, and Alexa Fluor 488 donkey anti-goat (Invitrogen, A11055) for Brachyury detection were applied in a 1/200 dilution overnight in a humid chamber in 5% serum in PBTT. Sections then underwent three one-hour washes in PBTT at room temperature. They were then mounted under cover slips with ProLong® Gold Anti-Fade Reagent containing DAPI counterstain (Invitrogen, P-36931) and left to dry in a dark cupboard for 48 hours.

2.7 Imaging using Laser Scanning Confocal Microscopy

Once the mounted slides were dry, they were kept covered in a plastic slide box (Fisherbrand, FB70883) and were brought to the Zen Zeiss LSM 700 confocal microscope in The National Children's Research Centre, Our Lady's Children's Hospital, Dublin. Each slide was scanned

using the Zen 2009 Light Edition™ software. Selective sections were scanned using the 40x lens (400x magnification) to capture the foregut, the notochord and the neural tube, and the 60x lens (600x magnification) was used to capture the notochord alone. Images were then saved as .lsm files on an external hard drive to be further edited and analysed.

2.7.1 Image analysis

Images collected from all groups of control and treated embryos were opened using Zen 2009 Light Edition™ software and edited. Sections where a Z-stack had been collected were analysed and the best single-plane image was chosen. Brightness and contrast were adjusted to produce the clearest picture without distorting antibody detection. Images were saved as single-plane files in .tif format to be used with other editing software.

2.7.2 Overview of specimens investigated

Within each detection group, images were grouped based on somite number (Table 2.5). Control and adriamycin treated specimens were analysed and details were noted with regards to notochord position and shape and antibody localisation. Different scoring criteria were devised to record features of the notochord.

Table 2.5 Number of embryo specimens analysed for each of the sets of markers of the extra-cellular matrix, according to stage group (number of somites).

Group	Laminin & Brachyury	E-cadherin & Brachyury
6-9 Somites	4 Control 5 Adriamycin-treated	4 Control 7 Adriamycin-treated
14-18 Somites	3 Control 5 Adriamycin-treated	3 Control 7 Adriamycin-treated
20-22 Somites	4 Control 7 Adriamycin-treated	5 Control 4 Adriamycin-treated
24-28 Somites	4 Control 6 Adriamycin-treated	3 Control 5 Adriamycin-treated

2.7.3 Scoring criteria used in the investigation of notochord position

The position of the notochord with respect to the foregut and the neural tube was recorded in transverse sections of each control specimen across all stage groups. Notochord position was subdivided into five categories according to D/V position: (vc) ventral, contacting the dorsal foregut endoderm, (v) ventral, close to foregut endoderm, (m) middle between foregut and neural tube, (d) dorsal, close to the floor plate and (dc) dorsal, contacting the floor plate (section 5.2.1, Figure 5.1). Scoring the position of the notochord for each embryos was given by two independent investigators to avoid bias.

2.7.4 Scoring criteria used in the investigation of E-cadherin localisation

Inter-cellular detection of E-cadherin within the notochord was arbitrarily scored for intensity by eye ranging from 0-3 stars (*). A score of 0 indicates no E-cadherin detection, 1 indicates a low level of detection (*), 2 indicates moderate (**) while 3 indicates heavy (***) detection between the cells of the notochord (examples are shown in section 5.2.4, Figure 5.4 e-h).

Scoring for intensity of detection of E-cadherin for ech embryos was given by two independent investigators to avoid bias.

2.8 Statistical analysis

Statistical analysis of quantitative data in Chapter 3 were performed using the Mantel-Haenszel X-squared test which is designed to test the association between two dichotomus variables where one variable is outcome (delay vs not in development) and other variable is animal treatment (control vs adriamycin treatment). Statistical evaluation of the quantitative data (notochord position and E-cadherin expression) in Chapter 5 were performed using Chi squared analysis.

Both analyses were preformed using free software Rv2.10.0.

Chapter 3

Abnormal notochord branching is associated with foregut abnormalities in an Adriamycin treated Mouse Model

The data presented in this chapter were published in PLoS ONE (Hajduk *et al.*, 2011).

3.1 Introduction

Congenital malformations of the foregut are common in humans and represent a challenge to the paediatric surgeon both in terms of surgical repair and the management of long term morbidity (Tomaselli *et al.*, 2003). Oesophageal atresia (OA) encompasses a group of congenital anomalies where the oesophagus does not connect with the stomach. The most common form of the condition is OA with distal tracheo-oesophageal fistula (TOF) where affected newborn babies have an oesophagus that ends blindly and an abnormal communication, or fistula, between the trachea and the stomach (Brunner and Bokhoven, 2005; Clark, 1999; Gross, 1953; Spitz, 2007). It is one of the most life-threatening anomalies in the newborn baby. The incidence of OA with or without a fistula is reported to be 1 in 2500 to 1 in 4500 newborns (Gross, 1953; Spitz, 2007). Although a number of theories have been proposed to explain the occurrence of the malformations (Kluth, 2003; Merei and Hutson, 2002), little is known about the etiology of these defects. The high incidence of associated anomalies in OA points to a very early disturbance of the developing embryo.

The precise steps in normal development of the foregut that are disturbed in OA/TOF are unknown but some new insights are emerging from the study of animal models. The foregut develops from the embryonic endoderm that involutes early from the most anterior part of the primitive streak initially forming a sheath of cells lying ventral to the mesoderm and ectoderm germ layers (Lawson *et al.*, 1986). The anterior endoderm folds over posteriorly to form a diverticulum called the foregut pocket that pushes under the headfold while more posterior regions of the gut primordium fold laterally, as the mouse embryo turns (Wells and Melton,

1999). Initially the endoderm is in very close proximity to the notochordal plate but from about E9 the notochord delaminates from the endoderm in the mid regions of the embryo and by about E9.5 it is separated from the anterior foregut by mesenchyme, becoming more closely associated dorsally with the neural folds/neural tube (Jurand, 1974) where it is well known to contribute to dorso-ventral (DV) patterning of the developing Central Nervous System (CNS) and laterally to patterning of the somites. Signals from the notochord are also important in patterning the foregut and its associated mesenchyme ventrally (Cleaver and Krieg, 2001).

Both the respiratory and digestive anlagen arise from the foregut; the trachea forming ventrally and the oesophagus dorsally. The first morphological evidence of this is at E9.5 with the appearance of two ventrolateral bulges which subsequently elongate to form the bronchi and lung buds in conjunction with surrounding mesenchyme (Cardoso and Lu, 2006; Morrisey and Hogan, 2010). Anterior to this, the single foregut diverticulum septates laterally to separate the trachea and oesophagus (Cardoso and Lu, 2006; Morrisey and Hogan, 2010; Qi and Beasley, 2000). There is some disagreement in the literature about how the process of septation progresses. Recent work measuring the respective lengths of the undivided and divided regions of the foregut overtime indicates that septation progresses anteriorly from an initial point (Ioannides *et al.*, 2010). Although similar work from another group concluded that progressive separation is achieved through posterior elongation from the point of septation (Williams *et al.*, 2003), it is clear that separation is presaged and accompanied by differentiation of foregut cells distinguishing dorsal (e.g. *Sox2* expressing) and ventral (e.g. *Nkx2.1* expressing) aspects that will form digestive and respiratory tissues respectively

(Ioannides *et al.*, 2010; Minoo *et al.*, 1999; Que *et al.*, 2007). Development of the lung primordia progresses with extension of the bronchial stalks and stereotypic branching and budding as the bronchial and bronchiolar tubules form between approximately E11 and E16 (Maeda *et al.*, 2007).

A valuable animal model of OA and TOF was established in mice (reviewed in section 1.4). Adriamycin treatment of pregnant female mice was found to produce a spectrum of tracheo-oesophageal and notochord malformations in embryos (reviewed in section 1.4). The model has been used to facilitate research toward understanding the developmental pathogenesis of OA/TOF (Dawrant *et al.*, 2007a; Dawrant *et al.*, 2007b; Gillick *et al.*, 2008; Hajduk *et al.*, 2010a; Ioannides *et al.*, 2002; Ioannides *et al.*, 2003; Ioannides *et al.*, 2010; Que *et al.*, 2006).

A number of mouse mutants replicate aspects of OA/TOF shown in the adriamycin model indicating that complex signaling events are involved in normal foregut development and disturbed in OA/TOF. Sonic hedgehog (*Shh*) signalling is implicated since *Shh* null mutants display OA/TOF with an increase in apoptosis in the lung mesenchyme (Litingtung *et al.*, 1998). Inactivation of the *Noggin* gene ($Nog^{-/-}$) implicates *BMP* signalling since *Nog* null embryos replicate notochord branching defects and OA/TOF with associated effects on lung branching morphogenesis (Que *et al.*, 2006; Weaver *et al.*, 2003). The morphological similarity of foregut abnormalities seen on the one hand in a number of mutants with different genetic lesions and on the other produced by adriamycin treatment, indicate that common processes are being disturbed. The adriamycin mouse model, therefore may allow us to understand the mechanisms disturbed during the pathogenesis of OA/TOF.

While analysis of abnormalities in the adriamycin treated mouse model has provided some insight into the pathogenesis of OA/TOF, studies to date have been limited to partial viewing of the overall effects largely through histological sections. There is also variability in the effects that could not be fully captured. The aim of this study was to carry out a more comprehensive analysis of whole embryos using molecular markers and 3D imaging to describe the spectrum of morphological abnormalities produced by Adriamycin treatment. I used 3 dimensional (3D) imaging of whole embryos in a systematic analysis of 78 adriamycin treated and 71 control embryos across embryonic days 10 to 12 for morphological defects. OPT is a rapid technique for 3D imaging of whole biological tissue specimens recording morphology while also allowing visualization of the tissue distribution of RNA, protein or histological stains in developing organs (Alanentalo *et al.*, 2007; Roddy *et al.*, 2009; Sharpe *et al.*, 2002; Summerhurst *et al.*, 2008). In this way I use OPT together with an endoderm marker (HNF3β) to visualize foregut and lung bud morphology at critical periods of development in control and adriamycin treated embryos. I also reveal defects at a molecular level using selected markers.

In addition to revealing delayed development in treated litters, this work shows the full spectrum of abnormalities and their frequency of occurrence. The abnormalities induced correlate with the spectrum of clinical presentations in newborns with OA/TOF. In addition this work reveals a close association between abnormal notochord branching seen in the mouse model and certain foregut malformations indicating a causative link between abnormalities in these neighbouring tissues. I propose that disturbances to notochord

delamination and resulting abnormal notochordal signalling may be the mechanistic basis of certain foregut abnormalities.

3.2 Results

3.2.1 Delayed development in adriamycin treated embryos

A total of 149 embryos divided by embryonic day (E10-E12) of collection and adriamycin treated or control groups were analyzed in detail from 3D digital recordings which provide a permanent record of the morphological features in 3D that could be reanalyzed and compared from multiple perspectives. Figure 3.1B shows the external morphological features that can be viewed from a surface representation of a typical digital recording. Each embryo was staged using Theiler criteria (Theiler, 1989) from Theiler stage (TS) 14 to TS20. The appearance and shape of branchial arches, forebrain vesicles and anterior and posterior footplates were key morphological criteria used here. Examining the range of stages at each embryonic day for control embryos, it was found that the predominant stage at E10 was TS16, at E11 was TS18 and at E12 was TS20. At E10, 5% of control embryos were staged below TS16 (TS15) compared to 25% adriamycin treated embryos. At E11, 31% of control embryos were staged below TS18 (TS17) in comparison to 42% in the adriamycin treated group. At E12, 25% of control embryos were staged below TS20 (TS19) compared to 75% in the adriamycin treated group. Statistical analysis using the Mantel-Haenszel X-squared test showed a significant delay ($pvalue<0.01$) in development of the treated embryos in comparison to controls across

all investigated stages (Figure 3.1).

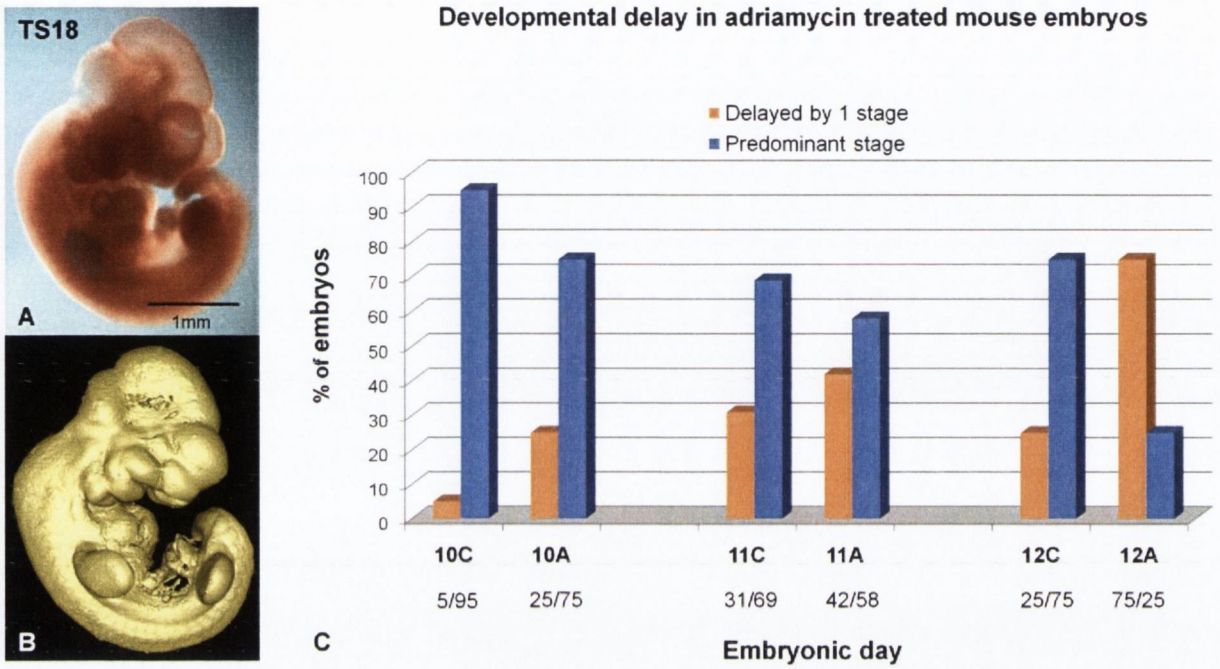


Figure 3.1: Theiler staging of adriamycin (a) and control (c) embryos revealed a significant delay in development following adriamycin treatment. (A) External view of an E11 control embryo. (B) Surface rendered view of the OPT 3D reconstruction of the same embryo showing morphological features used for staging purposes, staged as TS18. Scale bar as indicated. (C) Graphical representation of staging analysis across days E10 to E12 (n=44; n=72; n=26 respectively) the percentage of embryos collected on each day of development that fall into the predominant stage (E10, TS16,; E11, TS18; E12, TS20) is represented in blue bars; orange bars represent the percentage of embryos delayed by 1 stage. Mantel-Haenszel X-squared tests show significant differences in the proportions of delayed embryos in treated groups versus control groups (pvalue<0.01) on each day E10, E11 and E12.

3.2.2 A spectrum of foregut abnormalities are caused by adriamycin treatment

To assess the spectrum of effects on foregut development in adriamycin treated embryos 78 adrimaycin treated embryos and 71 control embryos from E10 to E12 were immunostained to localize the endoderm and notochord marker HNF3β and OPT scanned. HNF3β is a forkhead

domain transcription factor specifically expressed in floor plate, notochord and endoderm tissue including the foregut and lung buds, frequently used as an endoderm marker (Sharpe et al., 2002). Figure 3.2A shows an example of HNF3β labelled tissues in a control embryo, viewed following whole mount detection and OPT scanning. The 3D digital recordings of each embryo were analysed to assess the morphology of the foregut.

Eight morphological alterations were noted in adriamycin treated embryos: (1) abnormal branching of the notochord, (2) atresia of the foregut (complete discontinuity), (3) foregut stenosis (narrowing of the lumen), (4) oesophageal atresia (OA) with upper pouch, showing a blind dorsal pouch of the anterior foregut, (5) total laryngotrache-oesophageal cleft (LTEC), characterized by the absence of a septum dividing the trachea and oesophagus, (6) tracheal atresia, characterized by a blind ventral pouch of anterior foregut, (7) stomach agenesis, (8) fistula from carina or bronchi, where there is a narrow connection between the respiratory tract and the stomach. Table 3.1 summarises the percentage incidence of the each of the abnormalities above, across the days of collection. The number of embryos showing multiple malformations was not recorded. Figure 3.2 shows examples of each abnormality.

In the control groups there were no anomalies found. Most adriamycin treated embryos showed some abnormalities with only 2 embryos across stages appearing normal in all respects scored. Abnormal position (ventral displacement) and notochord branching was seen in almost all treated embryos; in 18/19 at E10. At E10 in adriamycin treated embryos, the full spectrum of foregut malformations was recorded. Foregut stenosis and LTEC were the most frequently recorded abnormalities, found in 33% and 27% respectively. Fistula was found only

in 7% of the embryos.

At E11 the incidence of LTEC (45%), tracheal atresia (24%) and fistula (63%), become more frequent with a striking increase in the incidence of fistula. Foregut stenosis was recorded only in 9% of cases. At E12 I noted an increased incidence of OA with posterior pouch (60%) and stomach agenesis (18%). The incidence of lower fistula was still high (55%). Foregut atresia, LTEC and tracheal atresia were recorded less frequently. The reduced incidence of the very severe anomaly of complete foregut atresia may be related to an increase in embryo reabsorption noted at this stage (not shown). The decrease in LTEC may indicate that separation of the oesophagus and trachea occurs later in some adriamycin treated embryos.

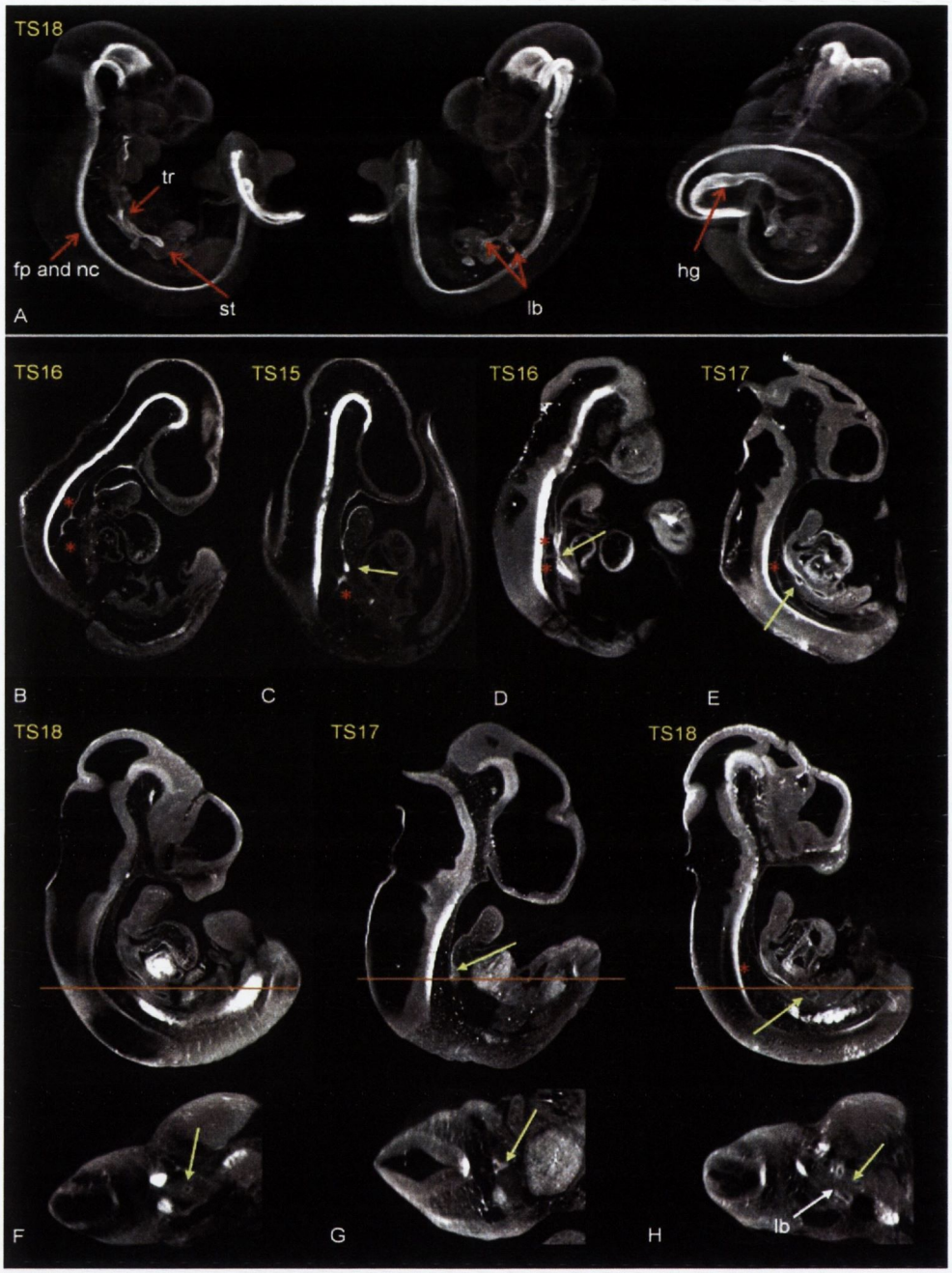


Figure 3.2: Morphological analysis of the spectrum of effects of adriamycin treatment on foregut and notochord development. (A) External views from different angles of a 3D reconstruction of a control embryo showing HNF3β labelled endoderm, notochord and floor plate (in white). (B-H) Virtual sections through 3D reconstructions of adriamycin treated embryos immunostained for HNF3β showing examples of the morphological abnormalities observed. Abnormal notochord branching (red stars) and foregut abnormalities (green arrows) are indicated. (1) abnormal notochord delamination (B, C, D, E; red stars), (2) foregut atresia (C), (3) foregut stenosis (D), (4) OA with upper pouch (E), (5) LTEC (F), (6) tracheal atresia (G), (8) fistula from the right bronchii (H). Absence of stomach (7) can't be shown. The images underneath are transverse sections in the planes indicated. *lb*; lung bud, *fp*; floor plate, *nc*; notochord, *hg*; hindgut, *tr*; trachea, *st*; stomach.

Table 3.1: The spectrum of adriamycin induced abnormalities observed showing % incidence at each embryonic day. The number of embryos analysed at each stage for control (white) and adriamycin treated (green) conditions is given in brackets (e.g. E10C (24)). The number of embryos showing the abnormality, per scorable* embryos for that abnormality, is tabulated. *specimens were not scorable for a particular trait if the reconstuction was not clear in the relevant region

Adriamycin induced abnormalities	E10C (24)	E10A (23)	E11C (35)	E11A (40)	E12C (12)	E12A (15)
1. Notochord branching	0/24 0%	18/19 94%	0/35 0%	33/38 87%	0/12 0%	9/14 64%
2. Foregut atresia	0/24 0%	1/15 7%	0/35 0%	2/35 6%	0/12 0%	0/11 0%
3. Foregut stenosis	0/24 0%	5/15 33%	0/35 0%	3/35 9%	0/12 0%	1/10 10%
4. OA with upper pouch	0/24 0%	2/15 13%	0/35 0%	5/35 14%	0/12 0%	6/10 60%
5. LTEC	0/24 0%	4/15 27%	0/35 0%	16/35 45%	0/12 0%	2/11 18%
6. Tracheal atresia	0/24 0%	1/15 7%	0/35 0%	8/34 24%	0/12 0%	0/11 0%
7. Stomach agenesis	0/24 0%	1/13 8%	0/35 0%	3/33 9%	0/12 0%	2/11 18%
8. Fistula from carina or bronchii	0/24 0%	1/15 7%	0/35 0%	22/35 63%	0/12 0%	6/11 55%

3.2.3 Abnormal notochord branching in adriamycin treated embryos is associated with the location and severity of foregut abnormalities

Abnormal notochord branching was the most frequently recorded anomaly across the stages and was most prominent at E10 (94%) and E11 (87%) respectively. In normal development, by E12 the notochord is no longer visible perhaps explaining the lower incidence of the abnormality recorded in older embryos. In addition to abnormal branches extending ventrally, the entire structure was frequently ventrally displaced with respect to the floorplate of the neural tube (Figure 3.2 B). Notochord branching in adriamycin treated embryos was scored according to number, thickness and positioning of the branches at E10 and E11, as well

association with foregut malformations (Table 3.2). The anterior-posterior (AP) level of the branching and the number of branches could be accurately scored from virtual sections cut through multiple planes in the computer reconstructed specimens. Figure 3.3 shows examples of sections through the reconstructions showing the position and extent of the branching. To further demonstrate that the HNF3 β positive abnormal branches seen to extend ventrally from the notochord are notochord in character, they were shown to express the gene encoding Sonic hedgehog (*Shh*), an important signaling molecule produced by the notochord (Figure 3.3 D) (Echelard *et al.*, 1993). Notochord branching was subdivided into three categories according to AP position of occurrence: (1) anterior, at the level of pharynx (Fig 3.3 A), (2) more posterior, at the level of the site of tracheal separation (Fig 3.3 B) and (3) posterior, between the site of tracheal separation and the stomach (Fig 3.3 C). Each embryo was also scored for the appearance of foregut abnormalities to reveal any association between notochord branching and specific foregut abnormalities (Table 3.2). Posterior localised (level 3) thick branching of the notochord, attached to the dorsal wall of the foregut was found more often associated with foregut atresia (2) and foregut stenosis (3) (Fig 3.3 D, E). More posterior branching of the notochord (level 2+3) was found to be associated with OA with upper pouch (4) and stomach agenesis (7). LTEC (5), tracheal atresia (6) and fistula (8) were associated with notochord branching at all levels. Fistula (8) is an interesting case since the abnormality is necessarily localised posteriorly, at the level of the stomach, but its occurrence is associated with branching at all levels (Table 3.2).

Table 3.2: Scoring of notochord branching and co-incidence of specific foregut abnormalities 2-8 (as per table 3.1, represented by different colours) in 50 E10 and E11 adriamycin treated embryos. For position 1= anterior to the pharynx; 2= level of the trachea; 3= between trachea separation and stomach. Number of stars represents the relative thickness of branch, Y= y shaped double branch of notochord.

Position and thickness of notochord branching	Morphological abnormalities (as per table 3.1)						
	2.Foregut atresia	3.Foregut stenosis	4. OA with upper pouch	5. LTEC	6. Tracheal atresia	7.Stomach agenesis	8.Fistula
1*							
1*							
1*Y							
1*							
1*							
1*							
1*							
2*							
2*							
2*							
2*							
2*							
2*Y							
2*							
2*							
2**							
2**Y							
2**							
3***Y							
3**Y							
3*							
3**							
3***							
3**							
3***							
3**Y							
3**Y							
3*							
3***							
1*,2*,3*							
1*,2*,3*							
1*,3**							
2*,3*							
1*,2**							
1*,3*							
2*,3*Y							
2*,3*							
1*,2*,3*							
2*,3*							
1*,3*							
2*,3*Y							
2**,3*							
2*,3*Y							
1*,2*Y							
1*,2*							

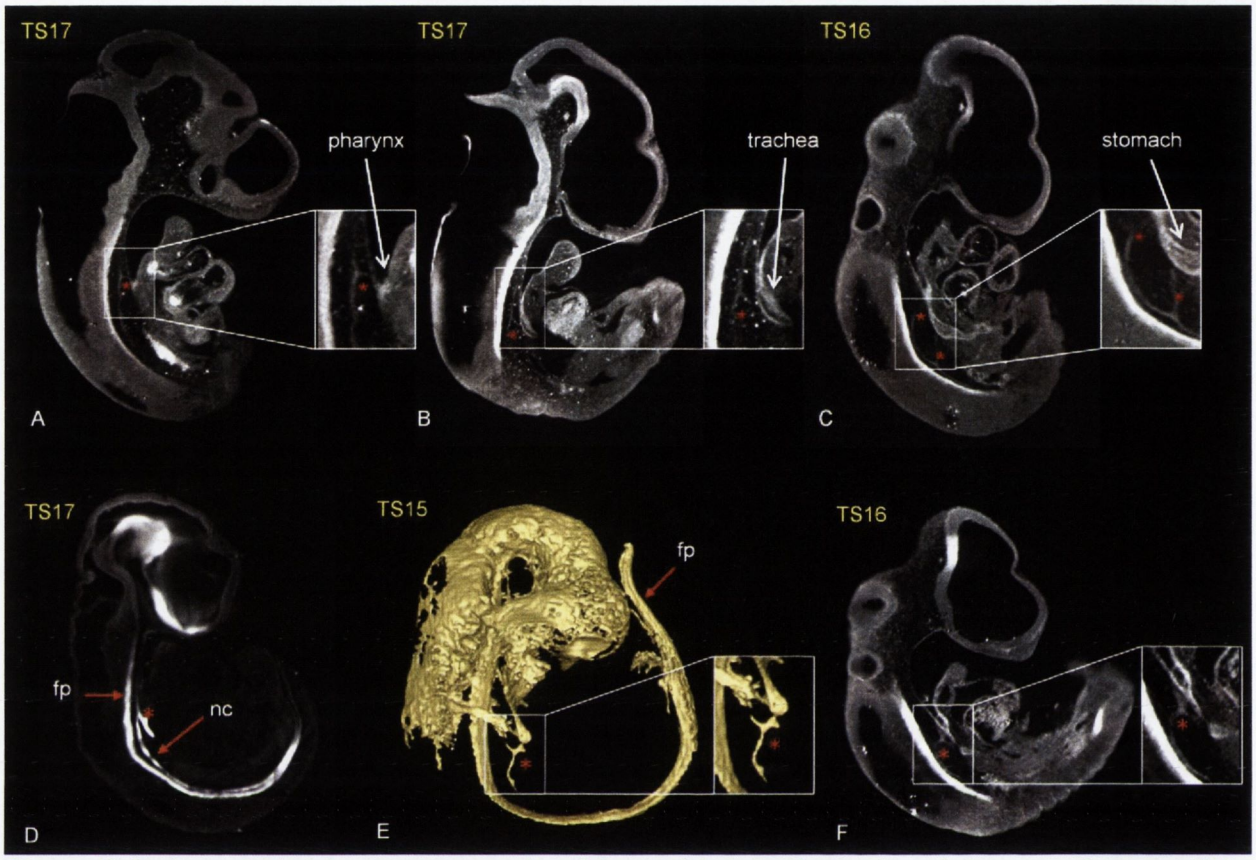


Figure 3.3: Association between notochord branching (red stars) and foregut abnormalities in 6 Adriamycin treated embryos (A-F); A-C and E,F show immunolocalisation of HNF3β, D shows *Shh* gene expression following whole mount in situ hybridisation. Virtual saggital sections of OPT reconstructions (A-C) demonstrate the different A-P levels of the abnormal branching notochord noted in table 3.2; anterior to pharynx (A), at the level of the trachea (B), between the site of tracheal separation and the stomach (C). (D) shows *Shh* expression in an abnormally delaminated and branched notochord (red star). (E) shows a surface rendered reconstruction of HNF3β immunolocalisation illustrating association between an abnormal, thick branch of the notochord (red star) and foregut atresia. (F) illustrates association between an association between an abnormal, thick branched notochord in a posterior location (red star) attached to the dorsal wall of the foregut and foregut stenosis. *fp*; floor plate, *nc*; notochord.

3.2.4 Patterning of the foregut is disturbed at the site of abnormal notochord branches

Shh expression in the foregut normally shifts from being expressed in the ventral endoderm of the prospective trachea prior to separation at E10.5 to being dorsally restricted to the separated

oesophagus at E11.5 (Ioannides *et al.*, 2003). A number of adriamycin treated embryos showed a lack of dorso-ventral restriction of *Shh* expression at the site of an unseparated foregut at E11.5, indicating a disturbance of normal D/V patterning (Ioannides *et al.*, 2003). We investigated if *Shh* expression in the foregut is specifically disturbed in the vicinity of ectopic notochord branches (Figure 3.4). At E11 ectopic *Shh* expression was seen through abnormal notochord branches of various length and thickness (Figure 3.4 A, B, C). In addition, there was an abnormal dorsal shift of the expression in the foregut specifically at the point where a thick ventral notochord branch was positioned adjacent to the foregut (Figure 3.4 Cb, Cc). Where there was limited ventral extension of the branch (Figure 3.4 A) or the branch was light (Figure 3.4 B), *Shh* was normally restricted to the ventral endoderm as expected at this stage.

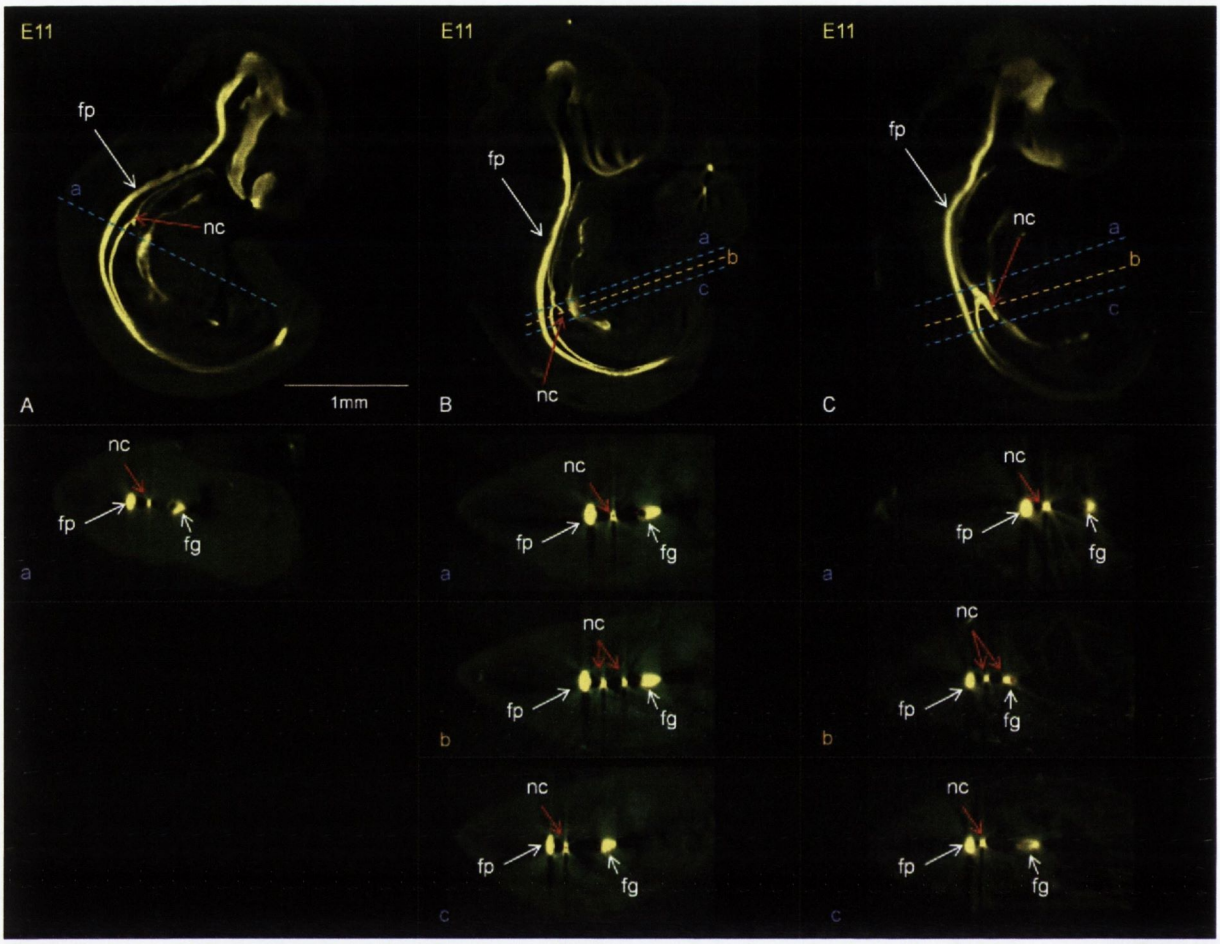


Figure 3.4: *Shh* expression in the branched notochord and disturbed *Shh* expression in the foregut following adriamycin treatment. Embryos at E11 showing notochord branches at different anterioposterior levels, different thickness and different distances from the foregut: A) short anterior branch; the cross section in a) shows normal localization of *Shh* expression in the ventral foregut (dorsal foregut outlined in red). B) long narrow notochord branch. Cross section at b shows the branched notochord; cross sections at a, b and c show normal ventral restriction of *Shh* expression. C) Thick notochord branch adjacent to the foregut; a,b,c cross sections show abnormal notochord branch in b and abnormal expression of *Shh* through the dorsal foregut in c. *fp*; floor plate, *nc*; notochord, *fg*; foregut.

We furthermore investigated expression of the *Foxf1* gene, which encodes a forkhead or winged helix transcription factor and is expressed during organogenesis in the mesenchyme adjacent to the endodermal epithelia of the gastrointestinal tract (Mahlapuu et al., 1998; Peterson, 1997). Haploinsufficiency of *Foxf1* leads to a phenotype similar to *Shh* null mutant mice including hypoplastic lungs and lobulation defects, oesophageal and tracheal stenosis, or

oesophageal atresia and trache-oesophageal fistula (Litingtung *et al.*, 1998; Mahlapuu *et al.*, 2001). We therefore examined the expression of *Foxf1* in adriamycin treated and control embryos and found that mesodermal expression of the gene around the foregut of treated embryos showed less of a ventral bias and was more symmetrically distributed around the foregut, specifically in the vicinity of abnormal notochord branches (Figure 3.5). To further investigate the coincidence of ectopic notochord branches and abnormal dorso-ventral expression of *Shh* and *Foxf1* in and around foregut endoderm, we measured the extent of foregut affected anterior and posterior to the notochord branch by counting the number of consecutive transverse virtual sections affected in a sample of treated embryos at E10 and E11 (Table 3.3). Although there was much variability in the extent of the effect, the pattern in general corroborated the example shown in Figure 3.4, where thick multiple branches (** and ***) were associated with the most affected specimens (up to 490μm) whereas single, fine branches (*) were associated with limited or no disturbance (e.g. 0, 30, 150 μm).

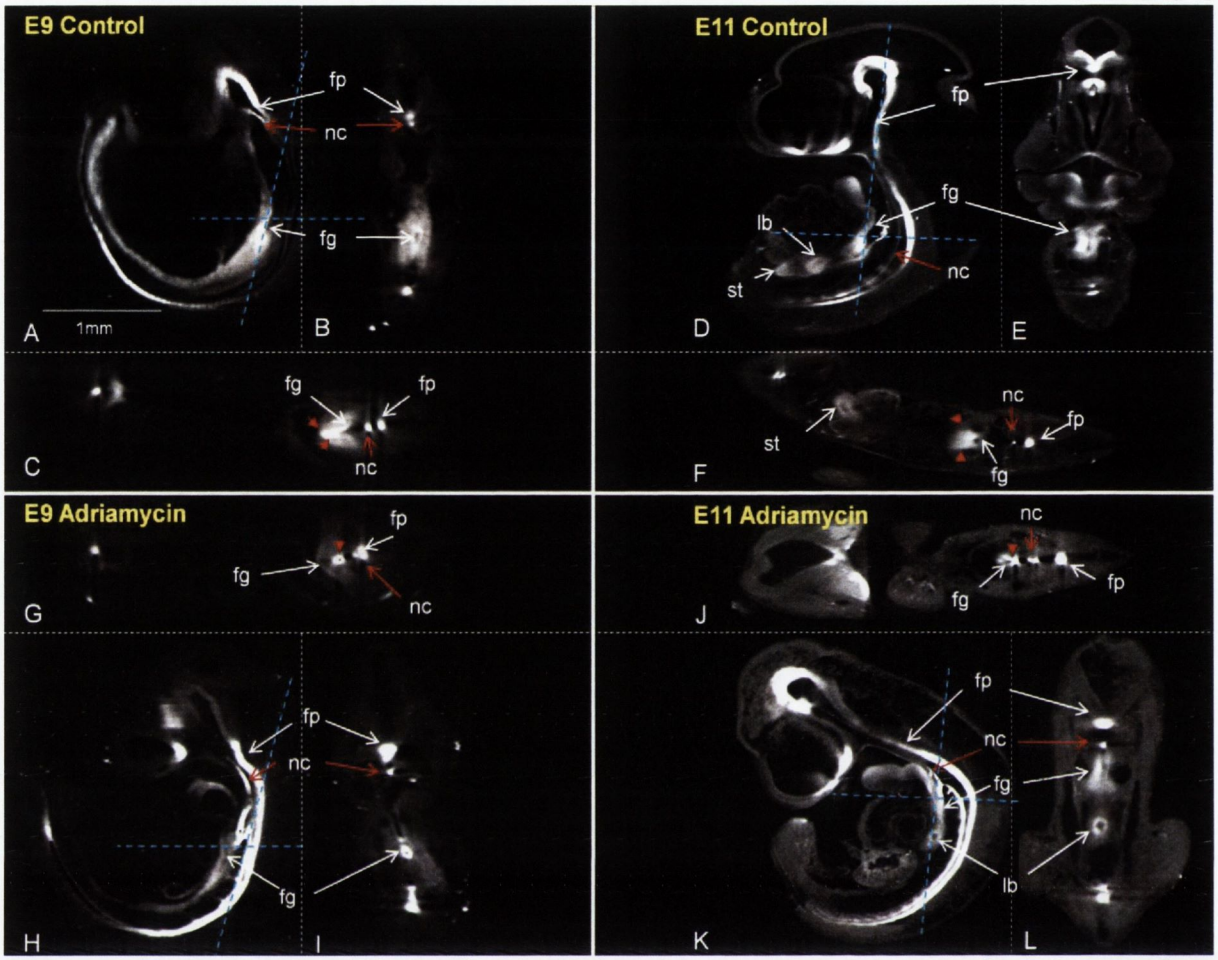


Figure 3.5: Expression of *Foxf1* in adrimycin treated and control embryos show abnormal expression in the foregut associated mesenchyme in the vicinity of ectopic notochord branches. Control (A-F) and adriamycin treated embryos (G-L) represented by virtual, sagittal (A,D,H,K), coronal (B,E,I,L) and transverse (C,F,G,J) sections of OPT reconstructions following whole mount in situ hybridisation with *Foxf1* antisense probe show expression in the floor plate, notochord, foregut endoderm and associated mesenchyme. Blue dotted lines indicate the planes of coronal and transverse sections. Red arrow heads on transverse sections of control embryos at E9 and E11 (C, F) indicate the ventral bias in distribution of *Foxf1* transcripts in the foregut mesenchyme. Note the absence of this pattern in treated embryos (G, J). *fp*; floor plate, *nc*; notochord, *fg*; foregut, *lb*; lung bud.

Table 3.3: Extent of foregut (μm) in which dorso-ventral localised expression of either *Shh* or *Foxf1* was disturbed in individual Adriamycin treated embryos at either E10 or E11. The right hand column shows the anterior/posterior position and relative thickness and proximity of the notochord branches (as indicated in Table 3.2).

Specimen	Gene expression analysed	Extent of disturbed expression pattern	Relative heaviness/ proximity of notochord branch
E10 2018	*Shh*	260 μm	2***Y
E10 2019	*Shh*	100 μm	2***Y
E10 2020	*Shh*	230 μm	2**, 3**
E10 2054	*Shh*	160 μm	1*,3*
E10 1817	*Shh*	490 μm	3***Y
E11 1785	*Shh*	180 μm	1**,2**
E11 1787	*Shh*	30 μm	2*
E11 2025	*Shh*	312 μm	2***
E11 2058	*Shh*	112 μm	2***
E11 361	*Shh*	221 μm	2**
E11 362	*Shh*	0	1*
E10 1828	*Foxf1*	390 μm	2**Y
E10 2041	*Foxf1*	130 μm	3**
E10 2036	*Foxf1*	250 μm	2***Y
E10 2040	*Foxf1*	250 μm	3***Y
E10 2039	*Foxf1*	460 μm	2***,3**
E11 2046	*Foxf1*	53 μm	1**,2**, 3*
E11 2045	*Foxf1*	350 μm	3***
E11 2047	*Foxf1*	420 μm	1*, 2***, 2*
E11 1789	*Foxf1*	150 μm	2*
E11 1790	*Foxf1*	300 μm	2**
E11 1791	*Foxf1*	255 μm	2**Y

Dorsoventral patterning of the foregut is also reflected in dorsal expression of *Sox2* and ventral expression of *Nkx2.1* and in *Nkx2.1* null embryos *Sox2* expression spreads ventrally accompanied by failure of trachea-oesophageal separation (Ioannides *et al.*, 2010; Minoo *et al.*, 1999; Que *et al.*, 2007). We therefore examined *Sox2* and *Nkx2.1* gene expression in adriamycin and control embryos and found that while *Nkx2.1* expression was normally confined to the ventral domain, dorsal *Sox2* expression was absent in the vicinity of an ectopic

notochord branch (Figure 3.6). Moreover *Nkx2.1* gene expression was seen in the endoderm of the lung buds in both control and treated groups and was expanded into the endoderm of the fistula of adriamycin treated embryos from E11 (Figure 3.6 F).

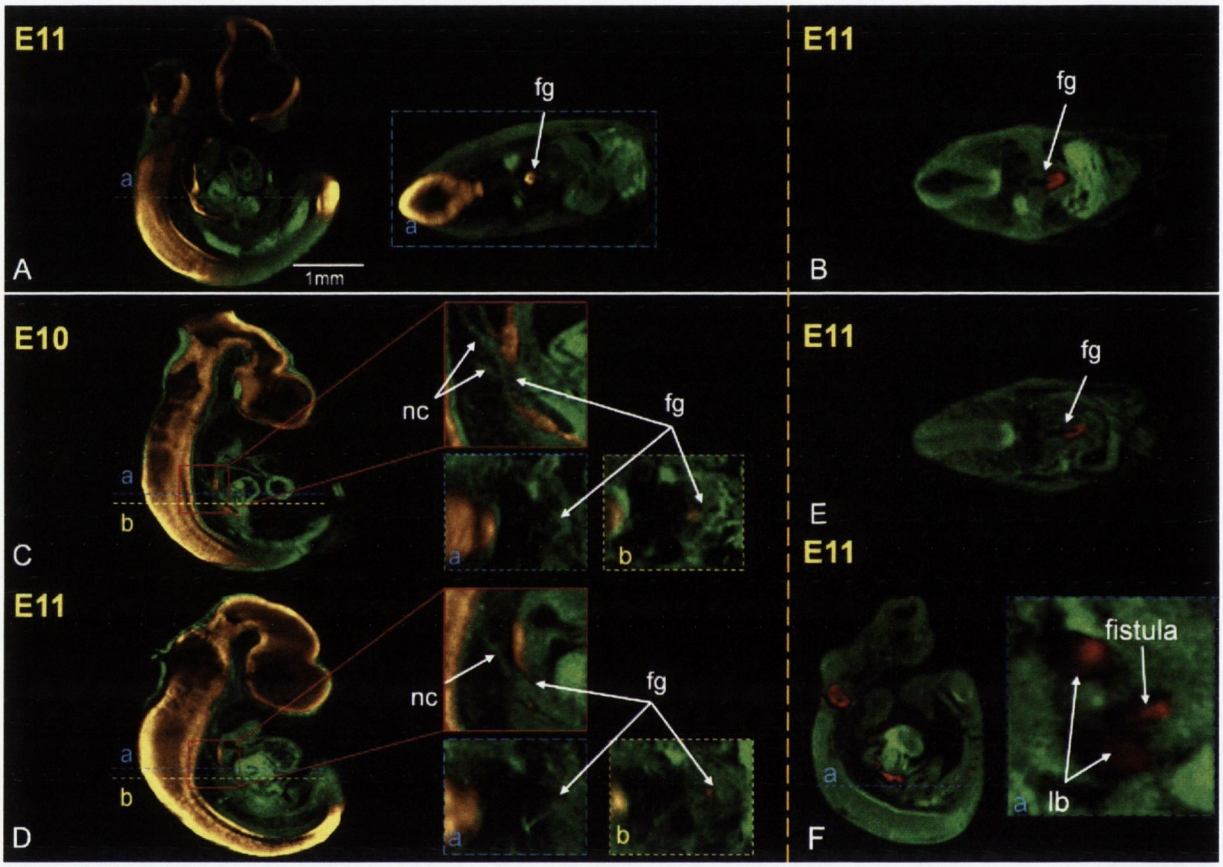


Figure 3.6: *Sox2* expression (A, C and D, shown in yellow) and *Nkx2.1* expression (B, E and F, in red) in control (A, B) and adriamycin treated (C, D, E and F) embryos at embryonic days 10 and 11 as indicated. *Sox2* expression in the dorsal foregut is lost at the site of abnormal notochord branches while *Nkx2.1* expression remains localized to the ventral foregut. *Nkx2.1* expression is seen in the endoderm of the lung buds and expanded is into the endoderm of the fistula in terated embryos (F). Sagittal sections are shown on the left of A, C, D and F with transverse sections on the right in A and F (in planes indicated), and in B and E. Higher magnification views at a notochord branch are bounded in red in C and D. Transverse section in the planes indicated as a and b at and below the site of a notochord branch are shown bounded in blue and yellow respectively. *nc*; notochord, *fg*; foregut, *lb*; lung bud.

3.2.5 Tracheal separation and lung branching in adriamycin treated embryos

Normal lung development could be followed in control embryos using OPT imagining and the endoderm marker HNF3β (Figure 3.7). The lung bud primordia start forming at TS15 (Figure 3.7 A) with very specific triangular widening of the foregut (Fig 3.7 F). From TS16-TS17 the oesophagus starts to separate from the trachea (Figures 3.7 B, C, G). Further elongation of the trachea and lung bud branching morphogenesis were recorded from TS18 up to TS20 (Fig 3.7 D, E, H). This normal progression is consistent with previous findings (Maeda *et al.*, 2007; Metzger *et al.*, 2008). Each adriamycin treated embryo was also staged according to external morphological criteria (Theiler, 1989) and the extent of tracheal separation and lung bud branching assessed through viewing virtual saggital, coronal and transverse sections. In adriamycin treated embryos, otherwise morphologically staged at TS15 and TS16, lung primordia were not present in 33% (4 out of 12) or present as only an oval widening of the foregut in 73% (8 out of 12) (Fig 3.7 I) of specimens. In treated embryos staged as TS17 only 20% (3 out of 15) of the embryos presented with separation of the trachea from the oesophagus and lung bud division, 53% (8 out of 15) of the embryos presented without tracheal separation but with appearance of lung buds and 27% (4 out of 15) of the embryos presented with only oval widening of the foregut.

In treated embryos staged as TS18 0 out of 22 embryos had normal trache-oesophageal separation, 18% (4 out of 22) of the embryos had lung bud division and 82% (18 out of 22) oval or transverse widening of the foregut. In treated embryos staged as TS19 14% (1 out of 7) of the embryos had normal trache-oesophageal separation and lung bud division, 29% (2 out

of 7) of the embryos presented with lung bud division and 57% (4 out of 7) of the embryos showed only triangular widening of the foregut.

In treated embryos staged as TS20, 20% (1 out of 5) of the embryos presented with separation of the trachea from the foregut and division of the lung bud, 60% (3 out of 5) of the embryos had lung bud division but no tracheal separation and 20% presented with only oval widening of the foregut.

From the above it is clear that only a minority of adriamycin treated specimens, even at TS20, show separation of the trachea and oesophagus. Even when separation was noted, the distance between the dorsal wall of the trachea and the ventral wall of the foregut was reduced and lung buds separated more posteriorly in comparison to control embryos (Fig 3.7 J).

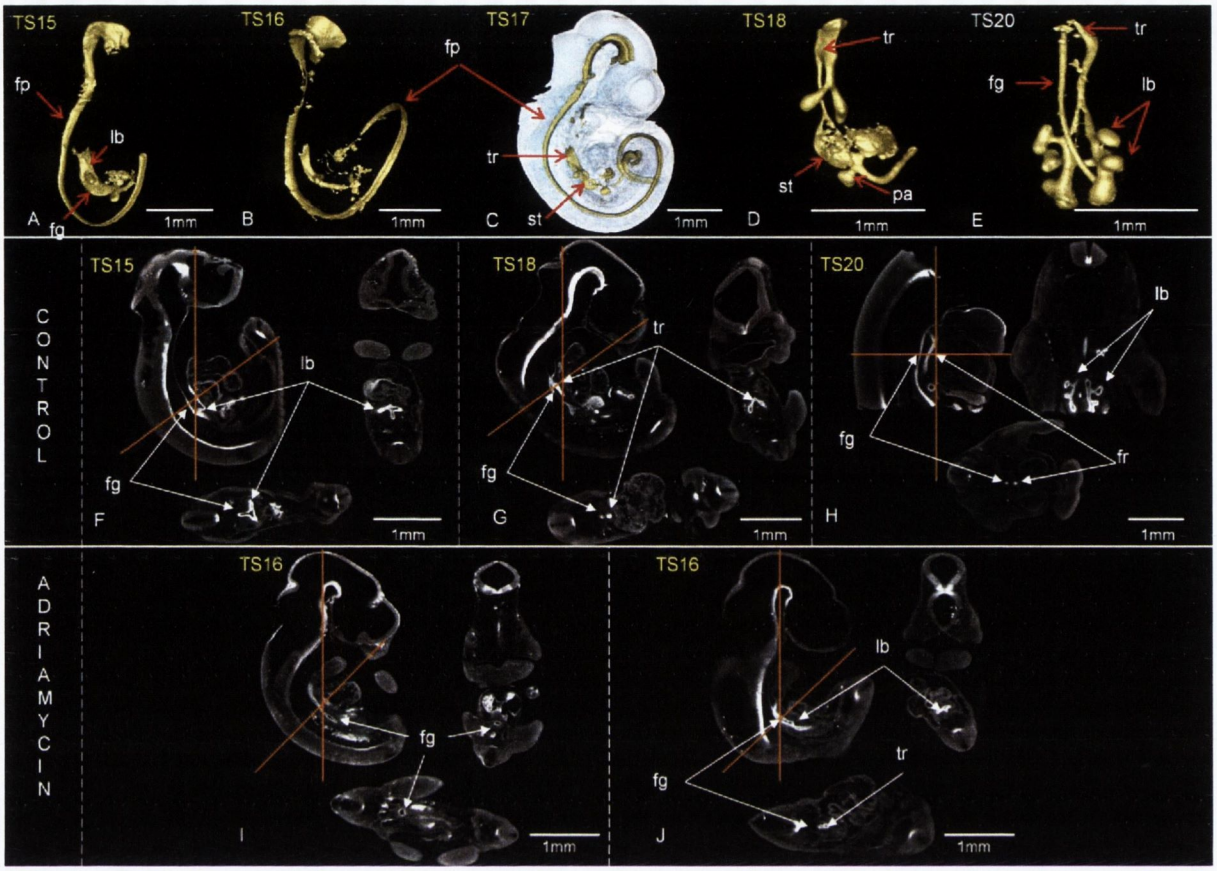


Figure 3.7: Abnormal trachea-oesophageal separation and lung morphogenesis in adriamycin treated embryos. A-E; normal trache-oesophageal separation and lung bud branching morphogenesis from TS15- TS20 revealed through 3D surface representation of HNF3β immunolocalisation. C shows surface representation of the HNF3β positive domain (in yellow) in the context of the whole embryo (blue, transparent). Sections through 3D reconstructions in saggital (main images), coronal (to the right) and transverse (below) orientations of control (F-H) and adriamycin treated (I-J) embryos. The position of coronal and transverse sections are indicated with red lines. At TS15 ventrolateral bulges on the foregut indicate the first appearance of the lung buds (A and F). At TS16 and TS17 the lung buds elongate (B, C). From TS17 separation of the trachea begins with extended separation at subsequent stages (C, D, E and G, H). Branching morphogenesis of the lung buds is extensive at TS20 (E and H). Scale bars as indicated. Examples of adriamycin treated embryos (I-J), at TS16 show abnormal oval widening of the foregut instead of lung primordia (I). The site of lung bud separation from the foregut is more posterior in comparison to control embryos (I). Abnormal tracheal separation, where the trachea remains close to the ventral wall of the foregut (J). *fp* floor plate, *lb* lung bud, *fg* foregut, *tr* trachea, *st* stomach, *pa* pancreas. Scale bars as indicated.

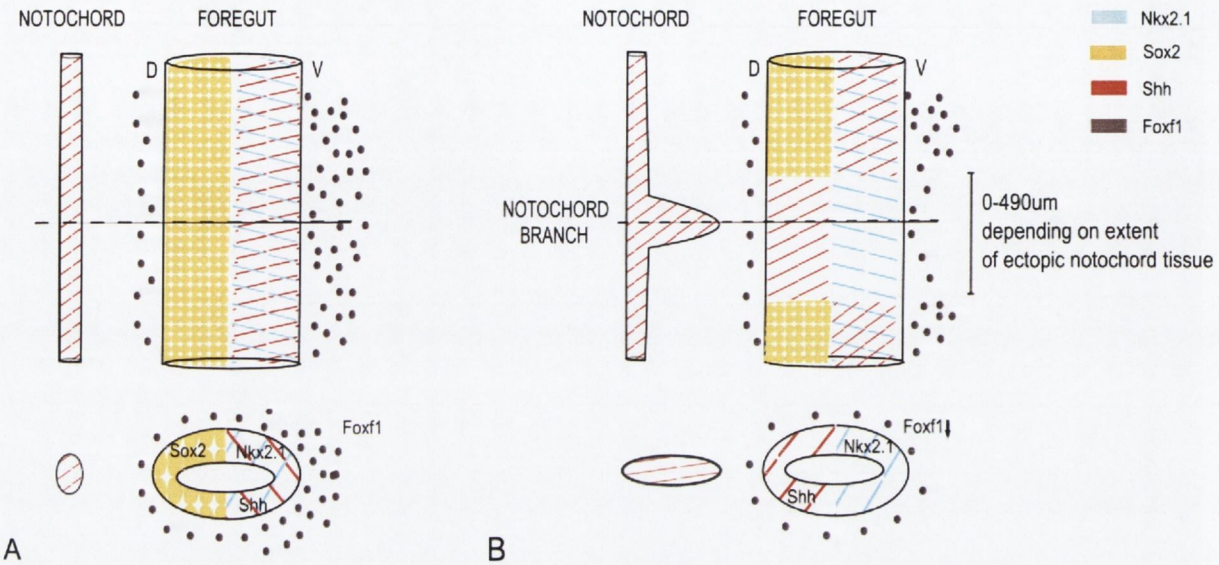


Figure 3.8: Schematic representation summarising the observed effects of adriamycin treatment on dorso-ventral patterning of the foregut, specifially in the vicinity of a ventral notochord branch. A and B summarise the observed expression of *Shh*, *Foxf1*, *Sox2* and *Nkx2.1* in control and treated E10 embryos respectively. The upper drawings represent lateral views of the notochord and adjacent foregut; the lower drawings represent transverse sections in the plane indicated above. In the vicinity of a *Shh* expressing notochord branch, *Sox2* expression is lost in the dorsal foregut, *Shh* expression is abnormally expressed dorsally and the normal ventral polarisation of *Foxf1* expression in the adjacent mesenchyme is lost.

3.3 Discussion

Here I show systematic detailed morphological analysis of a substantial number of mouse embryos exposed to adriamycin *in utero*, an established model of foregut congenital abnormalities termed OA/TOF. We reveal delayed development and a full spectrum of abnormalities and their frequency in adriamycin treated embryos. A very frequent abnormality noted was ventral displacement and branching of the notochord in 94% of E10 and 87% of

E11 embryos. The whole 3D embryo imaging approach allowed an association to be revealed between the position and severity of notochord branching and particular foregut abnormalities suggesting a mechanistic link between the effects on the notochord and the foregut. This is further emphasised by the observations of altered dorso-ventral patterning of the foregut, in terms of localized *Shh, Foxf1* and *Sox2* gene expression, specifically in the vicinity of a notochord branch (summarized in Figure 3.8).

Like all embryonic events, foregut and lung development involve complex changes in the shape and structure of tissues over short periods of time. It is therefore important to view and analyse normal and altered events in three dimensions. Although previous studies have used 3D reconstructions from serial embryo sections (Sasaki *et al.*, 2001; Williams *et al.*, 2001; Williams *et al.*, 2003), OPT scanning offers several unique advantages over section reconstructions and permitted a more complete analysis of a relatively large number of specimens in this study. First, because OPT scanning involves direct 3D image capture, the approach does not suffer from the difficulties of loss of tissue and distortion suffered in section reconstruction methods (Sharpe *et al.*, 2002). Second, OPT scanning is relatively rapid and significantly less time consuming that sectioning specimens, permitting a relatively large number of specimens to be analysed. Third, because OPT allows capture of colourimetric and fluorescent stains (Sharpe, 2003; Sharpe *et al.*, 2002), molecular markers can be used to visualize specific cells and tissues, as well as gene expression patterns; this was used to advantage here visualizing the endoderm and notochord marker HNF3β. In the approach used here, a permanent 3D computational representation of each treated and control embryo is recorded and can be analysed repeatedly from multiple perspectives. For example, using

MAPaint, software, developed by the Edinburgh Mouse Atlas Project (EMAP; http://genex.hgu.mrc.ac.uk), the 3D computer specimens can be digitally sectioned in any arbitrary plane of orientation and position, with multiple planes viewed simultaneously. We created 3D digital records of 149 control and adriamycin treated embryos across early stages of development from E10 to E12. The combined use of the HNF3β tissue marker and full 3D imaging, allowed a more comprehensive analysis of the full spectrum of abnormalities found in adriamycin exposed embryos.

Despite the increased comprehensivity of analysis, not all scanned embryos were fully interpretable. In some specimens the HNF3β marker signal was not strong and was obscured in particular locations meaning not all embryos were scorable for all abnormalities. This is possibly due to incomplete penetration of the antibody or other staining components in some cases. When an embryo was not scorable for a particular abnormality, it was not included in the analysis (Table 3.1).

It was shown that the dose and timing of exposure of embryos to Adriamycin is critical in producing foregut malformations (Dawrant *et al.*, 2007c). The exact preparation of adriamycin, dose and treatment regime used here was that previously shown to have the strongest effect in the Dawrant *et al* study (2007c). While the overall effects on the foregut are broadly consistent between studies some differences are likely to be due to differences in the treatment regime. Ionnides *at al.* reported high incidance (60%) of LTEC at E12.5 with a dose of 4mg/kg of adriamycin, administered at E7.5 and E8.5 (Ioannides *et al.*, 2002). In contrast, in this work where a higher dose was given earlier (6mg/kg at E7 and E8) the incidance of

LTEC at E12 was 18% and the incidance of OA was 60%. The very high incidance of OA with upper pouch seen here in comparison to 15.6% in embryos at E18 seen in an earlier study with the same treatment regime (Dawrant *et al.*, 2007a) may be explained by the fact that the most severely affected embryos may not survive past E12.

To assess if adriamycin exposure has an effect on the rate of development, embryos were staged according to Theiler morphological criteria and the range of stages at each embryonic day of development were compared between control and adriamycin treated groups. This showed a significant delay in development in treated groups across all days of development with a steady increase in the extent of delay over time. It is recognised that there can be a 6 to 12 hour difference in embryonic development between embryos within the same litter (Kaufman, 1999) so it is important to compare across a large number of embryos in control and treated groups. The method used here, where a predominant stage was identified for control embryos on each embryonic day and the proportion of embryos at a less advanced stage noted, allowed the increasing delay in treated embryos to be revealed in a robust manner. Because the criteria used to stage the embryos spanned multiple developing systems including facial, brain and limb features, we conclude that this level of adriamycin exposure delays development processes in general. In addition, 3D imaging showed the normal progression of lung development over a series of Theiler developmental stages and a marked specific delay in lung progression in treated embryos relative to overall development judged by other morphological criteria was observed. The observation that in 20% of treated embryos staged at TS20, the trachea and oesophagus had separated whereas at TS18 no separation was observed (an event observed at TS17 in control embryos) indicates that in some treated embryos there

may be some recovery in the effects on lung development, however the effects are very severe and the system is unlikely to fully recover.

The notochord is a key embryonic structure common to all members of the phylum Chordata. In higher vertebrates it exists only transiently but has a potent influence as a source of inductive signals patterning adjacent tissues including the neural tube dorsally, the somites laterally and the gut endoderm ventrally (Cleaver and Krieg, 2001; Dodd *et a*l., 1998; Halpern *et al.*, 1993; Kim *et al.*, 1997; Placzek, 1995; Stemple, 2005). The cells of the notochord derive from the node during gastrulation and initially form a notochordal plate embedded in the dorsal gut endoderm (Cleaver and Krieg, 2001; Jurand, 1974). The notochord cells reorganize into a rod-shaped structure that detaches from the endoderm, becomes separated from it by intervening mesenchyme, and comes to lie in closer association with the neural tube dorsally (Cleaver and Krieg, 2001; Jurand, 1974). The mechanisms regulating this dorsal delamination of notochord cells in a timely manner are not known. The existence of abnormal ventral 'branches' extending from the notochord has previously been noted in adriamycin exposed rat and mouse embryos (Dawrant *et al.*, 2007b; Mortell *et al.*, 2005; Orford *et al.*, 2001; Possoegel *et al.*, 1999; Williams *et al.*, 2001) indicating that the delamination process does not proceed correctly. Here we observe two clear sets of defects during development of treated embryos (delamination of the notochord and abnormal foregut development) and although these may be caused independently, the close physical association between abnormalities of the notochord and the foregut suggests a causative link whereby abnormal delamination of the notochord leading to ventrally displaced notochord tissue may disturb foregut development, either through mechanical disturbance or by producing aberrant signals

misdirecting the patterning of the foregut. In support of this idea there are a number of compelling observations in the literature illustrating notochord defects and problems with development of endodermal tissues; for example the *Noggin* knock-out mouse which exhibits features similar to adriamycin treated embryos including abnormal branching of the notochord and also OA/TOF defects of the foregut (Cleaver and Krieg, 2001; Li *et al.*, 2007; Que *et al.*, 2006). These observations suggest that the timing and position of notochord signalling must be closely regulated for correct development of the gut tube.

In terms of molecular players important in signaling from the notochord to the foregut, gene inactivation studies show that *Shh* is essential for normal patterning of the foregut possibly through Foxf1 activation (Litingtung *et al.*, 1998; Mahlapuu *et al.*, 2001). We showed that the branched notochord expresses *Shh* at a high level and therefore branching of the notochord would lead to closer and increased signaling of *Shh* to the foregut. In the adjacent foregut we observed lack of *Sox2* expression in the dorsal endoderm, abnormal dorsal expression of *Shh* in the endoderm and absence of the normal ventral bias in the foregut mesenchyme expression of *Foxf1* at this level (Figure 3.8). In the case of *noggin* knock-out mice, also showing abnormal notochord branches, the *Foxf1* expression domain was expanded dorsally around the foregut compared with wild type embryos. Although the patterning defects in these two cases are not identical, both are consistent with the idea that abnormal signalling from ventrally displaced notochord alters patterning of the adjacent foregut. It is not surprising that the defects are different in these cases as although both involve ectopic notochord tissue close to the foregut, in the case of the *noggin* knock-out this tissue cannot express noggin and the signalling characteristics may therefore differ. In both cases the correct distinction between

dorsal and ventral endoderm is lost which may be important for the correct process of separation of dorsal digestive tract and ventral respiratory tract and may lead to the foregut abnormalities of OA/TOF observed in both.

It is intriguing that haploinsufficiency of *Bmp4*, presumably lowering the level of *Bmp4* produced, can rescue notochord branching and the OA/TOF phenotype in *Nog* null mutants (Que *et al.*, 2006), supporting the suggested idea that the precise level of *BMP* signalling, normally regulated by *Noggin*, is crucial for correct morphogenesis of the notochord and foregut patterning. In adriamycin treated embryos *Bmp4* signalling activity might be disturbed as a consequence of ectopic *Shh* expression through the notochord branches (Litingtung *et al.*, 1998). This might also lead to reduced expression of *Fgfs* in the mesoderm (Stottmann *et al.*, 2001; Weaver *et al.*, 2000) supported by our previous observation of delayed of mesodermal *Fgf10* expression in the adriamycin model (Hajduk *et al.* 2010) and delayed outgrowth of the primary lung buds from the foregut observed here. The disturbed expression of *Sox2* in the dorsal foregut endoderm in the region of a notochord branch is interesting in light of recent observations that *Sox2* repression in the ventral foregut promotes respiratory identity (Domyan *et al.*, 2011). It is clear however that a complex balance in inter-regulated signalling pathways is involved in normal development since truncation of the trachea and lung maturation is also affected in mutants with disrupted *Wnt* signalling pathways (Li *et al.*, 2002; Li *et al.*, 2008a).

Implication of *Nkx2.1* gene expression in the endoderm of the fistula of treated embryos will be further discussed in Chapter 4 together with *Wnt2* and *Wnt7b* gene expression (section 4.3.5).

Conclusions

Although the accumulated observations presented here suggest a causative relationship between abnormal notochord branches and foregut abnormalities, this remains an open question. The mechanistic basis of abnormal notochord branching is still not known but the current findings add to the body of data in this area that allow possible mechanisms to be explored (Qi and Beasley, 1999; Williams *et al.*, 2001). Any model must take account of the various data on implication of molecular players and the association seen here between specific location and thickenss of notochord branches associated with foregut atresia and foregut stenosis. Mechanical disruption of normal foregut development cannot be ruled out and the altered dorso-ventral patterning observed suggests a fundamental signalling defect. This systematic approach, combining a morphological marker and 3D imaging improves our insight into the developmental sequence leading to such foregut abnormalities and affords the opportunity to study them with high precision. The observations confirm previous findings on morphological abnormalities in the adriamycin rat and mouse model and open new question for further directions of molecular study which may bring us closer to understanding the pathogenesis of OA/TOF in humans.

Chapter 4

Temporospatial gene expression analysis during the critical period of separation of the trachea and oesophagus in normal and adriamycin treated embryos

Some of the data presented in this chapter were published in Pediatric Surgery International (Hajduk *et al.*, 2010a; b).

4.1 Introduction

Experimental embryology and molecular biology studies have revealed that there are spatially and temporally co-ordinated signalling systems, mediated by transcription factors and secreted proteins, that control the proper stereotypic morphological patterning and differentiation of foregut development. The separation of the foregut into the trachea and oesophagus is controlled by several signalling molecules expressed either in the mesoderm around the anterior foregut at the level of the forming lung primordia, or in the notochord, which lies dorsal to the foregut. These molecules act on the foregut endoderm and pattern endoderm across its D/V plane (reviewed in section 1.2.2). Abnormal signalling during this critical period of foregut development may lead to faulty separation of the foregut and, in consequence, abnormal foregut morphology. Detailed study of the development of the tracheo-oesophageal malformations produced in the AMM described in chapter 3 have provided insights into the faulty morphological events that occur in this model. In chapter 3 the distribution of a number of gene transcripts were analysed showing abnormal dorsal expression of the *Shh* gene in the foregut endoderm at the level of abnormal notochord branches together with downregulation of its downstream target gene *Foxf1* gene in the ventral mesoderm of the lung primordia. Normal dorsoventral patterning of the foregut was reflected in ventral expression of *Nkx2.1* and dorsal expression of *Sox2* in control embryos. In treated embryos, while *Nkx2.1* expression was normally confined to the ventral domain, *Sox2* gene expression was not detectable across the foregut endoderm at the level of notochord branches. Although *Nkx2.1* gene transcripts were not detectably altered in their distribution and continued to be restricted to the ventral endoderm of the foregut, analysis revealed expression of the gene in the endoderm of the fistula.

The aim of this chapter is present comprehensive analysis of the AMM at the molecular level, examining the expression of a number of candidate genes implicated in normal foregut patterning (section 1.2.2). The focus is on expression around the foregut within a defined development period in which separation of the foregut becomes clearly defined (E9 to E12). The use of the 3D imaging technique OPT (Sharpe *et al.*, 2002) facilitated this work in allowing capture of the distribution of tissue specific markers and gene expression patterns, either colourometrically or fluorescently visualized, within a 3D morphological context. OPT has been routinely used for 3D recording and representation of gene expression patterns between E9.5 up to E11.5 in mouse embryos for investigation of facial development (Vendrell *et al.*, 2009), neural tube (Miller-Delaney *et al.*, 2011), otic vesicle (Lioubinski *et al.*, 2006), limb (Summerhurst *et al.*, 2008) or lung and foregut development (Sato *et al.*, 2008). In addition OPT was used to record gene expression patterns during brain development in human embryos (Kerwin *et al.*, 2004; Kerwin *et al.*, 2010; Sarma *et al.*, 2005). Once captured, data can be viewed and analysed in several different ways including virtual sections through the specimen in any orientation to view the precise distribution of the molecules or in 3D reconstructions as volume (where you can see through the specimen) or surface representations (Summerhurst *et al.*, 2008).

The candidate genes analysed for comparative expression (adriamycin versus control treatment) in this chapter are involved in three different sets of developmentally vital signalling pathways. Both Fgf10 and Tbx4 genes are co-expressed in the visceral mesoderm of the lung primordia at the same antero-posterior level where endodermal *Nkx2.1* expression is restricted to the ventral foregut (Sakiyama et al., 2003). Fibroblast Growth Factor signalling

has been implicated in normal patterning of the foregut and in development of the lung primordia. Misexpression of *Tbx4* or *Fgf10* in the visceral mesoderm posterior to lung primordia, result in posterior expansion of the *Nkx2.1* gene expression in the anterior foregut and failure of separation of the trachea from the oesophagus (Sakiyama *et al.*, 2003). This suggests that a *Tbx4-Fgf10* system acts as a signaling component of the inductive interactions specific to lung primordium mesoderm and that altered boundaries of expression can affect tracheo-oesophageal separation (section 1.2.2). Here expression of both *Fgf10* and *Tbx4* genes is compared in control and treated embryos.

Bmp4 is expressed in the ventral foregut mesoderm and endoderm (Li *et al.*, 2008b; Weaver *et al.*, 2000) and its signalling is modulated by extracellular antagonists, including noggin (Massague *et al.*, 2005). The *BMP* pathway is known to be important in foregut development through the evidence from *Bmp4* knockout embryos that show tracheal agenesis (Li *et al.*, 2008b). The *Noggin* gene encodes a *BMP* signalling antagonist that can modulate the pathway. *Noggin* knockout mutants show foregut and notochord malformations similar to those seen in AMM (section 1.2.2) further implicating the *BMP* pathway. Here expression of *Bmp4* and *Noggin* genes are compared in control and treated embryos.

Wnt2 and *Wnt2b* are expressed in the mesoderm surrounding the ventral aspect of the foregut endoderm from E9 in mice (Goss *et al.*, 2009). The *Wnt* signalling pathway is important for foregut and lung development (Goss *et al.*, 2009; Warburton *et al.*, 2005). *Wnt2/2b* double knock-out mutants result in absence of *Nkx2.1* expression in the anterior foregut endoderm at the level of lung primordia and display complete lung agenesis without foregut separation

(Goss *et al.*, 2009). *Wnt7b* is expressed in the lung epithelium with a more intense expression distally (De Langhe *et al.*, 2005; Warburton *et al.*, 2005). Inactivation of *Wnt7b* in mice resulted in perinatal death due to respiratory failure and lung hypoplasia (Shu *et al.*, 2002) (section 1.2.4). Here expression of *Wnt2* and *Wnt7b* genes is compared in control and treated embryos.

4.2 Results

4.2.1 *Tbx4* gene expression in control embryos and the effect of adriamycin treatment on gene expression patterns

The *Tbx4* antisense probe was first tested on normal embryos and found to give a clear and specific pattern of expression in the mesenchyme around the site of the lung buds, trachea, in a specific patch in the forelimb and extensively in the hindlimb (Figure 4.1). Figure 4.4 illustrates the 3D nature of the data generated through in situ hybridization and OPT scanning to visualize features of the *Tbx4* expression domain in detail.

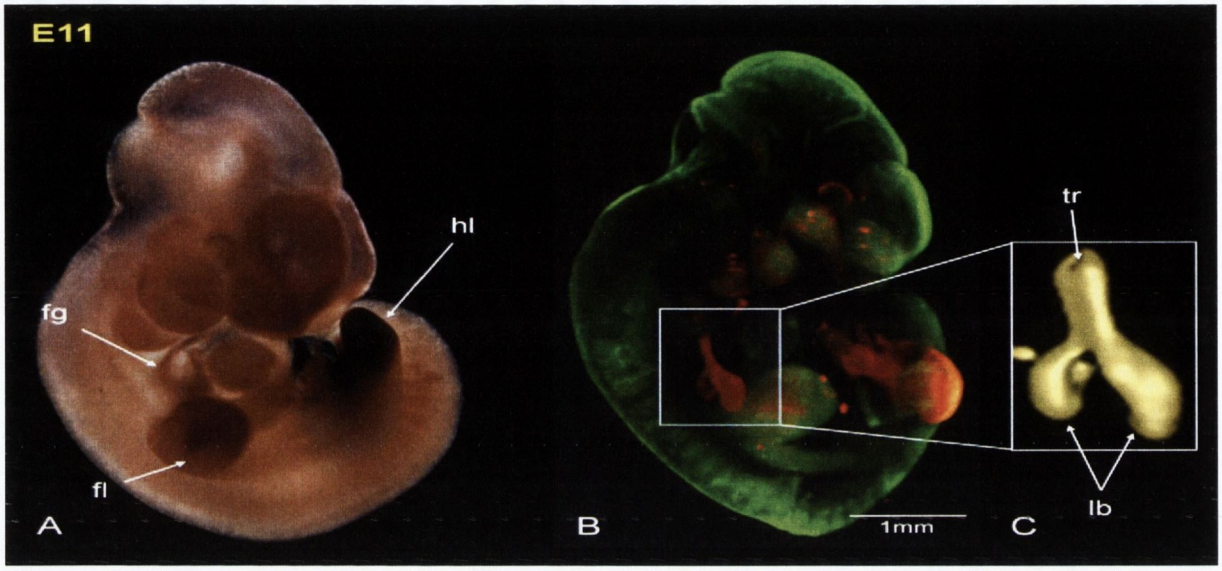


Figure 4.1: The expression of the *Tbx4* gene at E11. Photomicrograph of a lateral view of a whole mount *Tbx4* in situ hybridised specimen (A). The 3D nature of the data analysed in this study is shown in a still shot taken from a 3D reconstruction of the externally visible pattern of *Tbx4* expression following the merging of two OPT scans where the tissue (pseudocolorued in green) and the gene expression (pseudocolorued in red) were captured separately (B). The pattern of *Tbx4* expression around the trachea and lung buds is shown in more detail in this surface rendered image (C). fg; foregut, fl; forelimb, hl; hindlimb, tr; trachea, lb; lung bud.

Analysis of 3D computer reconstructed specimens of control and treated embryos across ages E9-E12 following OPT allowed the *Tbx4* gene expression patterns to be viewed in 2D virtual sections throughout the developing tissue (Figure 4.2). The intensity of staining and the spatial territory within which the *Tbx4* gene was expressed with respect to the forming foregut was compared visually between control and adriamycin treated groups at each time point of collection. In E9 adriamycin treated and control embryos *Tbx4* was expressed in the mesenchyme around the site of the lung buds (Figure 4.2 A-B, I-J). Any apparent difference in *Tbx4* expression pattern viewed on coronal sections (Figure 4.2 B, J) are due to relatively more advanced lung development in control embryos as previously noted (section 3.3.1). At E10 Tbx4 expression was clearly detected in the mesenchyme around the trachea (Figure 4.2 C) and in the mesenchyme around the lung bud (Figure 4.2 D). At this stage *Tbx4* expression

persisted in the lung bud region mesenchyme in treated embryos (Figure 4.2 K, L) even in cases where lung bud formation is lacking (not shown). At E11, virtual sections through the embryos showed *Tbx4* expression in the mesenchyme around the trachea in both control and treated embryos (Figure 4.2 E, M) and around the lung bud (Figure 4.2 F, N) without obvious changes in the spatial distribution or level of gene expression. At E12, embryos had enlarged considerably and the complexity of tissue increased. To ensure penetration of the RNA probe, the embryos were dissected to include only the trunk region from the first branchial arch to the base of the liver. Following OPT scanning and computer reconstruction, *Tbx4* gene expression was detected in the mesenchyme around the lung bud in control embryos (Figure 4.2 G-H) and treated embryos (Figure 4.2 O-P) without any difference in spatio-temporal expression between control and adriamycin treated embryos.

Although the adriamycin treated embryos showed a variety of the expected foregut abnormalities including complete laryngotracheo-oesophageal cleft (in 6 of 22 embryos), OA (in 6 of 22 embryos) and TOF (in 5 of 22 embryos), there were no differences in *Tbx4* gene expression pattern in the adriamycin treated groups, irrespective of the severity of the morphological abnormalities. Comparisons in this case are made according to embryonic day rather than Theiler stage because the progression of overall expression was so similar between control and treated embryos despite morphological differences, so staging differences were not an issue in interpreting the results.

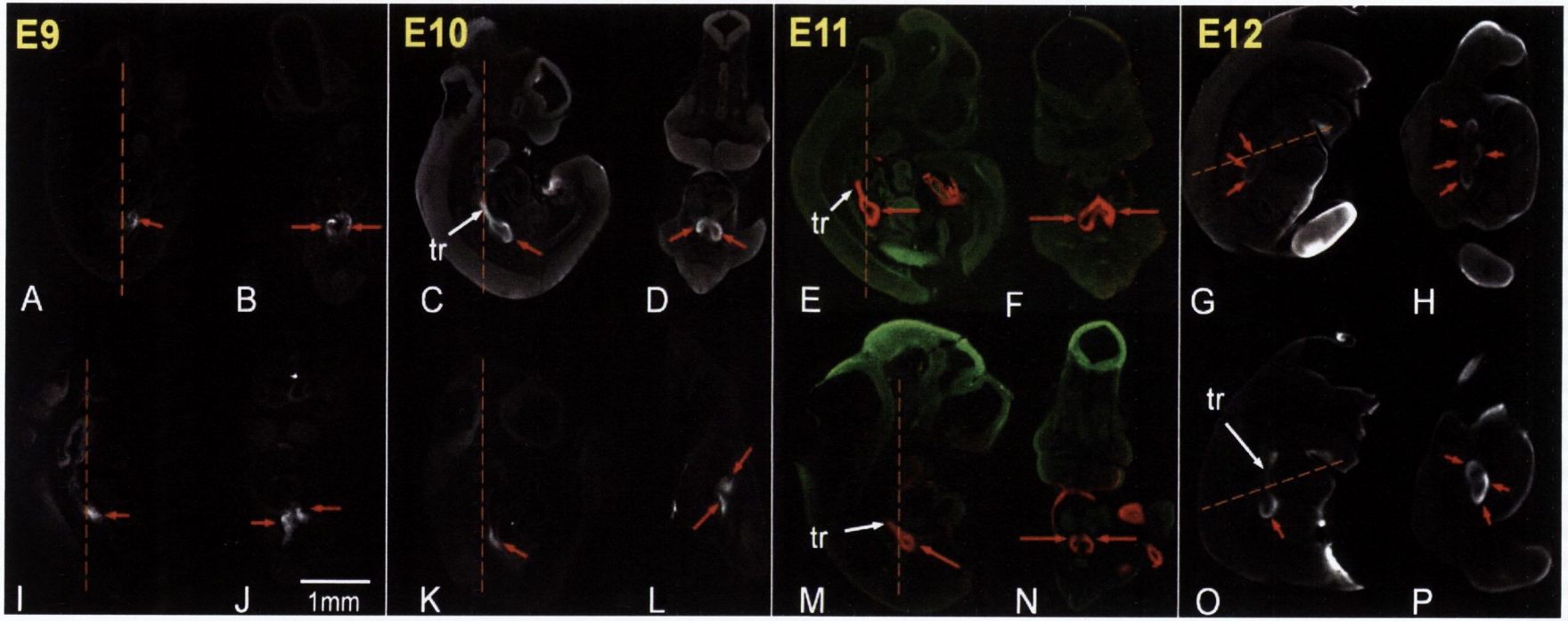


Figure 4.2: *Tbx4* gene expression in control (A-H) and adriamycin treated (I-P) mouse embryos at embryonic days E9 - E12 following whole mount in situ hybrydization. Mesenchymal *Tbx4* gene expression is revealed on virtual sections taken through the 3D data in different saggital (left of each panel) and coronal (right of each panel) planes, section planes indicated by orange lines. Red arrows indicate *Tbx4* expression around the site of the lung buds (A-P). White arrows indicate *Tbx4* gene expression around tracheal mesenchyme (C, E, M, O). E-F, M-N represents virtual sections taken through the 3D data following the merging of two OPT scans where the tissue (pseudocolorued in green) and the *Tbx4* gene expression (pseudocolorued in red) were captured separately. tr; trachea.

4.2.2 *Fgf10* gene expression in control embryos and the effect of adriamycin treatment on gene expression patterns

At developmental stages TS15 and TS16, *Fgf10* gene expression was not detected in the mesenchyme around the foregut in any of the embryos either from control or adriamycin treated groups. At TS17 *Fgf10* gene expression was clearly visualized in the distal mesenchyme around the tip of the two main bronchi in the control group (Figure 4.3 A - C) but no *Fgf10* gene expression was observed in treated embryos at these stages (not shown). As development proceeded, lung buds emerged laterally from the main bronchi and elongated from TS18 stage. Analysis of computer reconstructed specimens following OPT reconstructions of control embryos at TS18 revealed *Fgf10* gene expression in the mesenchyme around the tip of the developing buds in all of the specimens (Figure 4.3 D - F) as well as previously reported expression in other embryonic sites including forelimb, hindlimb, inner ear, forebrain and pharyngeal arches. In adriamycin treated embryos at TS18, *Fgf10* gene expression was detected around the foregut at the level of a transverse widening, indicating the site of lung bud development, which was clearly delayed, in 67% (4 out of 6) of the embryos (Figure 4.4 A - C). Two of the specimens had normal separation of trachea from the foregut and two had complete laryngo-oesophageal cleft. In 33% (2 out of 6) of the treated embryos at this stage (TS18) expression was not detected at all, lung buds were not seen and foregut instead formed an oval shape widening (Figure 4.4 D - F). Both these embryos demonstrated tracheal atresia (Figure 4.4 D). Other sites of the *Fgf10* gene expression were normal in comparison to control.

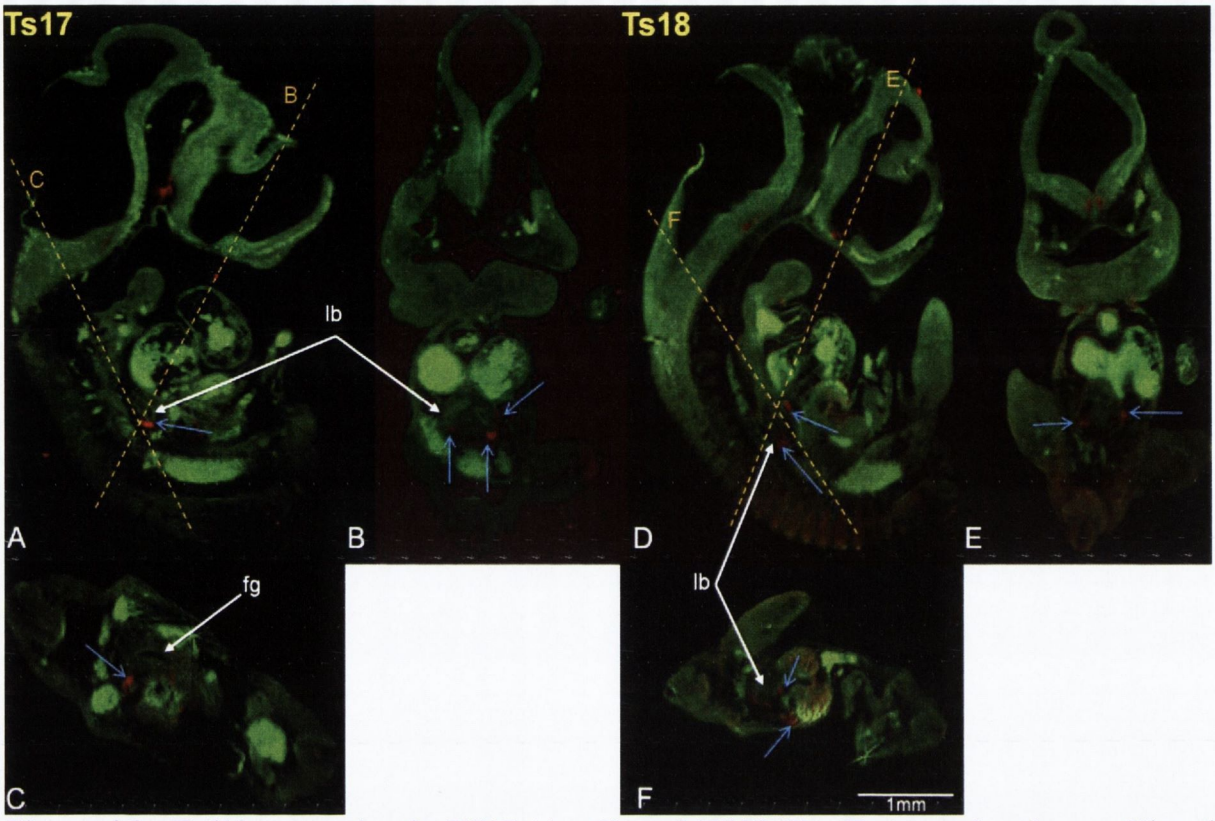


Figure 4.3: *Fgf10* expression in TS17 (A - C) and TS18 (D - F) control embryos. Virtual sections taken through 3D data in different planes are shown. A and D show saggital sections; B, C, E and F show sections in the planes indicated by yellow lines in A and D, following the merging of two OPT scans where the tissue (pseudocolorued in green) and the gene expression (pseudocolorued in red) were captured separately. Blue arrows indicate *Fgf10* gene expression around the tip of the of the lung buds. Expression of *Fgf10* is also visible in forebrain (infundibular recess (A) and optic stalk (D)), inner ear (D), first pharyngeal arch (E) and hindlimb (B). lb; lung buds, fg; foregut. Scale bar as indicated.

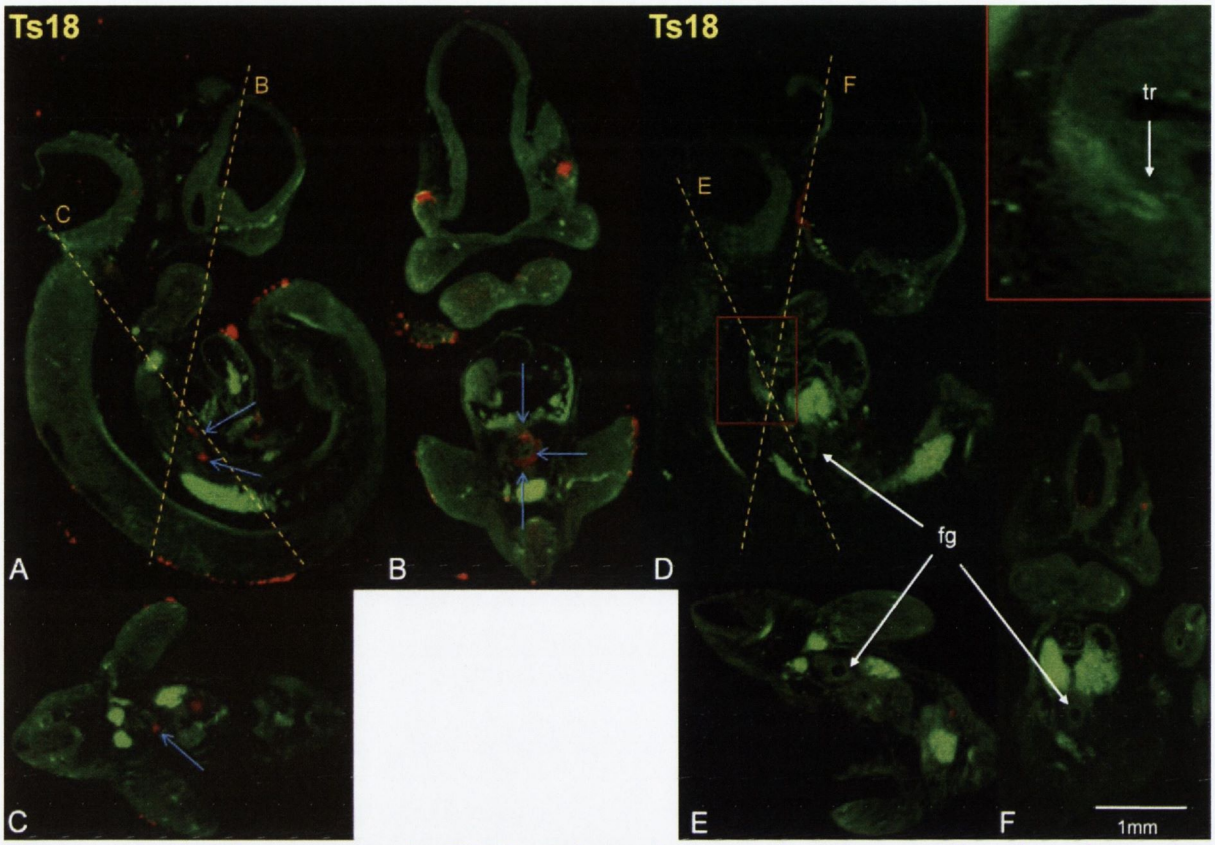


Figure 4.4: *Fgf10* expression in TS18 adriamycin treated embryos. Virtual sections taken through 3D data in different planes are shown. A and D show saggital sections; B, C, E and F show sections in the planes indicated by yellow lines in A and D, following the merging of two OPT scans captured separately. The red signal represents *Fgf10* gene expression with blue arrows indicating expression around the widened foregut (A – C). The specimen in D-F captures oval shape widening of the foregut without adjacent *Fgf10* expression. This specimen has a blind-ended trachea shown in the red frame (D). Expression of *Fgf10* is also visible in forebrain (D, F), eye on B. Green signal represents autofluorescence from the tissue, which highlights the overall anatomy of the embryo. fg; foregut, tr; trachea. Scale bar as indicated.

From TS19-TS21 lung buds normally begin to branch and the complexity of the bronchial tree increases in control specimens (Chapter 3, Figure 3.8). Expression of *Fgf10* was detected along edges of the distal mesenchyme of all lobes and from TS20 strong *Fgf10* expression was detected in the mesenchyme and endoderm of the buds in both control and adriamycin treated groups (Figure 4.5 A – D). Although the expression level and spatial territory of gene expression appeared similar in both groups, pulmonary branching morphogenesis was delayed

in the adriamycin treated group in comparison to controls, confirming my earlier findings (section 3.2.1).

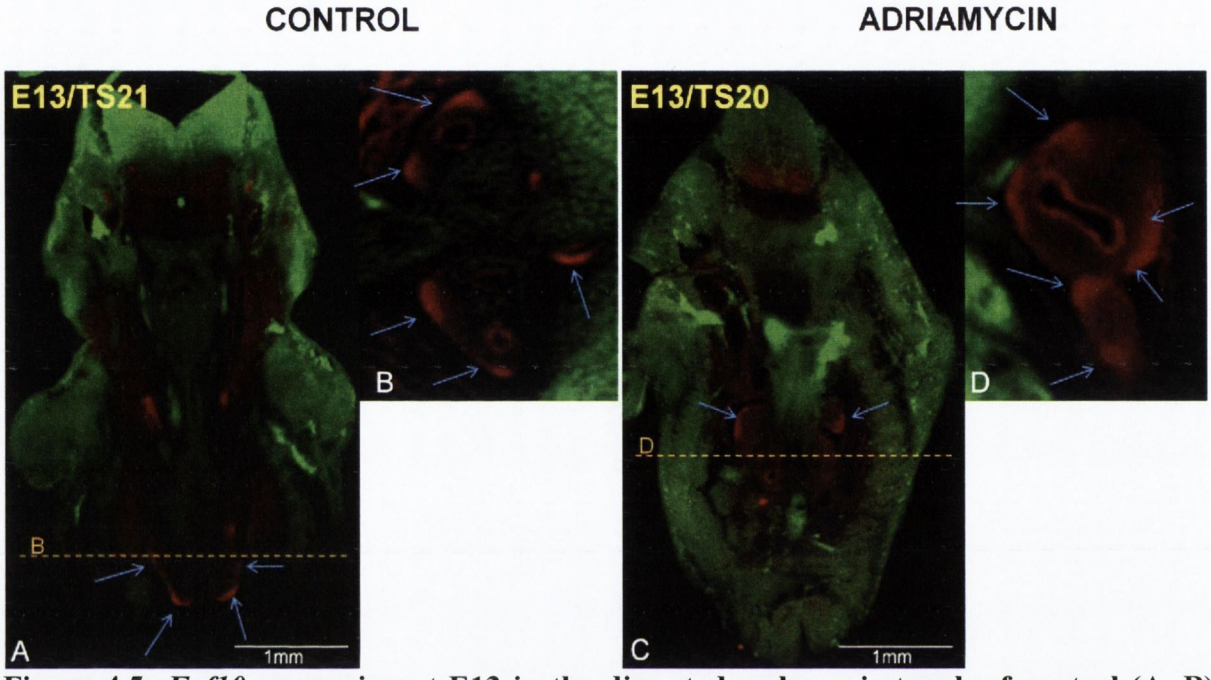


Figure 4.5: *Fgf10* expression at E13 in the dissected embryonic trunk of control (A, B) and adriamycin treated embryos (C, D). Blue arrows indicate *Fgf10* gene expression (in red) around the tip of the lung buds and in the mesenchyme between the buds. Strong *Fgf10* expression is also seen in the endoderm of the buds. Yellow lines correspond with the plane of transverse virtual sections (B and D). Scale bars as indicated.

4.2.3 The effect of adriamycin treatment on *Noggin* gene expression

4.2.3.1 *Noggin* gene expression in control embryos

Throughout the ages of embryos analyzed, *Noggin* expression was visible externally at the dorsal border of the somites (Figure 4.6 A,B), optic vesicles (Figure 4.6 B) and 3rd pharyngeal pouche (Figure 4.6 C,F). In section, strong *Noggin* expression was detected in the notochord, the dorsal and ventral midline of the neural tube (Figure 4.6 D, E). At E12, as the notochord

had almost disappeared, expression remained in the dorsal and ventral midline of the neural tube and 3rd pharyngeal pouch (Figure 4.6 F) and appeared in the interdigital region of the forelimb (Figure 4.6 C).

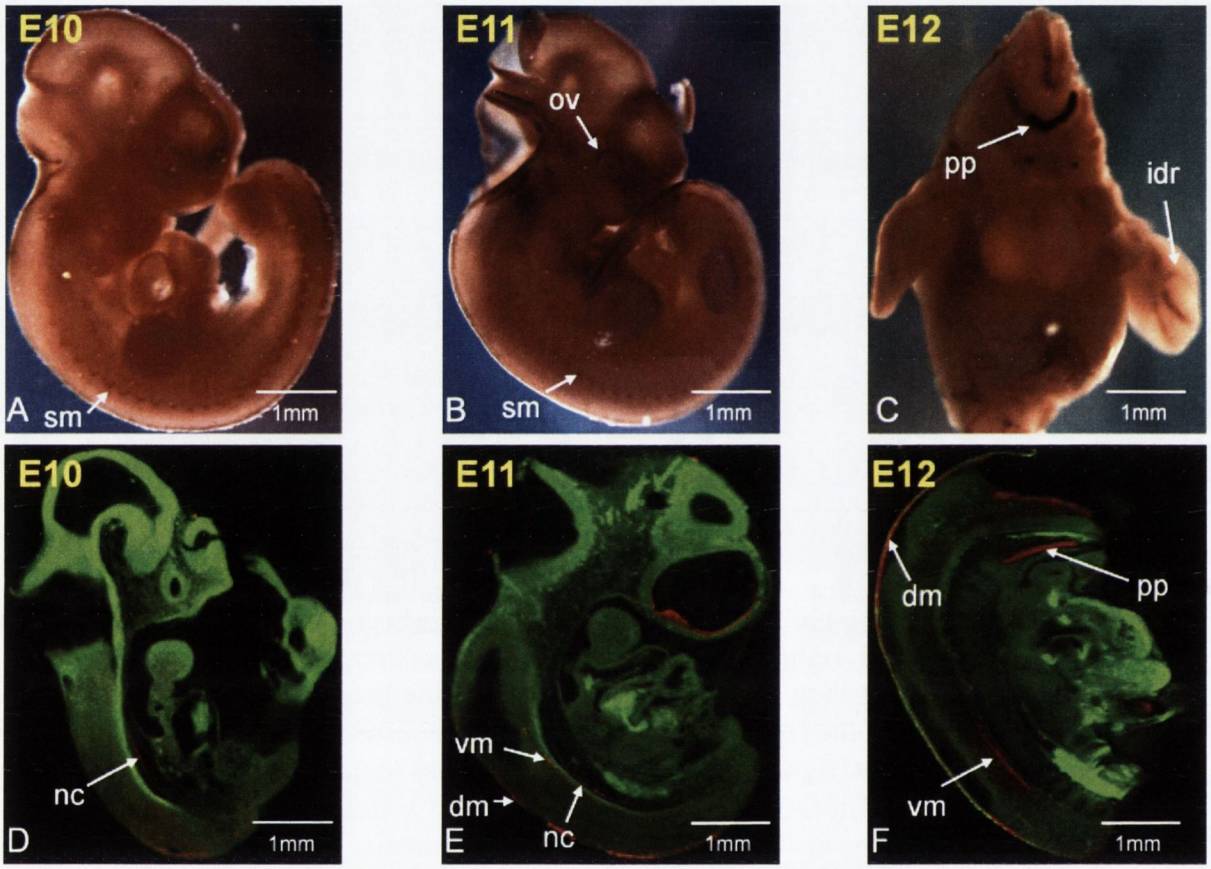


Figure 4.6: *Noggin* gene expression in control embryos. A and B show photomicrographs of whole embryos or embryo trunk (C) at E10, E11 and E12 respectively. D, E and F show virtual sections through the embryos with *Noggin* expression pseudocoloured in red, with arrows indicating *Noggin* gene expression in areas of interest. sm; somites, idr; interdigital region, nc; notochord, dm; dorsal midline of the foregut, vm; ventral midline of the foregut, ov; optic vesicle, pp; 3rd pharyngeal pouch. Scale bars as indicated.

4.2.3.2 Effect of adriamycin treatment on *Noggin* gene expression

At E10 and E11, *Noggin* gene expression was seen in the notochord, the dorsal and ventral midline of the neural tube throughout both control and adriamycin treated embryos (Figure

4.7). In treated embryos, *Noggin* expression was also seen in abnormal/ectopic branches of the notochord, with particularly strong expression in the tips of the branches in 12 out of 15 embryos (Figure 4.7 B, D). Five of these embryos exhibited total laryngotrache-oesophageal cleft (LTEC) and two exhibited foregut stenosis. Strong *Noggin* gene expression was also detected as a broad domain in the dorsal foregut endoderm close to and below the notochord branches in adriamycin treated embryos (6 out of 12) (Figure 4.7 D), whereas only very fine expression was detected in the foregut of control embryos (Figure 4.7 A). Also, in two of the treated embryos with no detected notochord branching, strong *Noggin* expression was seen in distinct patches in the dorsal endoderm of the posterior foregut (Figure 4.7 E). One of these embryos exibited LTEC and in the second the trachea is positioned abnormally close to the ventral wall of the foregut. Only one of the treated embryos analysed (n=15) had normal morphology without notochord branching and normal *Noggin* gene expression.

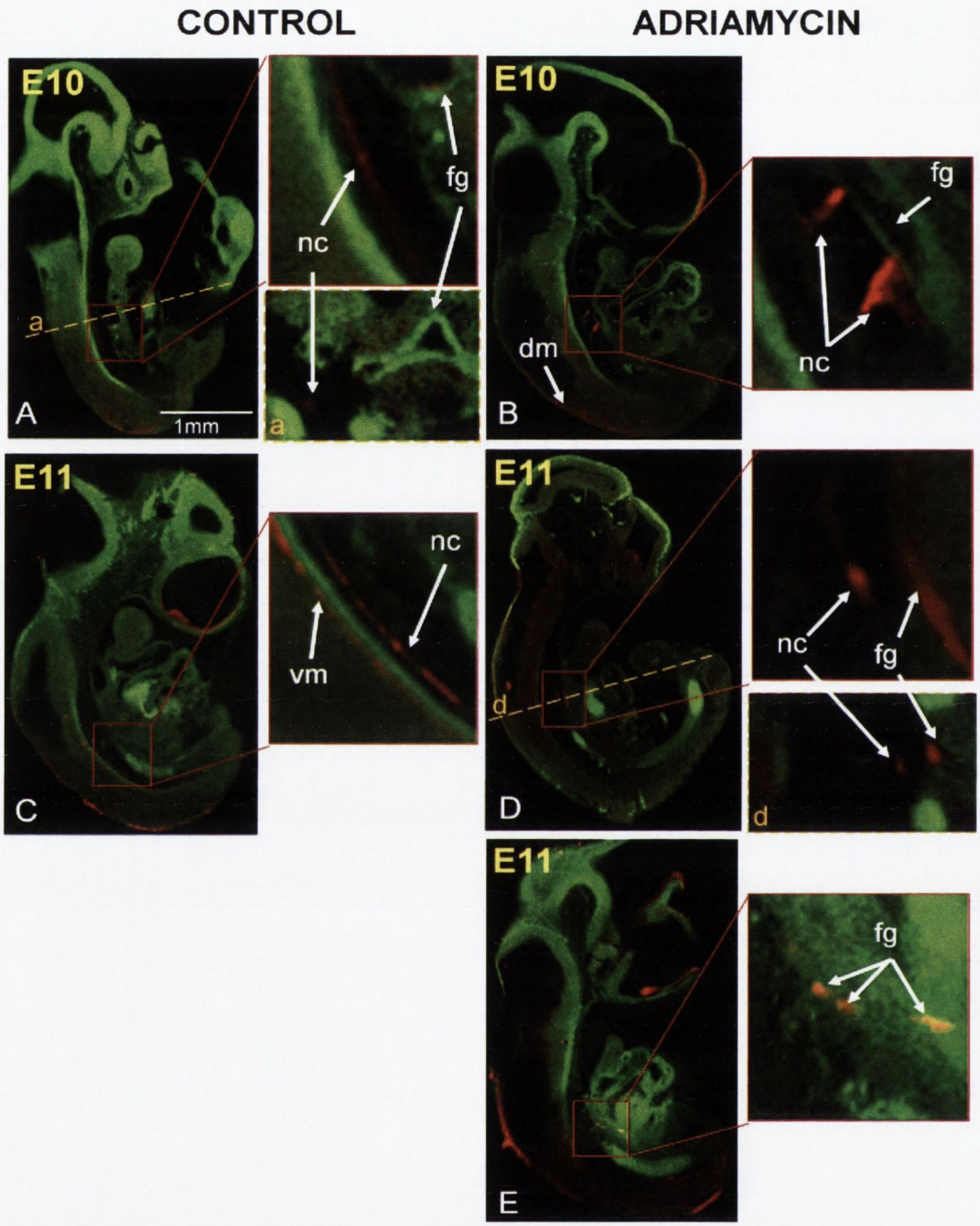


Figure 4.7: *Noggin* gene expression (pseudocoloured in red) in virtual sections of control (A, C) and adriamycin treated (B, D, E) embryos at E10-E11. The regions framed in red are enlarged on the right of each image. Yellow lines correspond with the plane of transverse virtual sections (a and d). Control embryos show *Noggin* expression in the normal notochord (A, C). Adriamycin treated embryos show increased *Noggin* expression in the tips of the notochord branches (B) and increased expression in the dorsal foregut endoderm in the proximity of the notochord branches (D). E; Adriamycin treated embryo at E11 without detectable notochord branches, but abnormal expression in dorsal foregut endoderm. nc; notochord, fg; foregut, dm; dorsal midline of the neural tube; vm; ventral midline of the neural tube. Scale bar as indicated.

By E12, the notochord has usually fully disappeared, and accordingly expression in this region had disappeared in both adriamycin-treated and control embryos. The expression in the ventral midline of the neural tube remained in both treated and control embryos. No differences in expression patterns were seen between treated and control embryos at this age (Figure 4.8). Four of the treated embryos present with fistula and one with oesophageal atresia with upper pouch.

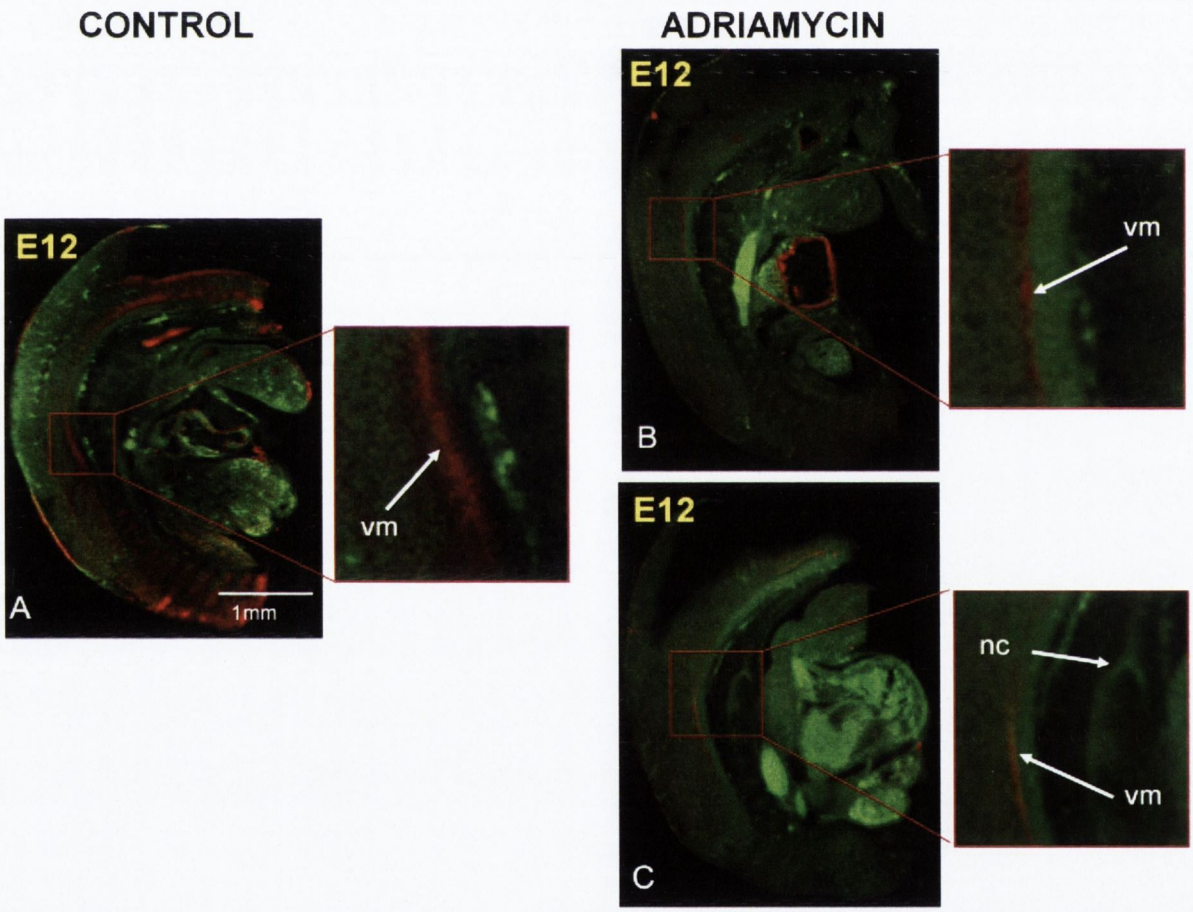


Figure 4.8: *Noggin* gene expression (pseudocoloured in red) in virtual sections of control (A) and adriamycin-treated (B, C) embryos at E12. The regions framed in red are enlarged on the right of each image. All embryos show expression in the ventral midline of the neural tube but no detectable expression in the notochord which would normally have regressed at this stage. C shows an adriamycin treated embryo with a visibly branched notochord still visible but showing no *noggin* expression. nt; notochord, vm; ventral midline of the neural tube. Scale bar as indicated.

4.2.4 The effect of adriamycin treatment on *Bmp4* gene expression

4.2.4.1 *Bmp4* expression in control embryos

At E10, *Bmp4* was seen to be expressed in several sites. In the dorsal region, strongest staining was observed in the dorsolateral half of the somites, in what appeared to be a gradient of expression fading out towards the dorsal border of the somites (Figure 4.9 A). In the limb, another apparent gradient of expression was seen, with the strongest staining in the apical ectodermal ridge, fading through the limb mesenchyme toward proximal (Figure 4.9 A). Further expression was also seen at the distal edges of the branchial arches and in the ectoderm of the ventral body wall.

In embryo sections, expression was seen in the ventral mesoderm sourrounding the lung primordia (Figure 4.10 A) and mesoderm around the tips of the lung buds (Figure 4.11 A). At E11 the expression pattern was very similar to E10, with extended expression seen at somite boundaries (Figure 4.9 B). In section, similar expression in the mesoderm around the lung buds was seen (Figure 4.11 C), as well as in the developing stomach (not shown). At E12, the boundary of expression in the limb became more defined to the limb mesenchyme close to the apical ectodermal ridge, whereas the expression in the somite region split into two distinct bands, one in the dorsal somite region (Figure 4.9 C) and the other close to the dorsal midline of the embryo (not shown). In section, expression was observed in only two of the five control embryos analyzed, probably due to poor probe penetration in the first in situ hybridisation. In the embryos that did show expression in section, *Bmp4* was expressed in the mesoderm around

the tips of the lung buds, which by then had started to branch (Figure 4.12 A). Expression in the stomach was also detected in these two embryos.

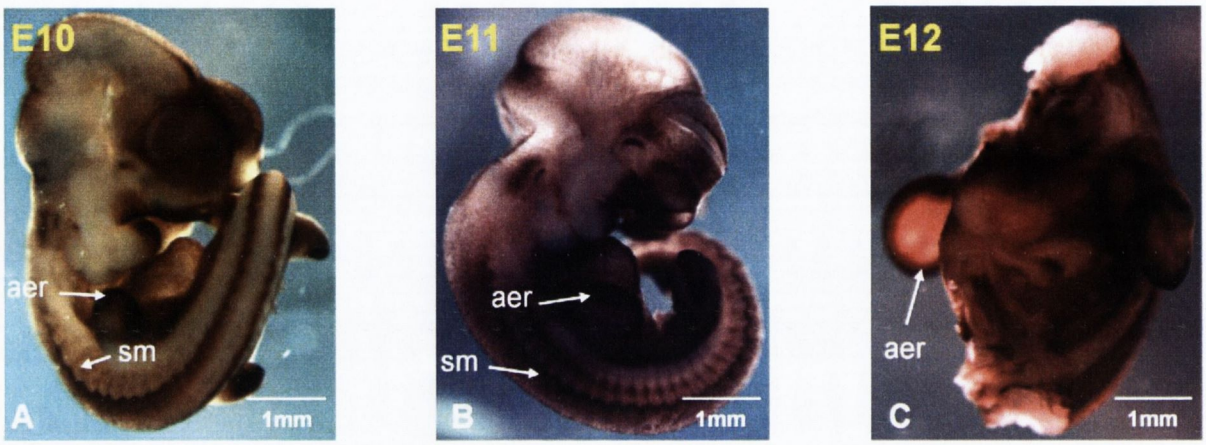


Figure 4.9: *Bmp4* gene expression in control embryos. A and B show photomicrographs of whole embryos or embryo trunk (C) at E10, E11 and E12 respectively. Arrows indicating *Bmp4* expression in areas of interest. *sm*; somites, *aer*; apical ectodermal ridge. Scale bars as indicated.

4.2.4.2 Effect of adriamycin treatment on *Bmp4* expression from E10-E12

At E10, *Bmp4* was expressed in the ventral mesoderm around the lung primordia (Figure 4.10 A and B) and in the mesoderm around the lung buds (Figure 4.11 A nd B) in both control and adriamycin treated groups. When comparing the expression patterns of embryos at the same embryonic day, no difference was seen between adriamycin treated and control embryos, although typical morphological alterations, including notochord branching (5 out of 6) and foregut stenosis (1 out of 6), were recorded.

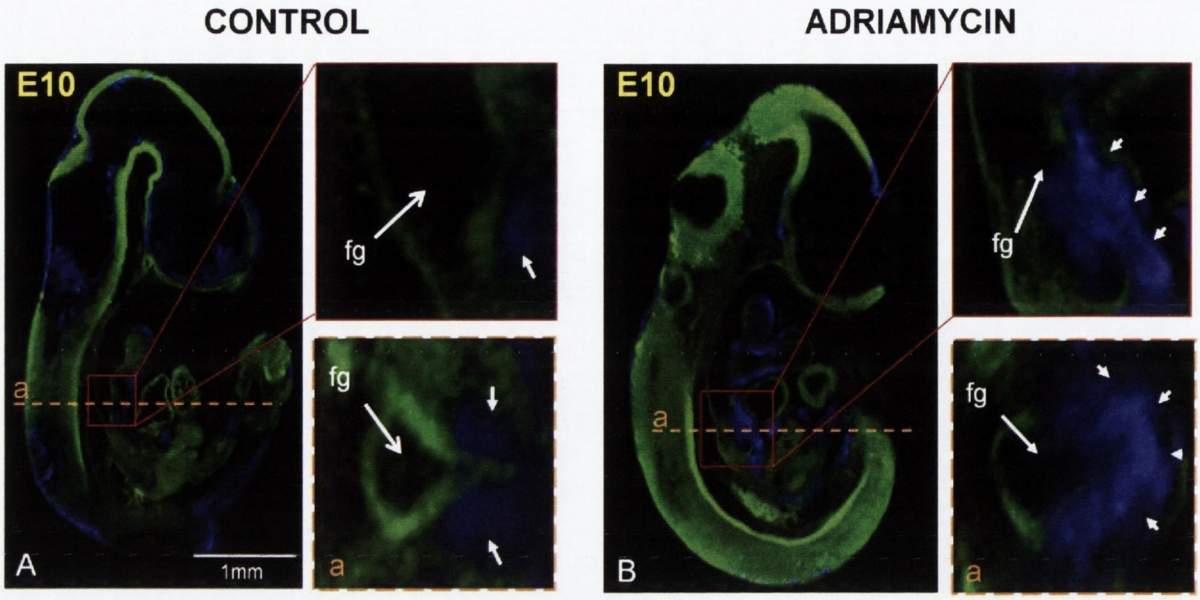


Figure 4.10: *Bmp4* gene expression (pseudocoloured in blue and highlighted by arrow heads) in virtual sections of control (A) and adriamycin treated (B) in E10 embryos. Images on the right show the boxed area enlarged (above) and transverse sections in the plane indicated (a; below). Both, control and treated embryos show *Bmp4* gene expression restricted to the ventral mesoderm surrounding lung primordia (arrow heads). fg; foregut. Scale bar as indicated.

At E11, both adriamycin treated and control embryos expressed *Bmp4* in the tips of the lung buds (Figure 4.11 C and D), and no expression was ever recorded around the foregut. Adriamycin treated embryos were again delayed and typical morphological abnormalities were recorded including notochord branching (4 out of 6), LTEC (4 our of 6), foregut stenosis (1 out of 6), but no difference in expression pattern between adriamycin treated and control embryos was seen.

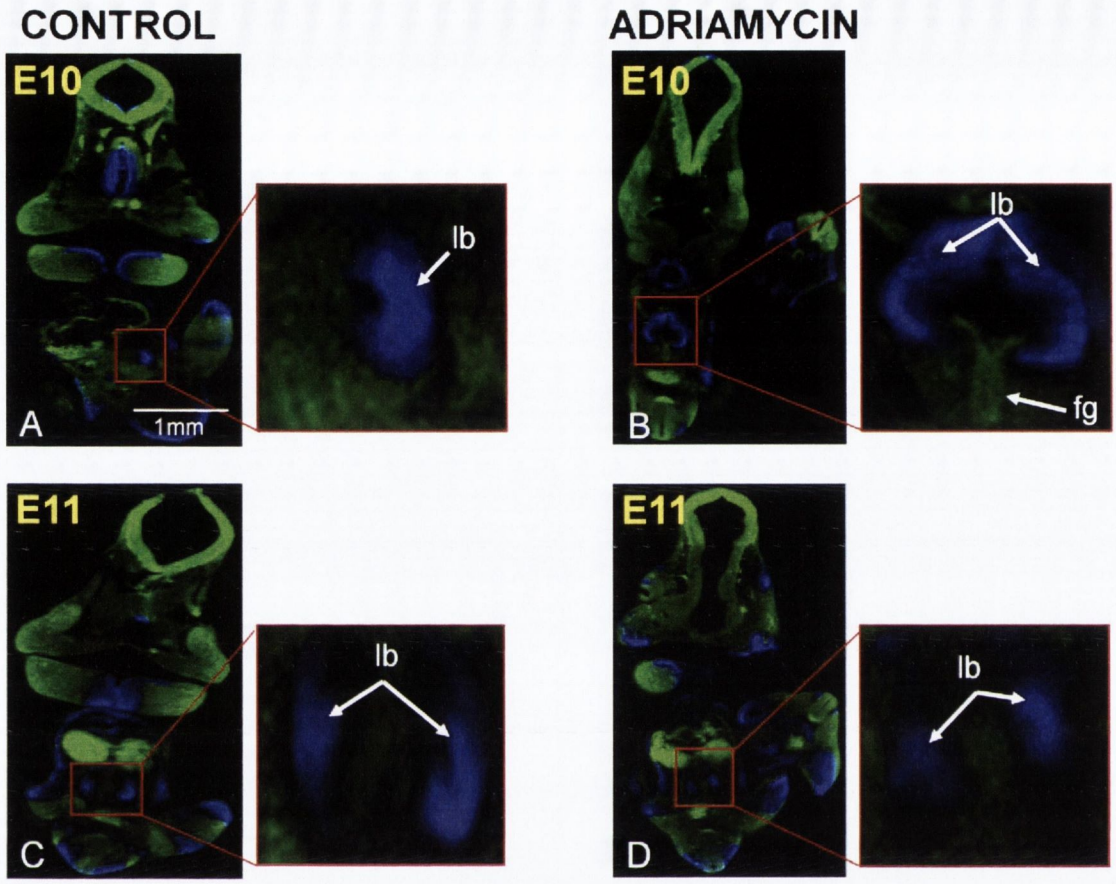


Figure 4.11: *Bmp4* gene expression (pseudocoloured in blue) in virtual sections of control (A, C) and adriamycin treated (B, D) embryos at E10 and E11. The regions framed in red are enlarged on the right of each image. Control and treated embryos show expression restricted to the mesoderm of the developing lung buds with no differences in distribution of the transcript. lb; lung buds, fg; foregut. Scale bar as indicated.

At E12, both treated and control embryos showed *Bmp4* gene expression in the lung bud mesoderm (Figure 4.12 A and B) and stomach (not shown), with no difference in expression pattern noted between them. One out of five treated embryos showed oesophageal atresia with upper pouch.

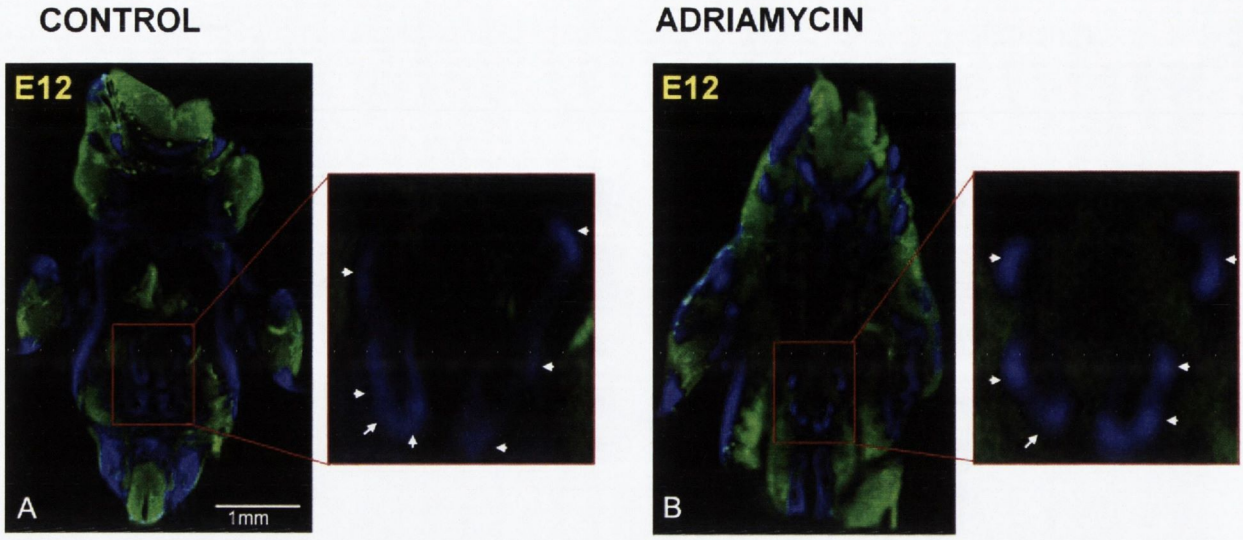


Figure 4.12: *Bmp4* gene expression (pseudocoloured in blue and highlighted by arrow heads) in virtual sections of control (A) and adriamycin treated (B) embryos at E12 showing Bmp4 expression pseudocoloured in blue. The regions framed in red are enlarged on the right of each image. Strong *Bmp4* expression is seen in the mesoderm of the lung buds in both groups (arrow heads). Scale bar as indicated.

4.2.5 The effect of adriamycin treatment on *Wnt2* gene expression

4.2.5.1 *Wnt2* gene expression in control embryos

In embryo section, *Wnt2* gene exprerssion was seen in the ventral mesoderm surrounding lung primordia from E10 (Figure 4.13 A). As development progresses, at E11, Wnt2 expression was recorded in the lateral mesoderm sourrounding newly formed lung buds (Figure 4.13 B). Very strong *Wnt2* gene expression was recorded from E12 in the mesoderm of the lung buds, which show advanced branching morphogenesis at this stage (Figure 4.13 C).

4.2.5.2 Effect of adriamycin treatment on *Wnt2* gene expression

Wnt2 gene expression in adriamycin trated embryos was seen in the ventral mesoderm around the lung primordium from E10 (Figure 4.13 D). Spatial distribution of the gene transcripts was not altered in comparison to control embryos although notochord branching was recorded in all of the analysed specimens (5 out of 5). At E11 lung buds did not separate from the foregut in most of the treated embryos (4 out of 5) however *Wnt2* gene expression was restricted to the ventro-lateral mesoderm of the foregut in the region where lung buds would normally emerge (Figure 4.13 E). Even in two of the five embryos exhibiting LTEC and foregut stenosis, *Wnt2* gene expression was not altered. At E12 lung buds underwent branching morphogenesis in all investigated embryos (5 out of 5). *Wnt2* gene expression was very strong and gene transcript restricted to the mesoderm sourrounding lung buds in all of the embryos with no differences in comparison to the control group (Figure 4.13 F). Three out of five embryos exhibited fistula from the carina or bronchii into the stomach and in all of these specimens *Wnt2* was expressed in the mesoderm sourrounding the fistula and anterior part of the stomach (Figure 4.13 F).

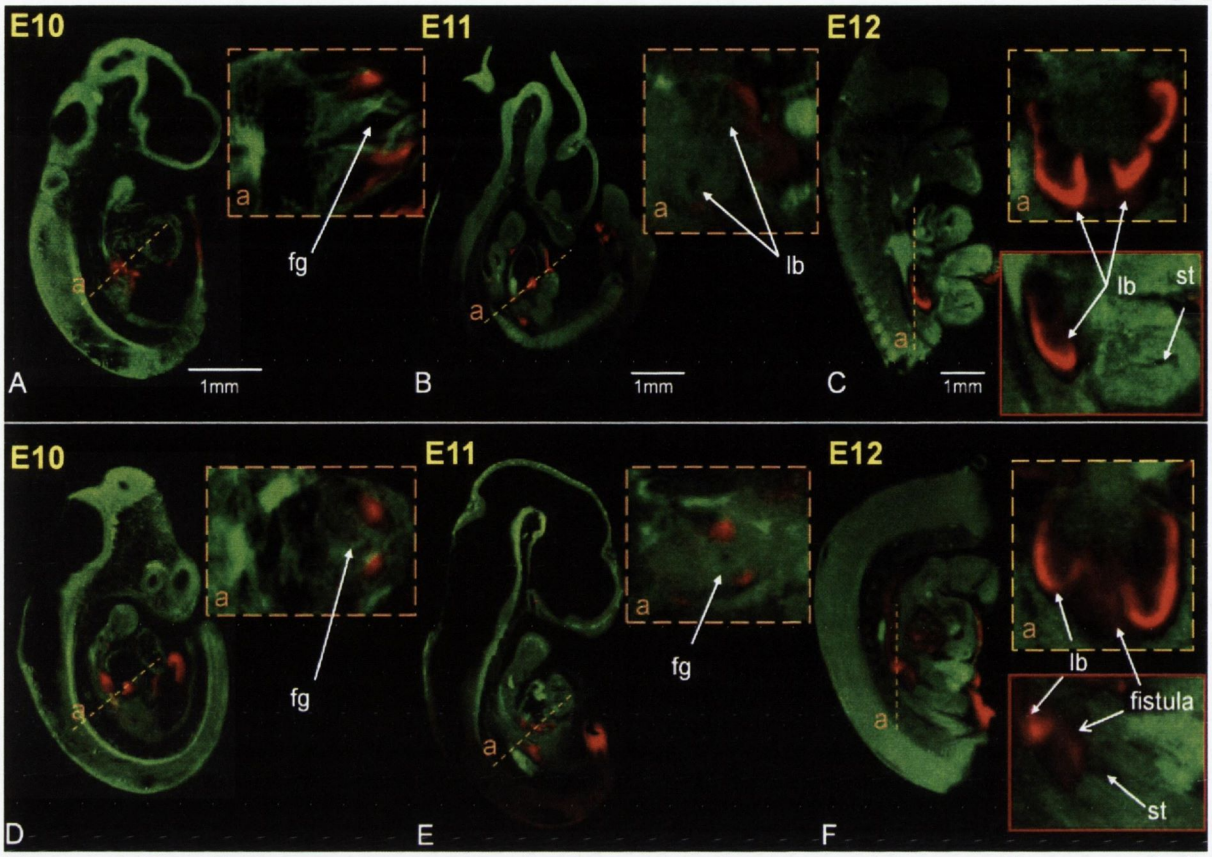


Figure 4.13: *Wnt2* gene expression in the mesenchyme on the ventral aspect of the developing foregut and around the lung buds. Virtual sections of control (A-C) and adriamycin treated (D-F) embryos at E10 to E12, with *Wnt2* expression pseudocoloured in red. Sagittal sections of the control and adriamycin treated embryos with enlargement of the expression in the mesoderm around the foregut and lung buds in transverse sections in the planes indicated (a) in orange (A, B, D, E). C and F additionally show enlargment of the region of interest in red frame. In F, *Wnt2* expression around an abnormal fistula is indicated. fg; foregut, lb; lung bud. Scale bars as indicated.

4.2.6 The effect of adriamycin treatment on *Wnt7b* gene expression

4.2.6.1 *Wnt7b* gene expression in control embryos

Endodermal expression of the *Wnt7b* gene was evident in the ventral foregut and at the tip of the lung primordia from E10 in virtual sections of embryo reconstructions (data not shown).

From E11 strong expression was recorded in the endoderm of the trachea and tip of the lung buds (Figure 4.14 A). As branching morphogenesis progresses *Wnt7b* transripts were seen very clearly in the trachea and lung bud endoderm (Figure 4.14 B).

4.2.6.2 Effect of adriamycin treatment on *Wnt7b* gene expression

Wnt7b gene expression in adriamycin trated embryos was seen in the ventral endoderm of the lung primordium from E10 in all of the adriamycin treated embryos (data not shown). In this group of treated embryos none had foregut anomalies at this stage although 3 out of 5 had abnormal notochord branches. Spatial distribution of the *Wnt7b* gene transcripts was not altered in comparison to control. At E11, *Wnt7b* gene expression was restricted to the trachea and lung bud endoderm (Figure 4.14 C). The pattern of gene expression was not altered in the embryos that exhibit foregut abnormalities (3 out of 5) at this stage, or notochord branching (3 out of 5). The *Wnt7b* gene expression pattern was not altered in any of the treated embryos analysed (5 out of 5) in comparison to control specimens. At E12 lung buds underwent branaching morphogenesis in all investigated embryos (5 out of 5). *Wnt7b* gene expression was very strong and gene transcripts were restricted to the tracheal and lung bud endoderm in all of the embryos (6 out of 6) with no differences in comparison to the control group (Figure 4.14 D). Four out of six embryos exhibited fistula from the carina or bronchii into the stomach and in all of these specimens *Wnt7b* gene was expressed in the endoderm of the anterior foregut and lung buds but not in the fistula.

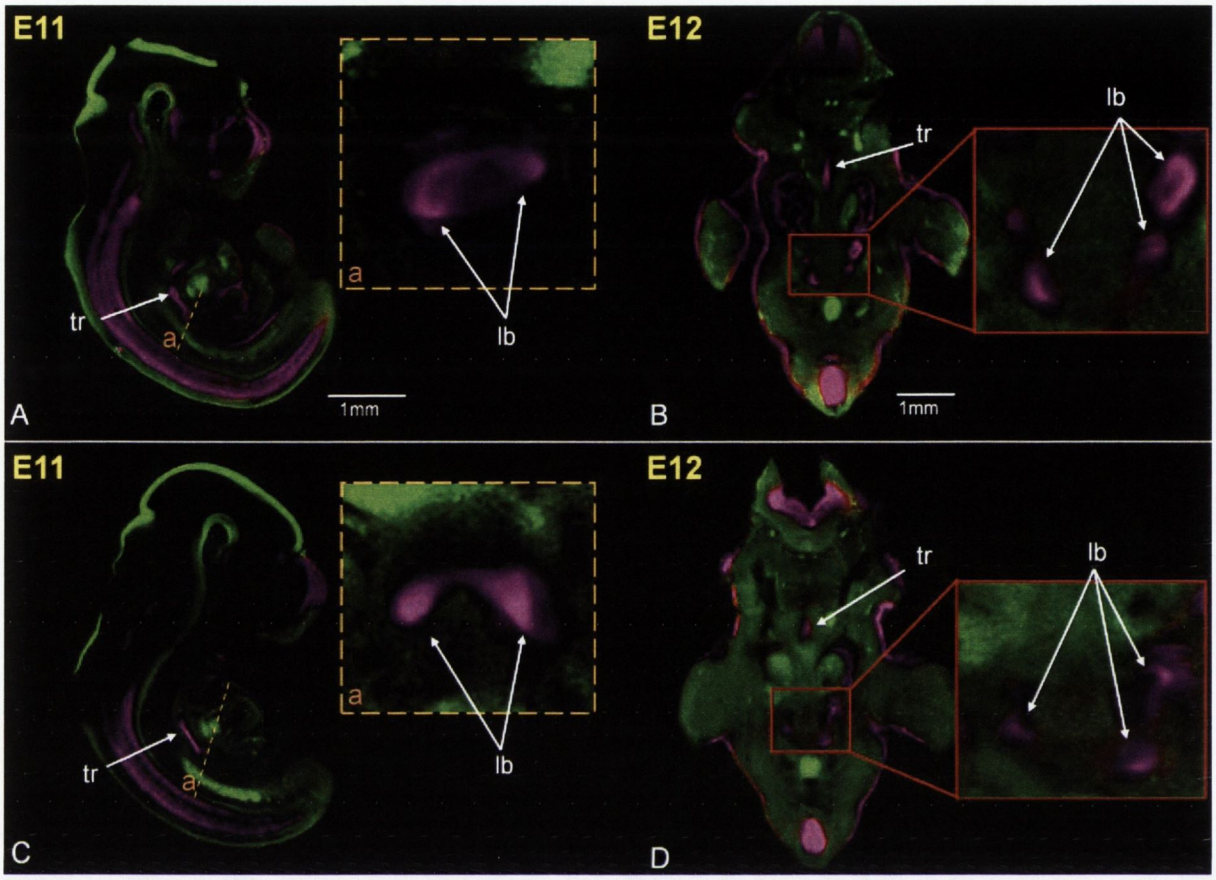


Figure 4.14: *Wnt7b* gene expression in the developing foregut and lung in control (A, B) and adriamycin treated embryos (C, D) at E11 and E12; gene expression is pseudocoloured in purple. Virtual sagittal sections taken through the 3D recontructions show *Wnt7b* gene expression in the tracheal endoderm (A, C) and enlargements of the gene expression in the endoderm of the developing lung buds. Orange frames show coronal sections in the plane indicated by the orange line *a* (A, C). B and D show similar coronal virtual sections through the specimens at E12 with enlargements of the region shown in the red frames. tr; trachea, lb; lung bud. Scale bars as indicated.

4.3 Discussion

This chapter aimed to use OPT technology to reveal the expression patterns of candidate genes implicated in foregut development as a preliminary way of identifying which genes may be affected when the congenital abnormalities OA and TOF are induced by adriamycin treatment.

Making use of the 3D nature of OPT generated data, comparisons of expression patterns in treated and control embryos, combined with an analysis if morphological defects, was facilitated.

4.3.1 Overview of findings

The *Noggin* gene was found to be expressed in the same territory in control and adriamycin treated embryos. Additionally, in adriamycin treated embryos *Noggin* was expressed throughout the notochord with particularly strong expression in the tips of the notochord branches at E10 and E11. Moreover in some of the treated embryos *Noggin* gene transcripts were recorded in an extensive layer of the dorsal endoderm of the foregut, more extensive than in control embryos in the same region. Abnormal accumulation of *Noggin* gene transcripts in the tip of the notochord branch or the dorsal wall of the foregut was associated with a wide spectrum of foregut abnormalities.

Expression of the *Fgf10* gene in both control and adriamycin treated embryos was found to be restricted to the distal mesenchyme of the bronchii. Although there was no differences in spatial distribution of the transcripts between the groups, delayed gene expression was seen in treated embryos. In some of the treated embryos, lack of *Fgf10* gene expression at TS18 was associated with tracheal atresia. *Tbx4* gene expression was restricted to the ventral mesoderm of the foregut from very early stages of development and as lung development progressed in later stages gene expression was restricted to the mesoderm surrounding trachea and lung

buds. There was no differences in temporo-spatial distribution of *Tbx4* transcript between the control and treated groups across the investigated stages.

Bmp4 gene expression was seen in ventral mesoderm around the lung primordia and strong *Bmp4* gene expression was recorded around the mesoderm of the lung buds from E10 in both groups. There was no differences in temporo-spatial distribution of the transcripts across all stages in control and adriamycin treated groups.

Wnt2 and *Wn7b* gene expression in this study was seen in the ventral foregut mesoderm (*Wnt2*) and endoderm (*Wnt7*) around the lung primordia and lung buds. No differences were observed in the expression of either genes in these sites in control and treated embryo groups and across all stages. However, in all of the treated embryos at E12 presented with a fistula *Wnt2* gene expression was seen in the mesoderm around the fistula and proximal part of the stomach. *Wnt7b* was not expressed in the fistula.

4.3.2 Expression of the *Fg10* gene is delayed in the ventral mesoderm of the anterior foregut of treated embryos: implications for outgrowth of lung primordia.

Once the respiratory field is established in the ventral foregut endoderm, accompanied by localized *Nkx.2.1* gene expression (Desai *et al.*, 2004; Morrisey and Hogan, 2010), outgrowth and extension of the lung primordia into surrounding mesenchyme is entirely dependent on the localized expression of *Fgf10* in the mesenchyme overlying the tips of the primary lung buds and expression of the receptor *Fgfr2b* in the endoderm of the foregut (De Moerlooze *et al.*, 200; Sakiyama *et al.*, 2003; Sekine *et al.*, 1999). In Chapter 3 I showed that *Nkx2.1* gene

expression was normally confined to the ventral domain of the foregut endoderm in adriamycin treated embryos, similar to control (Figure 3.6, summarised in Figure 4.15). Here I showed that mesenchymal *Fgf10* gene expression, was detected from TS17 in control embryos and restricted to the distal mesenchyme of the two main-stem bronchi. Expression of the *Fgf10* gene in adriamycin treated embryos was delayed and first detected at TS18 at approximately the same level and spatial territory, as in control embryos detected as early as TS17. However, *Fgf10* gene expression was detected in only two-thirds of the embryos at TS18 indicating that expression is just commencing at this stage. Our detailed 3D morphological study of the AMM presented in chapter 3 showed that lung bud formation and separation from the foregut is delayed in treated embryos in comparison to controls. This delay in *Fgf10* gene expression and in outgrowth of lung primordia in the AMM indicates that failure to express *Fgf10* in the ventral mesenchyme at earlier stages may at least contribute to delayed lung development.

A striking finding in this study was the lack of *Fgf10* gene expression in treated embryos which exhibited tracheal atresia (TA). This is reminiscent of the phenotype seen previously in mutants lacking *Fgf10*, where the trachea separates from the foregut although no bud extension occurs (Minoo *et al.*, 1999; Sekine *et al.*, 1999) suggesting that the same mechanism may be involved in the etiology of this malformation in AMM.

Fgf10 expression may be inhibited by ectopic *Shh* signaling through the abnormal branch of the notochord, as described in chapter 3. It was previously reported that *Shh* is part of an epithelial network of regulators that restricts expression of *Fgf10* in the mesenchyme around

the lung bud (Bellusci *et al.*, 1997b; Lebeche *et al.*, 1999). Although here *Shh* is downregulated in the ventral endoderm of the foregut (Chapter 3, Fig 3.4 Cb; summarised in Figure 4.15) in some of the adriamycin treated embryos, it is therefore unlikely that it is the cause of the delay in *Fgf10* expression. Alternatively, it is possible that adriamycin treatment affects the expression of other signalling molecules, not investigated in this work, involved in regulation of *Fgf10* expression, for example Retinoic Acid and *Tgfβ* (Chen et al., 2007).

The presence of a positive feedback loop between regulation of *Tbx4* and *Fgf10* expression was shown in chick during lung primordia formation (Sakiyama *et al.*, 2003). Ectopic *Fgf10* expression introduced into the visceral mesoderm alone induced ectopic budding of the foregut and caused ectopic mesodermal *Tbx4* expression around the anterior foregut. Inactivation of *Tbx4* function in the visceral mesoderm repressed *Fgf10* expression in corresponding mesoderm and led to failure of lung bud formation (Sakiyama *et al.*, 2003). In the present work *Tbx4* expression was detected adjacent to the foregut at an equivalent antero/posterior position and at approximately the same level in control and adriamycin treated embryos. This indicates that the morphological abnormalities seen in AMM are not accompanied by obvious changes in the spatial distribution or level of gene expression of *Tbx4* suggesting that *Tbx4* regulation is not altered in this model. This implies that the morphological abnormalities in AMM can occur in the presence of *Tbx4* transcripts. It also suggests that factors other than *Fgf10* positively regulate *Tbx4*.

4.3.3 Ectopic *Noggin* gene expression in the notochord and posterior wall of the foregut in adriamycin treated embryos: implications for foregut separation.

In chapter 3, analysis of ectopic notochord branches in AMM showed a possible relationship between position and thickness of ectopic notochord and severity of foregut abnormalities. From these observations it was proposed that abnormal notochord branching causes the disturbance of normal development of the foregut. Here all of the treated embryos analysed with abnormal notochord branches at E10 and E11, showed *Noggin* expression throughout the notochord with particularly strong expression in the tips of the notochord branches. It was shown that in cultured explants of mouse lungs, increasing concentrations of *Shh* results in an increase in Noggin gene expression (Weaver *et al.*, 2003). Therefore, in the presence of abnormally close notochord in AMM with strong *Shh* gene expression, as shown in Chapter 3 (Figure 3.4; summarised in Figure 4.15), *Noggin* gene expression might be upregulated. Shh however, is expressed very strongly through the entire notochord and abnormal branches. In contrast *Noggin* gene expression accummulated particularly in the tips of the notochord branches (Figure 4.7 B).

6 of the embryos at E11 also showed *Noggin* gene expression in a more extensive territory of cells of the dorsal foregut endoderm at the level of the branch or below. In control embryos, expression in the foregut was limited to a more restricted layer of cells of the dorsal foregut wall, consistent with previous reports (Que *et al.*, 2006). This implies that abnormally high levels of *Noggin* secreted from the ventrally displaced notochord in treated embryos may lead to altered gene expression in the dorsal endoderm of the foregut. However, this hypothesis is

in conflict with the observation that in two of the treated embryos with no detected notochord branching, strong *Noggin* expression was seen in distinct patches in the dorsal endoderm of the posterior foregut. An alternative hypothesis for the perturbed expression pattern of *Noggin* seen in the adriamycin model is that some of the cells that were meant to "become" notochord cells were "left behind" in the foregut endoderm when the chordomesoderm separated from it. Further evidence for such a hypothesis comes from the study of *noggin* knockout mice (Que *et al.*, 2006) where similar morphological abnormalities of the notochord and foregut were observed. These authors observed cells positive for the notochord marker Brachyury embedded within the dorsal foregut in $Nog^{-/-}$ mutant embryos. This is unlikely here following observation that Brachyury positive cells were not found embeded in dorsal wall of the foregut in AMM, shown further in Chapter 6.

It was hypothesised that elevated *BMP* signalling in the notochord and dorsal foregut endoderm due to the lack of the Noggin gene product in $Nog^{-/-}$ mutant embryos might promote intracellular adhesion and result in prolonged attachment of the notochord and faulty foregut separation (Li *et al.*, 2007; Que *et al.*, 2006). It was found that the notochord branching defect, together with foregut malformations could be rescued by reducing the gene dose of *Bmp4* by 50%. Therefore in this study, *Bmp4* was selected as a potential candidate due to its influance in the Noggin knockout mouse (Que *et al.*, 2006). However, in this project, no difference in the expression patterns of *Bmp4* was found between adriamycin treated embryos and controls. There are many possible explanations for these findings. First of all, it is important to note that the action of *BMP4* is inhibited by *Noggin* by not permitting *BMPs* to bind to their receptors (Gilbert, 2006). Therefore, just because *Bmp4* is being expressed, this does not mean that it is

having the effects that it is supposed to in the areas of interest. Also, despite their antagonistic relationship, the two genes do not directly affect the transcription of each other, and thus an upregulation of one is not necessarily followed by a downregulation of the other.

To further test our postulation that *BMP/Noggin* pathway is deregulated and may be causative of associated foregut abnormalities, investigation of the localisation of phosphorylated SMAD 1/5/8 (pSMAD 1/5/8), which accumulates only when the pathway is activated, would be beneficial for further study. Increased *BMP* signalling revealed by increased phosphorylated Smad1 antibody staining was found in *Nog*$^{-/-}$ mutant notochords at E8.5, with subsequent reduction in the level by E9, consistent with loss of *Noggin* function and agreement with the critical role of *BMP* antagonism during notochord detachment.

Que *et al* (2006) proposed that the lack of separation of the oesophagus and trachea seen in the *Nog*$^{-/-}$ mutants was caused by a lack of expression of *Noggin* in the dorsal foregut. Li *et al* (2007) also created *Noggin* knock out embryos and suggested that delayed and improper notochord delamination resulted from lack of *Noggin* gene expression in the notochord. In contrast all of the treated embryos in our series with abnormal notochord branches expressed the *Noggin* gene in the tip of the branches and 50% (6 ot of 12) expressed the *Noggin* gene in an extended territory of cells of the dorsal foregut endoderm. All of them exibited foregut abnormalities. These observations strongly suggest that *Noggin* has an effect on foregut morphology during development and leads to the conclusion that foregut malformations might be triggered by an imbalance of *Noggin* with respect to other signalling molecules.

In terms of the possible effect of *Noggin* on foregut patterning, explant studies in chick have demontrated that signals from Hensen's node, or its derivatives including the notochord, specify ingressing endoderm cells as foregut, inducing *Sox2* expression during gastrulation (Matsushita *et al.*, 2008). Moreover *Noggin* or *Chordin*, factors known to be secreted from Hensen's node and its derivatives induced endodermal *Sox2* expression in early chick embryos after 24-36 hours incubation (Matsushita *et al.*, 2008). *Sox2*, initially expressed throughout the entire foregut, is down-regulated in the respiratoty domain by E9.0 in mice (Sherwood *et al.*, 2009), coincident with up-regulation of *Nkx2.1* in this domain. Here increased *Noggin* gene expression in the tip of the branches was associted with loss of *Sox2* gene expression across the foregut endoderm at the level of the branch at E10 and E11 as described in Chapter 3 (Figure 3.6, summarised in Figure 4.16). Loss of *Sox2* gene expression was not associated with the dorsal expansion of *Nkx2.1* expression. Additionaly in $Nog^{-/-}$ mutants, the spatial expression pattern of *Nkx2.1* was restricted to the ventral endoderm of the foregut (Que *et al.*, 2006). This suggests that the *Noggin* gene is not involved in D/V patterning of the foregut in AMM.

Conditional inactivation of *Bmp4* in the foregut endoderm and surrounding mesenchyme results in tracheal atresia and lung hypoplasia (Li *et al.*, 2008b). Analysis of these mutants showed that ventral endodermal *Nkx2.1* expression is preserved at E9.5 - E10.5, before foregut separation, although at E12.5 an undivided single foregut tube is *Nkx2.1* negative. This led to the the conlusion that *Bmp4* is not required for the initial respiratory specification of the foregut (Li *et al.*, 2008b). Recent published studies showed that conditional inactivation of *Bmpr1a* and *Bmpr1b*, two principal *Bmp* receptors results in an undivided single foregut tube

in mouse mutants (Domyan *et al.*, 2011). Analysis of these mutants showed that ventral endodermal *Nkx2.1* expression is preserved at 19 somites (E9.25) although by 24 somites (E9.5) downregulation of *Nkx2.1* expression was observed together with ventral expansion of *Sox2* expression (Domyan *et al.*, 2011). Further expreriments showed that *Bmpr1a* represses the *Sox2* promotor in vitro (Domyan *et al.*, 2011). Because *Nkx2.1* and *Sox2* antagonise each other's expression (Que *et al.*, 2007) this led to the conclusion that *Bmpr1 a* and *b* may promote respiratory identity in an instructive fashion by inducing *Nkx2.1*, therby repressing *Sox2*. Alternatively, it could promote respiratory fate in permissive fashion by repressing *Sox2*, thereby allowing expression of *Nkx2.1* and tracheal formation (Domyan *et al.*, 2011). An analysis of the expression pattern of the *Bmp* receptors could thus be an interesting candidates for future study.

Assuming that *Bmp* signalling is inhibited in AMM by *Noggin* expression through the notochord branches, *Sox2* should be positevely regulated in the dorsal foregut endoderm of the treated embryos, not absent as I showed. However, in the developing mouse lens placode and taste papillae, *Bmp* signalling promotes *Sox2* expression (Beites *et al.*, 2009; Furuta and Hogan, 1998; Rajagopal *et al.*, 2009). These findings indicate that the effects of *BMP* on *Sox2* transcription are influenced by the specific developmental context, which is far different from normal in AMM (Figure 4.15).

4.3.4 *Wnt* signalling in the Adriamycin Mouse Model

The *Wnt* signalling pathway is known to be important for early tissue morphogenesis. Multiple

roles for *β-catenin* in cell proliferation and differentiation have been reported in the endodermal components of multiple tissues, including the liver pancreas, and lung (Apte *et al.*, 2007; Dessimoz *et al.*, 2005; Mucenski *et al.*, 2003; Shu *et al.*, 2005). The role for *Wnt* signalling in the development of the foregut has not been extensively studied or demonstrated as of yet. Due to their relationship with other signaling pathways and its critical role in the lung development, *Wnt* signalling might play an important role in the foregut separation (Goss *et al.*, 2009; Harris-Johnson *et al.*, 2009). For example *Wnt2/2b* double knock-out mutants revealed loss of the *Nkx2.1* expression in the ventral foregut endoderm at E9.5 associated with complete lung agensis in later stages, at E11.5 (Goss *et al.*, 2009) . Inactivation of *β-catenin* in ventral foregut endoderm at E10.5 results in absence of both trachea and lung (Harris-Johnson *et al.*, 2009). Specific loss of respiratory primordium is associated with lack of *Nkx2.1* expression in ventral foregut endoderm in these mutants.

Wnt2 gene expression in this study was seen in the ventral foregut mesoderm around the lung primordia in E10 and E11 embryos and there was no difference in gene expression in both control and treated groups of the embryos, even if foregut anomalies occurred. In all of the embryos presented with fistula in the later stage at E12, Wnt2 gene expression was seen in the mesenchyme surrounding the lung buds and additionally in the mesoderm around the fistula and proximal part of the stomach. The potent role for *Wnt/β-catenin* signalling in specifying lung endoderm progenitors suggested that activation of this pathway might dominantly expand lung endoderm progenitor identity outside the normal region in the foregut (Goss *et al.*, 2009; Harris-Johnson *et al.*, 2009). Activation of *Wnt/β-catenin* signalling reprograms posterior regions of the foregut endoderm to a lung endoderm progenitor fate (Goss *et al.*, 2009; Harris-

Johnson *et al.*, 2009). *Nkx2.1* gene expression, the earliest respiratory marker that labels tracheal endoderm, was expanded into the anterior stomach. These mutants moreover displayed defects in tracheal-esophageal separation similar to that seen in AMM with a common undivided foregut tube connected with the stomach. It was shown in ARM, in histological transverse sections through the foregut, that the fistula between the respiratory tract and the stomach was respiratory in origin, lined with ciliated respiartory epithelium emerging from the bifurcation of the trachea or from one of the main bronchii (Crisera *et al.*, 1999; Merei *et al.*, 1997). Investigation of the fistula in the adriamycin model shows that it is positive for *Nkx2.1* (Crisera *et al.*, 2000a; Ioannides *et al.*, 2010). Our study confirms expression of the *Nkx2.1* gene in endoderm of the fistula and proximal stomach from E11 (Chapter 3, Figure 3.6 F). Taken together these findings strongly suggest that the activation of *Wnt/β-catenin* through *Wnt2* expression in the mesoderm leads to formation of the *Nkx2.1* positive fistula in AMM.

Wnt7b, on the other hand, was considered as a candidate gene due to its relationship with *Nkx2.1* expression. It has been shown that *Wnt7b* promoter activity is regulated by *Nkx2.1* (Minoo *et al.*, 1995). In this study *Wnt7b* expression was not altered in adriamycin treated groups and *Nkx2.1* gene expression was confined to the ventral endoderm of the foregut without differences between the groups. This indicates that the morphological abnormalities seen in AMM are not accompanied by obvious changes in the spatial distribution or level of *Wnt7b* gene expression.

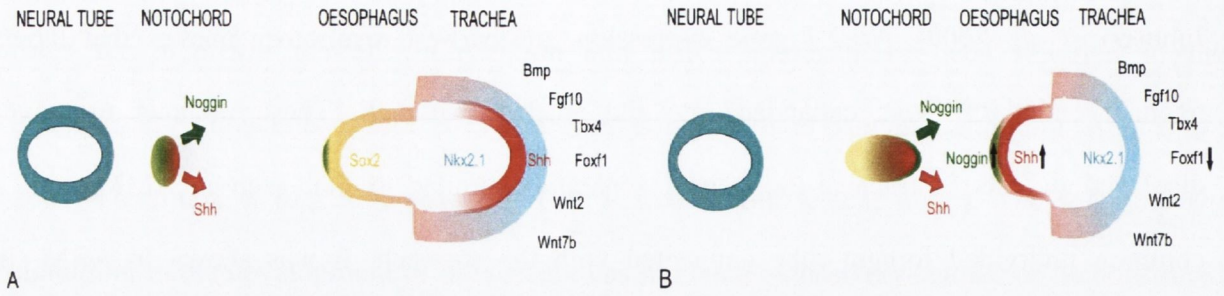


Figure 4.15: Diagramatic summary of candidate genes expression analysis in control (A) and adriamycin treated (B) transverse sections of developing notochord and foregut during separation of the trachea from the oesophagus at E10; summary of data presented in chapters 3 and 4. Ventral expression of *Nkx2.1* (blue), regulated through signaling from the ventral mesoderm (*Bmp, Fgf10, Tbx4, Foxf1 and Wnt2*,) determines the future trachea in control embryos (A). Higher *Sox2* expression (orange) in the dorsal foregut endoderm establishes the future oesophagus (A). Adriamycin treatment does not affect *Nkx2.1* expression in the ventral foregut endoderm although *Sox2* expression is repressed at the level of adjacent notochord branches (B). Abnormal notochord branches of the notochord are source of ectopic *Noggin* and *Shh* secretion and *Noggin* gene expression in the dorsal foregut endoderm is upregulated (B). *Shh* expression is shifted dorsally across the foregut endoderm and its downstream target *Foxf*1 gene is downregulated in the ventral mesoderm of the foregut at the level of notochord branch (B).

Chapter 5

Notochord Position and Cellular organisation in the Adriamycin Mouse Model

5.1 Introduction

The notochord is a relatively simple yet essential structure in vertebrate embryogenesis, playing an active role in cellular and tissue differentiation during crucial periods of morphogenesis. In addition to having a structural role defining the anterioposterior (A/P) axis of the embryo, it also has a well-established role in secreting signalling molecules that pattern the neural tube dorsally, the somites laterally and the foregut endoderm ventrally (reviewed in section 1.1.4). The cells that give rise to the notochord arise from the primary body organizer, the node, during gastrulation and initially form a midline structure called the prechordal plate that is located within the forgut endoderm (Jurand, 1974). Normal delamination of the notochord results in a rod like structure, detached from the endoderm and displaced dorsally toward the neural tube, by E10 in the mouse embryo (Jurand, 1974). It was originally reported by Qi and Beasley in the adriamycin rat model that the notochord can remain tethered to the

foregut in some embryos until E13 (Qi and Beasley, 1999). Branching and increased dorsoventral diameter of the notochord was also reported (Gillick *et al.*, 2003; Orford *et al.*, 2001; Possoegel *et al.*, 1999; Qi and Beasley, 1999; Williams *et al.*, 2001). Other studies corroborated notochord branching in the mouse (Dawrant *et al.*, 2007b). The drug has also been suggested to have a potent hypertrophic effect on the notochord with highest influence shortly after adriamycin exposure (Mortell *et al.*, 2005). In the current work, presented in chapter 3, disturbances of whole embryos from E9 to E12 were visualized using the HNF3ß marker and showed that ventral displacement and branching of the notochord were the most common defects induced by adriamycin exposure, occurring in 98% of E10 embryos. The work also showed a striking associated between the position of notochord branches and foregut malformations ranging from foregut stenosis to full atresia, and furthermore the severity of the foregut malformations corresponded to the number and heaviness of the notochord branches. Additionally, in chapters 3 and 4 I showed that abnormal branches of the notochord express the potent signalling molecule Shh and the *BMP* antagonist *Noggin*. Considering these results, I hypothesised that abnormal signalling from the notochord may be a primary cause of OA/TOF foregut anomalies seen in the AMM. In the work presented in this chapter I examine the effects of adriamycin on the delamination process and the cellular architecture of the early notochord as a primary disturbance in this model of congenital malformations. Extracellular matrix markers were visualised using confocal microscopy to assess cellular architecture.

The extracellular matrix (ECM) is an important aspect of the cellular environment. Composed of glycoproteins, proteoglycans and glycosaminoglycans, it provides mechanical support to

cells in the form of basement membranes or cell-to-cell adhesion, and contributes to important cellular events including differentiation, proliferation, survival, growth, polarity, migration, and chemotaxis of cells during development (Hynes, 2009). Many secreted proteins can contribute to the ECM in different cellular contexts; the particular combination of proteins endowing tissue specific characteristics. Both, laminin and E-cadherin are part of the ECM. Laminin is a major constituent of basement membranes, which separate parenchymal cells from connective tissue. It plays important roles in tissue morphogenesis and homeostasis by regulating tissue architecture, cell adhesion, migration and matrix-mediated signaling (Hamill *et al*., 2009). For instance, mice in which the α5 laminin subunit was inactivated present with a variety of developmental defects, including syndactyly and aberrant lung septation, whereas mice that lack the β2 laminin subunit suffer kidney failure owing to defective glomerular filtration (Miner and Yurchenco, 2004). The cadherin-superfamily of proteins is made up of calcium-dependent cell-to-cell adhesion molecules, where E-cadherin is the member specifically expressed in epithelial tissues of the developing ectoderm and foregut endoderm during early mouse embryogenesis (Nose and Takeichi, 1986; Takeichi, 1977). Cellular adhesion is a crucial aspect of cellular interaction processes involved in constructing differentiated and organised tissues in a multi-cellular organism. Any disruption to adhesion may alter cellular responses and tissue architecture. Due to their key roles in cell-adhesion and tissue morphology, cadherins are considered important regulators of morphogenesis (Takeichi, 1991). The importance of E-cadherin in early morphogenetic events was highlighted by the inactivation of the gene encoding it during mouse development, resulting in prenatal lethality at the time of implantation and the inability to form the trophoectoderm epithelium in preimplantation embryos (Larue *et al*., 1994).

Confocal laser scanning microscopy is a technique that produces high contrast images by scanning through different thin focal planes of a tissue section. The laser is scanned across the specimen, which excites specific fluorophores that have been used to label specific proteins, usually conjugated to secondary antibodies or RNA transcripts. These fluorophores fluoresce and emit light at a specific wavelength that is directed through a spatial pinhole construction (Semwogerere and Weeks, 2005). Due to this pinhole, the light passing through is restricted to a specific focal plane of the specimen, excluding most light that is not within that focal plane (Semwogerere and Weeks, 2005). This results in out-of-focus light being eliminated and the light detected creates a high-resolution image. Scanning at multiple focal planes thus allows the reconstruction of multiple horizontal focal planes, which can then be assembled to build a three-dimensional (3D) reconstruction of the section (Z-stack) that can then be digitally sectioned vertically. Confocal microscopes possess several advantages over conventional microscopy. First, confocal microscopy produces images of improved resolution, up to 1.4 times greater than standard microscopy, by eliminating out-of-focus light. Confocal microscopes also have a higher level of sensitivity compared to conventional microscopes, due to highly sensitive light detectors. Another key advantage of confocal microscopy is the ability to produce 3-dimensional reconstructions of thicker sections of the specimen, reducing the amount of analysis required and potential distortion (Semwogerere and Weeks, 2005).

The work presented in this chapter aimed to address the hypothesis that anomalies observed in the AMM could be a result of fundamental defects in cellular-architecture within the

notochord leading to abnormal delamination and ectopic placement of this potent signaling tissue during crucial stages of development. Confocal microscopy was used to investigate adriamycin exposed and control embryos at the cellular level, comparing the cellular organization and position of the notochord with respect to the foregut endoderm within a defined development period from E9 to E10, when delamination of the notochord normally occurs. The study employed immunohistochemical techniques to visualise markers of the extracellular matrix (namely E-cadherin and Laminin), in transverse sections. The overall aim was to reveal any early changes in notochordal tissue that might lead to ventrally displaced and ectopic notochord as a primary defect in this congenital model.

5.2 Results

5.2.1 Notochord position

The position of the notochord with respect to the foregut endoderm and the neural tube was assessed in all specimens assayed for E-cadherin or laminin expression. All control embryos (8 out of 8) within the group 6-9 somites showed a notochord with close contact with the foregut endoderm (position vc) (Figure 5.1 A). In the group 14-18 somites, 33% (2 out of 6) of embryos showed a notochord position with contact with the foregut endoderm and 67% (4 out of 6) of embryos showed a notochord position progressing towards the neural tube with mesenchymal cells intervening between the cells of the notochord and foregut, however there was no contact of the notochord with the cells of the floor plate (position d) (Figure 5.1 B). Among control embryos studied in the group 20-22 somites, 11% (1 out of 9) showed

notochord position in the middle between dorsal foregut endoderm and floorplate (position m) (Figure 5.1 C). In 22% (2 out of 9) of the embryos, the notochord had progressed towards the neural tube (position d) (Figure 5.1 D) and in 67% (6 out of 9) of the embryos the notochord was positioned adjacent to the floorplate with close contact with the cells of the floorplate (position dc) (Figure 5.1 E). In control embryos with 24-28 somites, the notochord approached the neural tube either without contact with the floorplate (71%, 5 out of 7) or with close contact with cells of the floorplate (29%, 2 out of 7). The overall progression of the notochord away from the foregut endoderm and toward the neural tube as embryos mature is shown diagrammatically in Figure 5.2A.

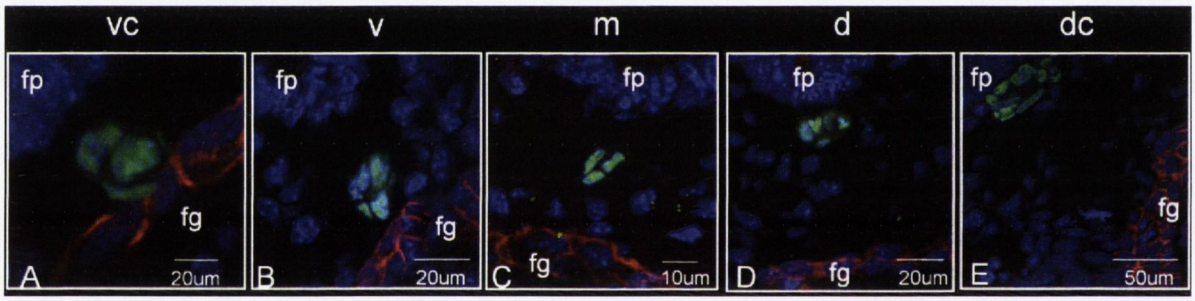


Figure 5.1: Example of five different positions (scored vc, v, m, d, dc, as described (section 2.7.3) of the notochord in relation to the dorsal wall of the foregut and floor plate in progressively more advanced control embryos; A; 8 somites, B; 14 somites, D; 21 somites E; 24 somites. Notochord cells are Brachyury positive (green). E-cadherin stained cells are seen in the foregut endoderm (red). Counterstaining with DAPI is shown in blue. *fp*; floor plate, *fg*; foregut. Scale bars as indicated.

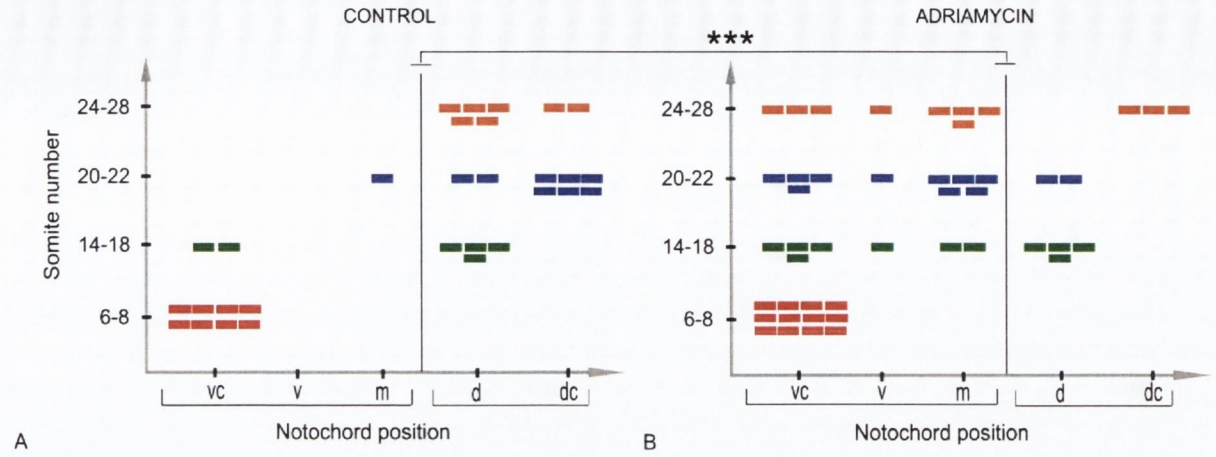


Figure 5.2: Graphical representation of recordings of notochord position along the dorsoventral axis in the thoracic region, comparing control (A) and adriamycin treated embryos (B). The specimens were divided into groups according to somite number (y axis). The number of embryos per group are indicated (each rectangle represents a specimen). Notochord position is scored as vc (ventral with foregut contact), v (ventral), m (mid), d (dorsal), or dc (dorsal with contact with the floorplate). Statistical analysis showed a strongly significant difference in ventral (vc, v, m) versus dorsal (d, dc) position between control and adriamycin treated groups (Chi-Square = 14.9, df=1, p>0.0001)

Comparing notochord position in adriamycin treated embryos across all stages shows that the notochord is ventrally displaced (Figure 5.2B). The notochord has a ventral position (vc, v or m) in 80% of adriamycin treated individuals (n=46 from 16 independent litters) and in 36% of control specimens (n=30 from 12 independent litters) (Chi-Square = 14.9, df=1, p>0.0001. Focusing on later stages only (20-28 somites), 1/16 (6%) control specimens and 18/23 (78%) adrimaycin treated embryos show a ventrally located notochord. Looking at the dynamics across the stages, normal progressive delamination seen in control specimens is disturbed. In specimens with 6-9 somites, close contact with the foregut endoderm (position vc) was seen in all specimens investigated (12 out of 12) and was the same as in the control group in the earliest stage category. In the adriamycin treated group with 14-18 somites, 45% (5 out of 11) of specimens had a notochord in ventral position close to the foregut (vc or v) in contrast to

33% of control specimens. In two embryos (18%) the notochord was seen midway between the dorsal wall of the foregut and the floor plate (position m). Only in four embryos (36%) the notochord was approaching the neural tube with no direct contact to floor plate cells (position d) compared to 67% of control specimens. In treated embryos with 20-22 somites 33% of the specimens (4 out of 12) still showed a notochord position in contact with the foregut endoderm, compared to 0 embryos in the control group. 8% (1 out of 12) showed a ventral position (v), 42% (5 out of 12) had a mid position (m), 17% (2 out of 12) were seen in a dorsal position (d) and none had reached contact with the floorplate of the neural tube compared to 67% of control embryos. Comparing notochord position in adriamycin treated embryos in the oldest stage category (24- 28 somites) shows that while 27% (3 out of 11) had achieved a dorsal notochord position adjacent to the neural tube (d or dc), compared to 100% of control specimens, 36% (4 out of 11) still showed a ventral position close to the foregut (vc or v) and 36% (4 out of 11) had a mid position (m) (Figure 5.2B). Notochord position close to the foregut was recorded in some treated embryos in all stage categories showing that the normal progression of notochord delamination in control embryos (Figure 5.2A) is not seen in treated embryos (Figure 5.2B).

5.2.2 Laminin localisation in control embryos

In all specimens across the stage groups, laminin was clearly detected as expected in the basal laminae of the neural tube, notochord and foregut. In control embryos within the stage group 6-9 somites, laminin localisation around the notochord showed a common basal lamina shared with the foregut endoderm (Figure 5.3 A). In 2 out of 4 (50%) control samples laminin

surrounding the notochord was complete on the ventral side, separating notochord cells from foregut cells, while in the other two embryos (50%) enclosure of the notochord by its own basal lamina was incomplete showing no localization of laminin at the ventral side of the notochordal cells (Figure 5.3 A). Within the stage group 14-18 somites, the notochord was displaced dorsally away from the foregut (Figure 5.3 B) as previously described and all three control specimens (100%) showed continuous laminin detection surrounding the notochord with two specimens showing streaks of laminin detection in a pattern extending from the basal lamina of the notochord to that of the dorsal foregut endoderm (Figure 5.3 B). This is consistent with the previously described process of notochord delamination in mouse embryos (Jurand, 1974). Again, in the stage group 20-22 somites there was continuous laminin detection surrounding each notochord in each specimen (4 out of 4) but at this stage no streaks of laminin were recorded extending from the foregut endoderm to the basal lamina of the notochord (Figure 5.3 C). All of the embryos (4 out of 4) in the final group of 24-28 somites showed complete laminin localisation around the notochord (Figure 5.3 D) while one embryo showed remnants of a streak of laminin extending from the foregut endoderm to the basal lamina of the notochord.

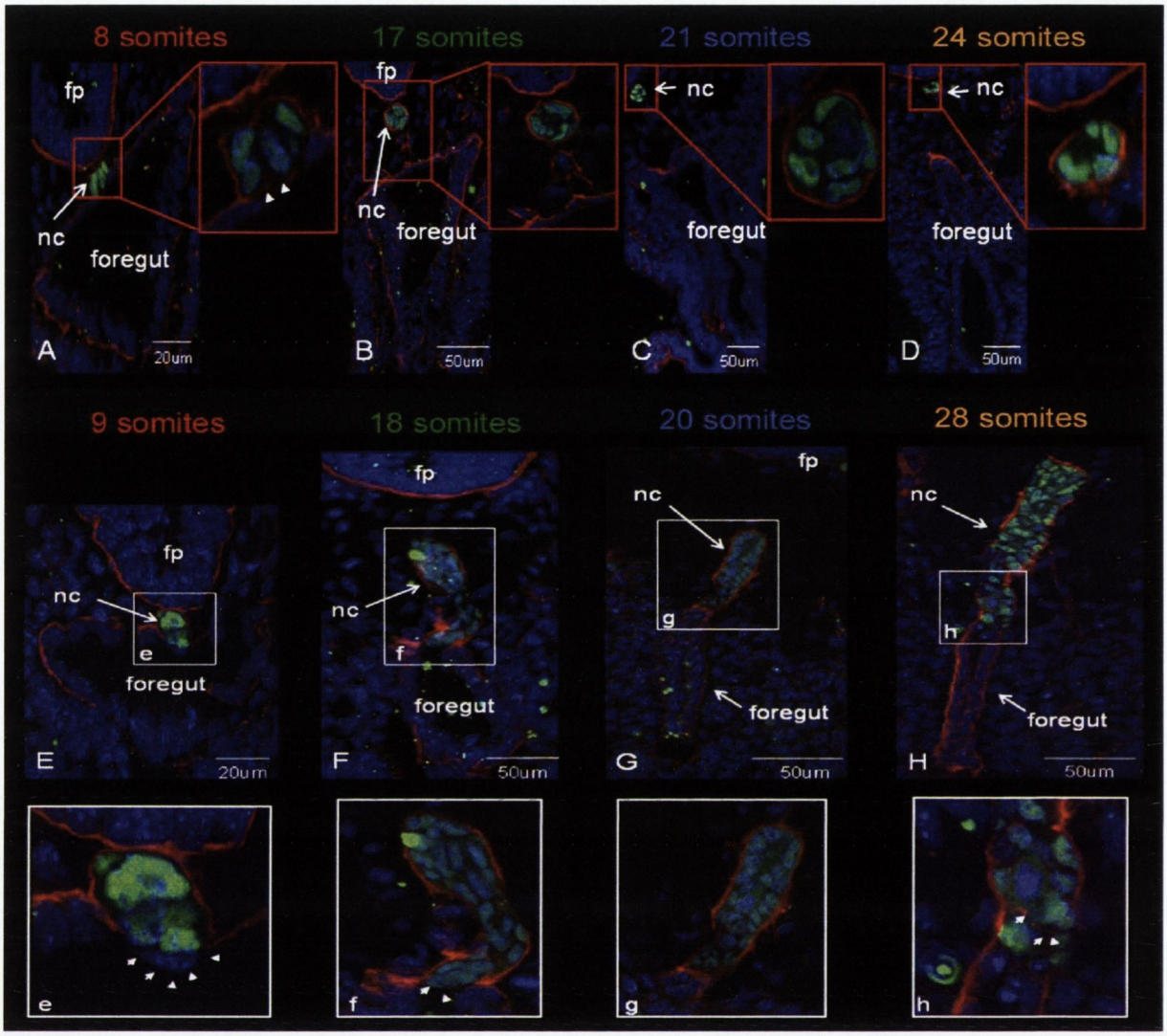


Figure 5.3: Laminin (red) and Brachyury (green) distribution in transverse sections through the thoracic region of control (A-D) and Adriamycin treated (E-H) embryos at progressively more advanced developmental stages. Each image shows a specimen with the number of somites indicated, representative of a stage group analysed; 6-9, 14-18, 20-22 and 24-28 somites. Image A shows notochord cells incorporated in the foregut endoderm (arrow heads) with a basal lamina shared with the dorsal wall of the foregut. As delamination progesses the notochord is separated from the endoderm but streaks of laminin were detected, extending from the foregut endoderm to the basal lamina of the notochord (B). At later stages the notochord is completely surrounded by its own basal lamina as it progresses away from the foregut endoderm (C, D). By contrast, in adriamycin treated embryos, E shows incomplete notochord delamination from the dorsal wall of the foregut (arrow heads). F-H show abnormally shaped notochords, elongated along the D/V axis still in contact with the foregut endoderm even at the latest stages. F and H show incomplete basal lamina ventrally (arrow heads). Counterstaining with DAPI is shown in blue. *fp*; floor plate, *nc*; notochord. Scale bars as indicated.

5.2.3 Laminin localisation in adriamycin treated embryos

In adriamycin treated embryos of the earliest stage group, 6-9 somites, 80% (4 out of 5) of treated embryos showed incomplete laminin detection on the ventral side of the notochord indicating the lack of a basal lamina separating notochord cells from the foregut (Figure 5.3 E). Complete enclosure of the notochord by its own basal lamina was seen in one embryo (20%), compared to 50% of control embryos at this stage. Five adriamycin treated embryos were studied in the stage group 14-18 somites. 60% (3 out of 5) showed complete Laminin detection surrounding the notochord as well as a streak of laminin extending from the notochord to the foregut basal lamina. Two embryos (40%) showed incomplete laminin surrounding an abnormally shaped notochord, elongated in the dorsal to ventral aspect (Figure 5.3 F). In contrast, notochords in all control embryos had developed a complete basal lamina of their own by this stage, had delaminated away from the endoderm and had a normal rod shape in cross section. Seven adriamycin treated embryos in the stage group 20-22 somites were investigated and showed that all (100%) had complete laminin expression surrounding the notochord although streaks of laminin extending from the notochord to the foregut basal lamina were still evident in 86% (6 out of 7) of embryos. One embryo showed a complete basal lamina surrounding the notochord although the notochord was abnormally elongated and remained in contact with the basal lamina of the dorsal foregut endoderm (Figure 5.3 G). Within the group 24-28 somites, 83% (5 out of 6) of treated embryos showed complete basal lamina surrounding the notochord. One embryo examined shared its basal lamina with dorsal foregut and laminin detection was incomplete on the ventral side of an elongated notochord (Figure 5.3 H). General observation of notochord shape shows that, in adriamycin treated

specimens the notochord is less rod shaped and more elongated along the D/V axis, most commonly showing contact with cells of the foregut endoderm in comparison to control specimens.

5.2.4 E-cadherin localisation in control embryos

Transverse sections of control embryos showed clear E-cadherin detection between foregut endoderm cells (Figure 5.4 A-D) as well as expression in the most ventral part of the neural tube, particularly on the ventricular aspect of the floor plate, in all stage groups. All control samples showed absence of E-cadherin immunodetection between the cells of the notochord (Figure 5.4 A-D) and the normal delamination of the notochord away from the foregut across the stages analysed.

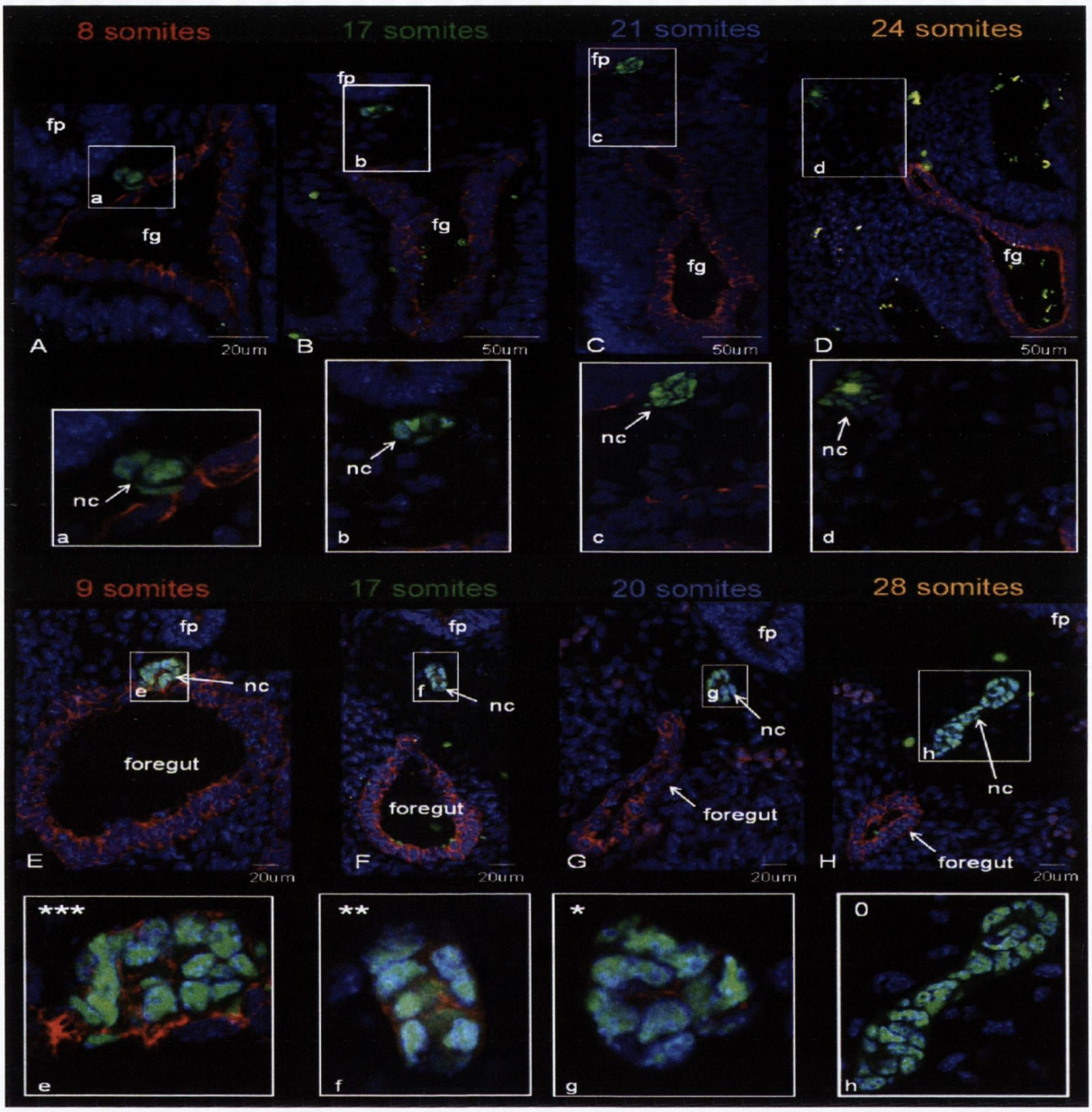


Figure 5.4: Detection of E-cadherin (red) and Brachyury (green) in transverse sections through the thoracic region of control (A-D) and Adriamycin treated (E-H) embryos at progressively more advanced developmental stages. Each image shows a specimen with the number of somites indicated, representative of a stage group analysed; 6-9, 14-18, 20-22 and 24-28 somites. In both groups E-cadherin immunodetection is seen between the cells of the foregut (A-H). In control embryos no immunodection of E-caherin is seen in between notochord cells (in green) across all the stages (A-D). By contrast in adriamycin treated embryos, E-Catherin immunodetection is seen in between notochord cells in three younger groups (E-G). No immunodetection is seen in oldest group of treated embryos although significant change in notochord shape was recorded (H). Images e – h shows examples of E-cadherin immunodetection scoring system range from zero to three stars. Counterstaining with DAPI is shown in blue. *fp*; floor plate, *fg*; foregut, *nc*; notochord. Scale bars as indicated.

5.2.5 E-cadherin localisation and position of the notochord in adriamycin treated embryos

As in control embryos, E-cadherin was detected between the foregut cells and in the ventral aspect of the neural tube across all somite groups in adrimaycin treated embryos (Figure 5.4E-H). However in addition, in treated embryos E-cadherin expression is altered with 60.2% (14/23) of treated specimens showing ectopic expression between cells of the notochord (Chi-Square= 14.5, df=1, $p>0.0001$). This effect is even more striking at early stages (6-18 somites) when 92% (12/13) of treated embryos show ectopic localization in the notochord compared to 0/6 for control. At later stages (20-28 somites) only 2/10 treated embryos showed abnormal expression between cells of the notochord compared with 0/7 for controls and in the majority of specimens E-cadherin was no longer detected between the cells of the notochord (Figure 5.4H). Assigning arbitrary scores to the intensity of expression also showed most severe effects at earlier stages. In the stage group of 6-9 somites, 6/7 (86%) embryos showed E-cadherin detection between the cells of the notochord and of those, 50% (3/6) received a relative intensity score of 3 (Figure 5.4 e), 33% (2 out of 6) a score of 2 and 17% (1 out of 6) a score of 1. In the stage group 14-18 somites, all (6 out of 6) embryos showed E-cadherin localisation between the cells of the notochord with 50% (3 out of 6) embryos receiving a relative intensity score of 2 (Figure 5.4 f) and 50% (3 out of 6) a score of 1. In the stage group 20-22 somites, 40% (2 out of 5) of adriamycin treated embryos showed clear E-cadherin expression between notochord cells with one specimen receiving a score of 2 and one receiving a score of 1 (Figure 5.4 g). Within the final stage group of 24-28 somites, all five specimens of adriamycin treated embryos examined showed no E-cadherin between the cells

of the notochord even in cases where the notochord shape and position were clearly abnormal (i.e. elongated along the D/V axis and abnormally close to the foregut) (Figure 5.4 h).

The observations with respect to notochord position and abnormal E-cadherin expression in notochord cells in treated embryos across developmental stages are combined and presented graphically in Figure 5.5. This shows a number of interesting features of the findings. 1) the most intense E-cadherin localisation in the notochord is seen in the earliest stages with just one specimen in the stage group up to 22 somites receiving a score of 2 for intensity. 2) The most intense abnormal E-caherin notochord expression is also seen in locations closest to the endoderm (vc or v). 3) As also clear from Figure 5.2, treated embryos at the latest stages examined still show a variety of positions from the most ventral to the most dorsal, however independent of position, none of these specimens show E-cadherin expression between notochord cells. Therefore there is correspondence between the intensity of expression and notochord position but only at early stages and this abnormal expression is lost at the latest stages (Figure 5.5).

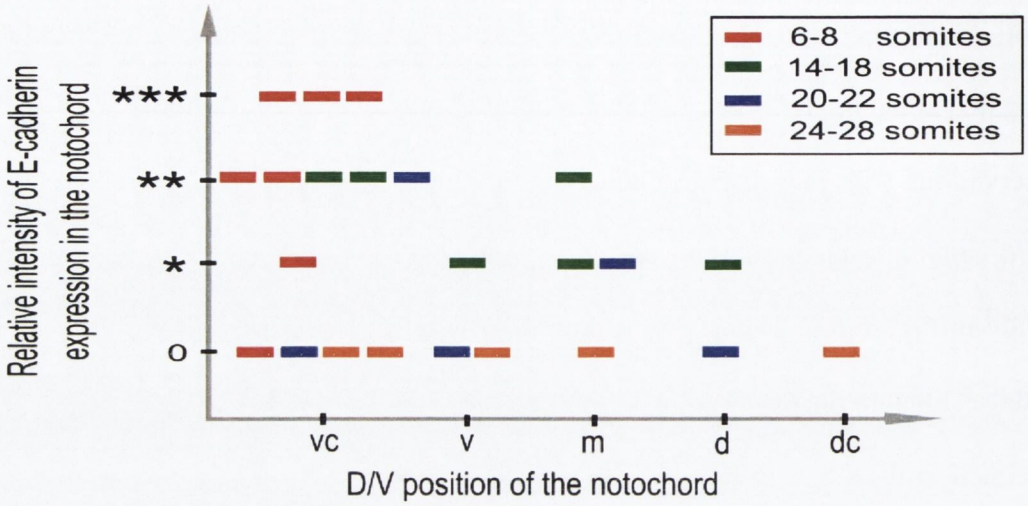


Figure 5.5: Integrating observations on abnormal notochord position (X axis) and relative intensity of abnormal E-cadherin detection in the notochord of adrimaycin treated embryos across stage groups (represented by different colours as indicated). The numbers of specimens analysed scored for each stage group are indicated (each rectangle represents an individual specimen). D/V position designated as ventral with foregut contact (*vc*,), ventral (*v)*, mid (*m)*, dorsal (*d), or dorsal with floor plate contact* (*dc)*. Relative intensity of E-cadherin expression is scored by: 0 indicates no detection, * indicates low, ** indicates moderate, *** indicates high level of detection.

5.3 Discussion

5.3.1 Overview of findings

This chapter aimed to explore a possible link between abnormal notochord development seen in the adriamycin mouse model and its architecture during development. The results indicate that three distinct alterations occur with respect to notochord structure following treatment with adriamycin compared to control specimens at equivalent stages of development. Firstly, analysis of notochord position revealed abnormal delamination of the notochord from the foregut endoderm (Chi-Square = 14.9, df=1, p>0.0001, for ventral displacement). Secondly,

the shape of the notochord was altered from the normal rod shape which is circular in transverse cross section, becoming elongated along the dorso-ventral axis with the ventral extremity remaining in contact with the foregut. Thirdly, abnormal cellular structure within the notochord of treated embryos was revealed by ectopic expression of the extracellular matrix protein E-cadherin, normally restricted to the epithelial cells of the endoderm and floorplate (Chi-Square= 14.5, df=1, $p>0.0001$). These cellular and tissue structure changes point to the embryological basis for hypertrophic and branched notochords previously described in the adriamycin mouse model at later stages.

5.3.2 Abnormal delamination of the notochord in adriamycin treated embryos: implications for notochord structure

In control specimens, notochord positioning was consistent with expected dorsal progression of notochord cells with respect to the foregut, or delamination, over the period studied (Jurand, 1974; Que *et al.*, 2006). At early stages the notochord cells were embedded within the endoderm, although most were separated by a continuous dorsal lamina. At progressively later stages the notochord was displaced dorsally with mesenchyme cells between the notochord and foregut, although initially, a strip of continuous laminin staining extended between the basal laminae of the notochord and gut endoderm. At the latest stages the notochord was positioned at a distance from the endoderm and completely separated from it, surrounded by an independent basal lamina. In adriamycin treated embryos, abnormal notochord position was seen in transverse section across all stages, indicating disturbed delamination. At the earliest stages, the notochord was embedded in the foregut endoderm similar to control specimens,

although not always separated dorsally by a basal lamina. The major difference was that close association with the endoderm was maintained in some specimens through all somite stages in treated embryos. This proximity was seen even in the oldest group of 24-28 somite embryos, in contrast to control embryos where the notochord had detached from the foregut by the 18 somite stage. In specimens that showed such prolonged attachment to the foregut endoderm, a misshapen notochord, elongated along the dorso-ventral axis was recorded in several cases.

Notochord development involves gross morphological changes that provide the notochord with its mechanical strength, including acquisition of large central vacuoles and formation of a notochordal basement membrane. It is suggested that internal turgor pressure generated by inflated vacuoles and resisted by the notochordal basement membrane produces the stiffness of the notochord, important for elongation and resistance to kinking (Adams *et al.*, 1990). If the basal lamina around the notochord is incomplete, as seen in this work, this may lead to loss of the turgor and to the abnormal delamination and branching of the notochord observed. Secondly, loss of turgor of the notochord would affect the shape of the notochord (Adams *et al.*, 1990) and in fact notochord shape was affected with many specimens showing elongation along the dorso-ventral axis so that the tissue was more elliptical than round in cross section, as was also noted previously in adriamycin exposed rat embryos (Possoegel *et al.*, 1999). The lack of a restraining basal lamina might also explain the increased volume of notochord tissue reported previously in the rat model (Mortell *et al.*, 2005).

The transition from the chordomesoderm of the prechordal plate to the notochord also involves changes in gene expression and the correct formation of the basal lamina has been

implicated in this process. In zebrafish mutants grumpy and sleepy, where laminin 1 protein is lost due to the disruption of the zygotic supply of β1 or γ1 chains, the basement membrane around the notochord fails to form and notochord cells do not become properly vacuolated. The mutant notochord cells also continue to express genes typical of the chordomesoderm that would normally be extinguished, such as echidna hedgehog (Coutinho *et al.*, 2004; Parsons *et al.*, 2002). Although in this work I did not investigate markers for notochord maturation, it is possible that the process of notochord maturation is disturbed due to delayed enclosure by its own basement membrane.

5.3.3 E-cadherin is abnormally expressed in the notochord of treated embryos: implications for notochord structure and signalling

Examining cellular characteristics within the notochord revealed that the extra cellular matrix cell adhesion molecule E-cadherin, not normally expressed in the notochord at any stage of development investigated, is detected between notochord cells in adriamycin treated embryos. E-cadherin detection was most prevalant in the notochord of treated embryos aged E9 that had developed between 6-9 somites. Lower levels of E-cadherin were still seen in treated embryos that had developed up to 22 somites, however no E-cadherin was detected in the notochord of embryos with more than 24 somites. This indicates an alteration in the character of notochord cells. A previous study of forced E-cadherin expression in the mouse intestinal epithelieum unveiled a number of effects on the tissue (Hermiston *et al.*, 1996). The increased level of the adhesion molecule caused delayed migration of cells up the villus and increased adhesion of villus epithelial cells in the intestine. This supports the idea that due to the adhesive nature of

E-cadherin, increased levels would increase cell to cell attachment, thus having an effect on tissue architecture. The observed abnormal distribution of E-cadherin therefore indicates that intercellular adhesion within cells of the notochord and possibly also between notochord cells and foregut cells have increased, perhaps contributing to impaired delamination.

While the results showed no E-cadherin expression in the notochord of treated embryos with over 24 somites, attachment to the foregut endoderm was noted in two out of five of the adriamycin treated embryos at this stage. It is suggested that sustained E-cadherin expression may not be necessary for the prolonged notochord abnormality; expression at earlier stages may have a long-term influence on cell behaviour. The precise profile of cadherin molecules expressed in a tissue is reflective of normal tissue differentiation, for example through a process known as 'cadherin switching', E-cadherin is downregulated and the expression of other cadherins (mainly N-cadherin) is upregulated in different tissues at later stages of vertebrate development (Inuzuka *et al.*, 1991; Kikuchi *et al.*, 2009; Oda *et al.*, 1998; Sakamoto *et al.*, 2008). This dynamic regulation of cadherins during morphogenesis is thought to influence cell sorting and cell movement behaviours.

It also must be noted that E-cadherin forms an important functional complex with the protein *β-catenin* of the multi-gene family of catenin proteins (Aberle *et al.*, 1996; Kemler, 1993). The intra-cellular domain of E-cadherin binds directly to *β-catenin*, which in turn binds to another catenin protein, α-catenin, connecting the actin cytoskeleton to the adherens junction. While *β-catenin* plays the role of the main binding partner of E-cadherin, uncomplexed *β-catenin* proteins are involved in the evolutionary conserved canonical *Wnt* pathway, which plays a

major role in organising the body plan of animals via cell-to-cell communications (Gilbert *et al.*, 2010; Willert *et al.*, 2003). A recent study highlighted that *Wnt* signalling is required for notochord progenitor cells to sustain their fate and is also needed for the posterior extension of the notochord during mouse embryogenesis (Ukita *et a*l., 2009). By ablating *β-catenin*, it was shown that the notochord precursor cells lost expression of notochord specific genes yet maintained the expression of genes normally expressed in both the notochord and endoderm (Ukita *et al.*, 2009). Additionally, E-cadherin, usually only present in the endoderm, was detected in the notochord. It was suggested that the cadherin-mediated cell adhesion complex was maintained in the *β-catenin* ablated embryos by the recruitment of the *β-catenin* cousin molecule *plankoglobin* and/or *β-catenin* residuals (Ukita *et al.*, 2009). This poses an interesting situation where intracellular changes occur to accommodate disruptions of normal developmental processes. Previous studies in *Drosophila* and *Xenopus* embryos suggested that over expression of cadherins led to a reduction in *β-catenin* levels available for signalling to the nucleus due to an increase in their recruitment in cadherin-catenin complexes at the cell membrane (Heasman *et al.*, 1994; Sanson *et al.*, 1996). A contrasting study however in mammalian cells showed that an increase in *Wnt-1* signalling consequently increased levels of *β-catenin*, which led to the stabilization of cadherin-catenin complexes at the cellular membrane, stabilizing cell adhesion (Hinck *et al.*, 1994). Although in chapter 4, *Wnt2* and *Wnt7b* gene expression was described in adriamycin treated embryos and no alteration in gene expression was found around the foregut or notochord, it may be useful additionally to investigate *β-catenin* protein in both the foregut endoderm and notochord cells of the adriamycin mouse model to delineate any changes in nuclear localisation compared to that in

the mouse during normal development and in conjunction with abnormal E-cadherin detection. No reliable what target genes are known for this system.

5.3.4 The possible impact of altered notochord architecture on the foregut endoderm: possible role in endodermal anomalies

The detection of laminin and the visualisation of the basal lamina highlight abnormal delamination of the notochord in treated embryos where the notochord continues to share a basal lamina with the foregut endoderm, failing to detach, for much longer periods. A shared basal lamina between the two structures was even found in the oldest group investigated; 24-28 somites. Moreover in one embryo from this group the basal lamina was found to be incomplete. The observed change in shape of the notochord and notochord branching indicate altered mechanical properties of the tissue. Abnormal E-cadherin expression, associated with increased cell adhesion, supports the idea of altered physical properties as well as reflecting altered molecular regulation. The reduced distance between notochord cells and those of the developing endoderm, together with altered mechanical and molecular characteristics in adriamycin treated embryos might impact normal development of the foregut in two major ways: 1) an abnormal mechanical influence might be exerted on the foregut endoderm or 2) the normal diffusion of signaling molecules from the notochord might be disturbed. An association between abnormal notochord position and heaviness, and certain foregut malformations was described in chapter 3. Evidence of altered signaling through notochord branches was described in chapter 3 and chapter 4. This chapter precisely shows how and

when the delamination abnormality progresses and shows a structural difference in notochord cells.

The basal lamina can act as a physical barrier for signaling molecules. It was discussed in chapter 3 that proximity of the notochord may increase its signaling and lead to foregut abnormalities. Here we show that enclosure of the notochord by its own basal lamina is delayed or, in some treated embryos, basal lamina is incomplete, even in later stages of development. The lack of a physical barrier may increase and/or prolong signaling from the notochord into surrounding tissue in addition to the abnormally close position of the notochord in relation to the foregut. In addition the link between E-cadherin levels and *ß-catenin* opens the possibility of altered *Wnt* signalling. It is possible that the severity of foregut malformations might depend on how severely the basal lamina is affected although the present work does not provide this evidence since laminin detection was not combined with whole embryo imaging where foregut abnormalities in a number of specimens could be assessed.

Conclusions

The importance of the axial structure of the notochord in vertebrate development has been delineated in many embryological studies. Its rigidity and axial determination properties along with its crucial signalling purpose in many stages of morphogenesis highlight that any alteration to its normal formation and function could lead to drastic effects on the developing organism. This study focused on the architecture of the notochord itself with emphasis on proteins of the extracellular matrix. The results show that changes in notochordal properties

are evident in the AMM that in turn may influence notochord delamination and signalling mechanisms from the notochord to the foregut endoderm, consistent with the hypothesis that the notochord may be the primary target of disruption and therefore may result in abnormal patterning of the foregut. This will be further explored in chapter 6. Between these results and previous studies, the abnormal development of the notochord and its possible influence on foregut malformations such as OA and TOF is reinforced.

Chapter 6

General Discussion and Future Directions

6.1 Summary of the findings and conclusions

The work presented in this thesis addresses how administration of adriamycin to developing mouse embryos impacts morphogenesis of the foregut and notochord and has shown that notochord abnormalities occur early and are closely associated with the position and extent of foregut patterning defects. By addressing the 3 objectives outlined in section 1.5 the following conclusions were drawn:

Morphological analysis of foregut development in control and adriamycin treated embryos.

1. Full 3D imaging and analysis of 149 individual control and treated embryos revealed a spectrum of 8 defects, together with their frequency. The most common defect was ventral displacement and branching of the notochord, observed in 98% of embryos at E10. This study revealed a number of features of the adriamycin mouse model not previously reported (Chapter 3).

2. Morphological analysis of the adriamycin treated embryos revealed a close spatial correspondence between the site of notochord branching and defects of the foregut. More severe foregut abnormalities including foregut atresia and foregut stenosis were associated with more posterior and thicker branches of the notochord. This spatial association indicated for the first time a causative link between abnormalities in these neighbouring tissues (Chapter 3).

3. Altered patterning along the DV axis of the foregut was observed adjacent to abnormal notochord branches. The whole 3D embryo imaging approach revealed altered distribution of transcripts of the patterning genes *Shh, Foxf1* and *Sox2*. Treated embryos not only showed ectopic expression of *Shh* throughout notochord branches but also a dorsal shift in expression in the adjacent foregut endoderm. Mesenchymal *Foxf1* gene expression was downregulated in the corresponding ventral foregut mesoderm and the normal dorsal restriction of *Sox2* gene expression was lost in the foregut endoderm in the region of notochord branches. The severity of these altered patterning effects corresponded with the proximity of the notochord branches. This implicates the notochord as a primary site of disturbance in such abnormalities and

underlines the importance of the model to further address the mechanistic basis of foregut congenital abnormalities (Chapter 3).

Candidate gene analysis in the AMM.

4. Gene expression analysis revealed disturbance of *BMP* signalling pathway components. The 3D analysis of expression of the *Noggin* gene, a modulator of *BMP* signalling, in control and treated embryos revealed not only ectopic expression throughout the notochord branch but more remarkably, strong *Noggin* expression at the distal tip of the notochord branches and in an expanded domain within the dorsal foregut endoderm. Although there were no differences in temporo-spatial distribution of Bmp4 transcripts across all stages in control and adriamycin treated groups, abnormal Noggin localisation suggests disturbances of this important signaling parthway. These disturbances to *BMP* pathway components observed in the mouse model might be causative of the foregut abnormalities (Chapter 4).
5. There were no differences in spatial distribution of the *Fgf10* and *Tbx4* transcripts between the control and adriamycin treated groups however delayed *Fgf10* gene expression was seen in treated embryos. Comparison of stage matched embryos revealed a lack of *Fgf10* gene expression at TS18 in some of the treated embryos, associated with tracheal atresia. This delay in *Fgf10* gene expression and in outgrowth of lung primordia in the AMM indicates that failure to express *Fgf10* in the ventral mesenchyme at earlier stages may at least contribute to delayed lung development. The morphological abnormalities seen in AMM are not accompanied by obvious changes in the spatial distribution or level of gene expression of *Tbx4* suggesting that *Tbx4*

regulation is not altered in this model. This implies that the morphological abnormalities in AMM can occur in the presence of *Tbx4* transcripts (Chapter 4).

6. Examining the abnormal fistula seen in 63% of adriamycin treated embryos at E11 (chapter 3), this work confirmed previous findings that the fistula expresses the respiratory marker *Nkx2.1* from an early stage of development. Moreover *Wnt* signaling pathway gene expression was found for the first time in the fistula. Mesoderm around the fistula was found to express *Wnt2*, a gene known as a marker of respiratory cell progenitors, reinforcing the hypothesis of a respiratory origin and character for the fistula (Chapter 3 and 4).

Analysis of notochord structure and delamination in the AMM

7. Changes in the position and shape of the notochord were seen from as early as the 8 somite stage in adriamycin treated embryos. Abnormal delamination was shown by the position of the notochord which remained close to the foregut even in 28 somite embryos, a stage at which the notochord had fully delaminated and was positioned close to the neural tube in 100% of control embryos. Notochord shape was also altered in adriamycin treated specimens where the normal rod shape was lost and appeared more elongated along the D/V axis. Often the dorsoventrally stretched notochord remained in contact with cells of the foregut endoderm as late as 28 somites (Chapter 5).
8. Application of adriamycin not only affected morphology of the foregut and notochord, it also appeared to impact the physical structure of the tissue, as indicated by changes in the ECM of the notochord in treated embryos. The abnormal expression of E-

cadherin, typical of epithelial tissue and known to increase cell to cell adhesion in tissues, would change notochord properties in a manner that may influence notochord delamination. The knock on effect of delayed delamination of a potent signaling tissue may be responsible for abnormal signaling from the notochord to the foregut endoderm. This is the basis of my proposal that the impact on the notochord may be one of the primary effects of disruption, leading secondarily to abnormal patterning of the foregut and the foregut malformations (Chapter 5).

6.2 Significance of the findings and future studies

The work presented in this thesis provides new insight into the regulation of embryonic foregut development in the mouse and the effects of adriamycin treatment in the Adriamycin Mouse Model of congenital foregut malformations. The use of 3D imaging enabled direct comparison of gene expression and foregut development both across developmental time and between control and treated embryos. This work demonstrates the integral role that the notochord plays in the development of the foregut. While this thesis indicates a causative role for notochord in the etiology of foregut malformations in the AMM, it is clear that we need to know more about the role of notochord signalling in foregut development and how this might be deregulated in foregut malformations.

6.2.1 Impact of the notochord on foregut patterning and development

D/V patterning of the foregut is critical for establishing the identity of emerging territories in the foregut and further foregut separation into the trachea and oesophagus. This process appears to be regulated, at least in part, by signalling from the notochord as indicated previously by observation made in *Noggin* knockout mice, where the notochord is disturbed and the foregut displays a lack of D/V separation (Que *et al.*, 2006). This is reinforced here through altered expression of patterning genes in the foregut in the vicinity of misplaced notochord tissue, further associated with abnormal foregut separation in the AMM. Although abnormal notochord signalling is not the only possible mechanism though which the process of D/V foregut identity might be modified following adriamycin treatment, and a direct impact on the foregut is also a possibility (Morrisey and Hogan, 2010), the impact of the notochord on the foregut is worthy of further exploration. The nature of the relationship between notochord signalling and foregut patterning would be further informed by a study exploring the influence of notochord transplants on foregut development. Given the position of the foregut deep within the embryo this would be best approached in explant culture. Explant cultures have been widely used to recapitulate development of particular organ systems in a controllable manner. This approach was used in the classical experiments demonstrating the patterning influence of the notochord on the neural tube (van Straaten *et al.*, 1988; van Straaten *et al.*, 1985b). Brigid Hogan's lab is using explant culture of the foregut to monitor separation of the trachea and oesophagus (Que *et al.*, 2007; oral presentation at the International Society of Developmental Biology meeting, Edinburgh, 2009). I propose that 3D explant cultures (for example, embedded in collagen matrix (Murphy *et al.* 1996)) could be used to compare

patterning and separation of the foregut examining morphology and expression of D/V patterning genes using 3D imaging. Explant co-cultures could be constructed where the notochord is 1) included in its normal position, 2) removed or 3) added in an abnormal position and/or at a different distance from the foregut. This would demonstrate the effects of decreased, increased or misplaced notochord signalling on foregut patterning.

The work presented here also leads to the more specific proposal that at least one aspect of the signal deregulation eminating from the adriamycin treated notochord is an impact on *BMP* signalling (Section 6.1 conclusion 4). This hypothesis, as well as effects on other interrelated signalling pathways, could be explored by altering the expression of components of these pathways in embryos *in vivo*. Using transgenic mouse models is one possibility but this could also be achieved in the chick model, perhaps more conveniently. The release of the first draft sequence of the chicken genome in March 2004 (Wallis *et al.*, 2004), together with the development of associated molecular and electronic resources, has dramatically increased the potential of the chick as a subject for molecular developmental research (Stern, 2005). The chick is now not only a great system for physical manipulation and observation of the embryo but also offers the possibility of gene manipulation that is more rapid and direct than the mouse. One of the most powerful new techniques to be developed is *in ovo* electroporation, which allows targeted introduction and expression of genes within specific structures or cell groups in the living chick embryo (Bron *et al.*, 2004; Nakamura *et al.*, 2004). Using *in ovo* electroporation in chick would allow examination of the effect of abnormal exposure of the developing foregut to specific molecules. The prime transgenic alterations to test in this way would be over expression/ectopic expression of *Noggin* and knockdown of specific *BMPs* and

other components of the pathway. The resulting embryos could be then analysed with a view to revealing changes in foregut morphology and patterning using our established methodology (OPT) and markers (e.g. HNF3beta, *Sox2, Nkx2.1*).

6.2.2 Adriamycin influences the physical characteristics of the notochord tissue: the significance of altered E-cadherin expression.

In this work I showed that changes in notochordal properties are evident in the AMM that in turn may influence notochord delamination and signalling mechanisms from the notochord to the foregut endoderm (Chapter 5). E-cadherin, not normally expressed in the notochord at any stage of development is detected between notochord cells in adriamycin treated embryos. It is also known that Adriamycin can induce E-cadherin-mediated cell-cell adhesion by increasing expression of E-cadherin and beta-catenin in the breast cancer cell line YMB-S (Yang *et al.*, 1999). This strongly supports the conclusion that the notochord may be the primary target of disruption in AMM resulting in abnormal patterning of the foregut. One possible way to further explore the effect of aberrant E-cadherin on notochord cells would involve over expression of E-cadherin in the notochord and to look at the effect on its delamination and gene expression. This could be achieved by ectopic expression of the E-cadherin gene using previously described *in ovo* electroporation in chick, followed by *in situ* hybridization to analyse the expression of candidate genes (e.g. *Shh, Foxf1, Sox2, Noggin*).

Several lines of evidence implicate cadherins in different developmental processes. In most cases, the effects of cadherin perturbation can be interpreted in the light of their roles in cell

adhesion, cell sorting, and cell migration. It was however found that cadherins are more directly involved in the differentiation of certain types of tissues by influencing specific gene activity, important in regulating spatial patterning in mouse embryos (Larue *et al.*, 1994). It was shown for example that the presence of E-cadherin can negatively regulate Brachyury expression in an embryonal stem cell line (Larue *et al.*, 1994). Notochord development is governed by a set of transcription factors including *Foxa2, Brachyury*, and *Noto* (Ang and Rossant, 1994; Ben Abdelkhalek *et al.*, 2004; Herrmann and Kispert, 1994). By ablating *β-catenin*, it was shown that the notochord precursor cells lost expression of notochord specific genes *Noto* and *Brachyury* (Ukita *et al.*, 2009). Additionally, E-cadherin, usually only present in the endoderm, was detected in the notochord. Towards this end, further exploration of the impact of the E-cadherin on notochord development is required. I have examined *Brachyrury* expression in adriamycin treated embryos and it is expressed throughout the displaced notochord tissue but in situ hybridisation could be used to analyse the expression of the other notochord specific genes, *Foxa2* and *Noto.* This could be followed by investigation of *β-catenin* protein in the foregut endoderm and notochord cells in control and adriamycin treated groups to delineate any changes in expression or nuclear localisation, comparing it with E-cadherin detection.

One of the fundamental processes involved in both differentiation and organization is establishment of cell polarity. Epithelial cells show the classic example of cell polarity, with various molecules sorting to distinct apical and basolateral membrane domains (Tepass *et al.*, 2000). The crucial role of classic cadherins and their associated catenins in epithelial differentiation has been well documented, and these protein complexes seem to be broadly

important for forming and maintaining epithelial tissues (Tepass *et al.*, 2000). For example cadherins seem to be directly involved in maintaining cell polarity by directing the localization of the sec6/8 complex, which specifies vesicle targeting to the lateral membrane. This recruitment, and the continuous polarized delivery of specific molecular components to the lateral membrane, establishes and maintains the lateral membrane domain of epithelial cells and contributes to epithelial apical/basal polarity (Grindstaff *et al.*, 1998).

The initial generation of cell asymmetry may either be cell autonomous, resulting, for example, from the unequal distribution of cytoplasmic contents, or alternatively it may result from intracellular interactions. In this thesis I suggested that abnormal distribution of E-cadherin might indicate that intercellular adhesion within cells of the notochord and possibly also between notochord cells and foregut cells have increased, perhaps contributing to impaired delamination. E-cadherins are characterized by long extracellular and the cytoplasmic domains. The extracellular domain of E-cadherin establishes interactions between neighboring cells and cytoplasmic tail associates with an array of intracellular proteins (Gumbiner *et al.*, 1988). These proteins link cell–cell adhesion to the actin–myosin network, vesicle transport, and cell polarity machinery. The best studied of these links is the binding of the cytoplasmic tail of E-cadherin to the Armadillo repeat in the *β-catenin* protein, which in turn binds *α-catenin*, which interacts with actin and several actin-binding proteins (Bershadsky, 2004; Yonemura *et a*l., 2010). Through the action of these intracellular binding partners, E-cadherin contacts modulate actin filament organization at the underlying cortex (Baum and Perrimon, 2001; Drees *et al.*, 2005; Perez-Moreno *et al.*, 2003). Therefore, in order to understand the contribution of cytoskeletal components in abnormal delamination of the

notochord in AMM, more ultrastructural analysis of the notochord and cytoskeleton markers is required. Electron microscopy could be then used to investigate in control and adriamvcin treated embryos within notochord and endodermal cells intracellular localization and organisation of *β-catenin*, *α-catenin* and *F-actin*.

6.2.3 Identification of further molecular role players

In this thesis I showed evidence that the *BMP/Noggin* pathway is deregulated in adriamycin treated embryos and I suggested that this might contribute to the foregut abnormalities observed (Chapter 4). I argue here that further work should focus on this pathway to work out which other components of the pathway are affected and to pin down how this could lead to the observed foregut malformations. Very little is known about *BMP* targets in general and particularly in the foregut, so adding to our knowledge of this signalling pathway would be very valuable in itself but work on this pathway in the AMM model would also provide extra candidate genes to investigate and build a more complete picture of the processes that are affected. This could be approached in two ways. In silico, where it would be possible to carry out computational analysis of all microarray data in the Gene Expression Omnibus database where the *BMP* pathway has been altered to select candidate genes that are a) misregulated in these experiments and b) also expressed in the gut (using gene expression databases such as MGI (web site) and EMAGE (web site). *In situ* hybridisation could then be used to confirm the localisation of the expression in the normal gut, adding to our knowledge of the normal developing gut, and to assay any alterations in expression in the AMM. In addition, an experimental approach to identify candidate genes could be undertaken, for example using an

endodermal cell line (Adamson *et al.*, 1985) or primary cells plated from the embryonic foregut, exposed to recombinant *BMP* protein or *Noggin* or Control and then carry out a microarray analysis (or whole transcriptome sequencing) to establish which genes are up or down regulated as a result of activation or blocking of the *BMP* pathway. The most consistent and promising candidates indicated in this way could then be tested in the cell culture system to see if the response to *BMP* signalling is direct or indirect by addition of cyclohexamide to block protein production- if up or down regulation still occurs in the presence of cyclohexamide the response must be direct. Any targets identified in this way could then be analysed in the AMM for alterations in expression.

6.3 Impact on our understanding of human OA/TOF; clinical implications

In recent years the accumulation of data arising from knock out mouse studies on abnormal signalling pathology, together with work on the AMM, is gradually building up a picture of key events that might lead to foregut malformations, however we appear to have only scratched the surface in terms of understanding the etiology of human OA/TOF. It is likely that the enormous advances in our understanding of the human genome will allow us to make best use in future of the information generated from the study of mouse genetics. For example array based technologies have been successful in delineation of the role of the 16q24.1 locus in the etiology of severe developmental malformations including OA/TOF (Stankiewicz *et al.*, 2009). Two genes, *FOXF1* and *FOXC2*, of the four genes in the region 16q24.1 have been reasonably well studied both in humans and the mouse therefore a comparison of the

phenotypes due to *FOXF1* and *FOXC2* mutations in humans, and to *Foxf1* and *Foxc2* inactivation in mouse was possible (Shaw-Smith, 2009). The identification of genes associated with oesophageal atresia shown in this work offers the prospect of improvements in genetic counselling for this disorder. For example the sequencing of genes in the cohort of patients, looking for mutations in candidate genes *SHH, FOXF1, FGF10, NOG* and *SOX2* could be carried out on a large scale on whole-genome amplified DNA, as has recently been described for the whole X chromosome (Tarpey *et al.*, 2009). The goal of these studies would be to complete the 'cytogenetic map' for osophageal atresia and tracheo-oesophageal fistula. Genes and/or proteins identified to play a role in etiology of OA/TOF could be then used as a marker for prenatal genetic testing. DNA chips could be used for high-risk pregnancies, such as those with familial history of congenital anomalies and those selected on the basis of prenatal ultrasound examination. This could provide important information about short and long term prognosis, thereby aiding in parental counseling and preparation of medical care. However, in this thesis I showed that multiple parts of the system can be disturbed leading to OA/TOF in mouse embryos. Therefore most probably it would be difficult to identify one factor responsible for the malformations in human. If so prenatal diagnosis would be challenging and also difficult to foresee how a prenatal therapy could be envisaged in the short term. However, more knowledge about the steps involved and how they can be disrupted will lead to new insights, perhaps on alternative types of treatment, or perhaps protection against notochord disorders.

The databases that store information on all patients with congenital anomalies, including OA/TOF, are pivotal in research of the etiology of these malformations. In Europe, a number

of birth defects registries have joined forces in EUROCAT, the European network of population-based registers for epidemiological surveillance of congenital anomalies (http://www.eurocat-network.eu/). The registries provide valuable information on trends in frequency of occurrence of birth defects and patterns of anomalies seen to facilitate early warning of teratogenic exposures. This international collaboration is especially valuable for rare exposure or rare anomalies, making it possible to combine data and draw more firm conclusions faster. The pooling of the data enables research questions to be answered on a large scale, making results more stable. A similar idea, expanding the data by collection of DNA from biological samples (blood, buccal swabs, urine, etc) from the children with OA/TOF and possibly their parents, could provide a DNA bank combined with detailed patient characteristics. This offers the big advantage for further genetic and epidemiological study of these foregut malformations. For example, studies on gene-environment interactions may lead to more targeted prevention strategies for groups or even individuals who are at higher risk because of the genotype. With better etiological knowledge we could recommend preventive measures, such as the advice to use folic acid in the periconceptional period as a means to lower the risk of neural tube defects in offspring.

In summary the research presented in this thesis has provided the following new insights in to our understanding of the origin of OA/TOF foregut malformations: 1) The notochord is a vulnerable tissue that may be the site of primary developmental disturbances leading to OA/TOF; 2) Developmental processes involved in foregut separation could be disturbed at multilple levels. This is supported both by human studies searching for a genetic basis to

OA/TOF and animal model studies, such as presented here; 3) Future studies should be directed at investigating the *BMP* signalling pathway.

Bibliography

Aberle H, Schwartz H, Kemler R. 1996. Cadherin-catenin complex: protein interactions and their implications for cadherin function. J Cell Biochem 61(4):514-523.

Ackerman KG, Herron BJ, Vargas SO, Huang H, Tevosian SG, Kochilas L, Rao C, Pober BR, Babiuk RP, Epstein JA, Greer JJ, Beier DR. 2005. Fog2 Is Required for Normal Diaphragm and Lung Development in Mice and Humans. PLoS Genet 1(1):e10.

Ackerman KG, Wang J, Luo L, Fujiwara Y, Orkin SH, Beier DR. 2007. Gata4 Is Necessary for Normal Pulmonary Lobar Development. Am J Respir Cell Mol Biol 36(4):391-397.

Adams DS, Keller R, Koehl MA. 1990. The mechanics of notochord elongation, straightening and stiffening in the embryo of Xenopus laevis. Development 110(1):115-130.

Adamson ED, Strickland S, Tu M, Kahan B. 1985. A teratocarcinoma-derived endoderm stem cell line (1H5) that can differentiate into extra-embryonic endoderm cell types. Differentiation 29(1):68-76.

Alanentalo T, Asayesh A, Morrison H, Loren CE, Holmberg D, Sharpe J, Ahlgren U. 2007. Tomographic molecular imaging and 3D quantification within adult mouse organs. Nat Meth 4(1):31-33.

Alcedo J, Ayzenzon M, Von Ohlen T, Noll M, Hooper JE. 1996. The Drosophila smoothened Gene Encodes a Seven-Pass Membrane Protein, a Putative Receptor for the Hedgehog Signal. Cell 86(2):221-232.

Alcedo J, Noll M. 1997. Hedgehog and its patched-smoothened receptor complex: a novel signalling mechanism at the cell surface. Biol Chem 378(7):583-590.

Alexandre C, Jacinto A, Ingham PW. 1996. Transcriptional activation of hedgehog target genes in Drosophila is mediated directly by the cubitus interruptus protein, a member of the GLI family of zinc finger DNA-binding proteins. Genes & Development 10(16):2003-2013.

Ang SL, Rossant J. 1994. HNF-3β is essential for node and notochord formation in mouse development. Cell 78(4):561-574.

Apte U, Zeng G, Thompson MD, Muller P, Micsenyi A, Cieply B, Kaestner KH, Monga SPS. 2007. β-Catenin is critical for early postnatal liver growth. American Journal of Physiology - Gastrointestinal and Liver Physiology 292(6):G1578-G1585.

Arsic D, Cameron V, Ellmers L, Quan QB, Keenan J, Beasley S. 2004. Adriamycin disruption of the Shh-Gli pathway is associated with abnormalities of foregut development. Journal of Pediatric Surgery 39(12):1747-1753.

Arsić D, Keenan J, Quan QB, Beasley S. 2003. Differences in the levels of Sonic hedgehog protein during early foregut development caused by exposure to Adriamycin give clues to the role of the Shh gene in oesophageal atresia. Pediatr Surg Int 19(6):463-466.

Auerbach AD. 2009. Fanconi anemia and its diagnosis. Mutation Research/Fundamental and Molecular Mechanisms of Mutagenesis 668(1-2):4-10.

Baum B, Perrimon N. 2001. Spatial control of the actin cytoskeleton in Drosophila epithelial cells. Nat Cell Biol 3(10):883-890.

Beck F, Erler T, Russell A, James R. 1995. Expression of Cdx-2 in the mouse embryo and placenta: Possible role in patterning of the extra-embryonic membranes. American Journal of Anatomy 204(3):219-227.

Beites CL, Hollenbeck PLW, Kim J, Lovell-Badge R, Lander AD, Calof AL. 2009. Follistatin modulates a BMP autoregulatory loop to control the size and patterning of sensory domains in the developing tongue. Development 136(13):2187-2197.

Bellusci S, Furuta Y, Rush MG, Henderson R, Winnier G, Hogan BL. 1997a. Involvement of Sonic hedgehog (Shh) in mouse embryonic lung growth and morphogenesis. Development 124(1):53-63.

Bellusci S, Grindley J, Emoto H, Itoh N, Hogan BL. 1997b. Fibroblast growth factor 10 (FGF10) and branching morphogenesis in the embryonic mouse lung. Development 124(23):4867-4878.

Ben Abdelkhalek H, Beckers A, Schuster-Gossler K, Pavlova MN, Burkhardt H, Lickert H, Rossant J, Reinhardt R, Schalkwyk LC, Müller I, Herrmann BG, Ceolin M, Rivera-Pomar R, Gossler A. 2004. The mouse homeobox gene Not is required for caudal notochord development and affected by the truncate mutation. Genes & Development 18(14):1725-1736.

Bershadsky A. 2004. Magic touch: how does cell-cell adhesion trigger actin assembly? Trends in Cell Biology 14(11):589-593.

Boulet AM, Capecchi MR. 1996. Targeted Disruption ofhoxc-4 Causes Esophageal Defects and Vertebral Transformations. Developmental Biology 177(1):232-249.

Bouwmeester T, Kim S-H, Sasai Y, Lu B, Robertis EMD. 1996. Cerberus is a head-inducing secreted factor expressed in the anterior endoderm of Spemann's organizer. Nature 382(6592):595-601.

Bragg AD, Moses HL, Serra R. 2001. Signaling to the epithelium is not sufficient to mediate all of the effects of transforming growth factor [beta] and bone morphogenetic protein 4 on murine embryonic lung development. Mechanisms of Development 109(1):13-26.

Bron R, Eickholt BJ, Vermeren M, Fragale N, Cohen J. 2004. Functional knockdown of neuropilin-1 in the developing chick nervous system by siRNA hairpins phenocopies genetic ablation in the mouse. Developmental Dynamics 230(2):299-308.

Brunner HG, Bokhoven Hv. 2005. Genetic players in esophageal atresia and tracheoesophageal fistula. Current Opinion in Genetics & Development 15(3):341-347.

Cardoso WV, Lu J. 2006. Regulation of early lung morphogenesis: questions, facts and controversies. Development 133(9):1611-1624.

Chapman DL, Garvey N, Hancock S, Alexiou M, Agulnik SI, Gibson-Brown JJ, Cebra-Thomas J, Bollag RJ, Silver LM, Papaioannou VE. 1996. Expression of the T-box family genes, Tbx1–Tbx5, during early mouse development. Developmental Dynamics 206(4):379-390.

Chen F, Desai TJ, Qian J, Niederreither K, LÃ¼ J, Cardoso WV. 2007. Inhibition of Tgfβ signaling by endogenous retinoic acid is essential for primary lung bud induction. Development 134(16):2969-2979.

Chen Y, Struhl G. 1996. Dual Roles for Patched in Sequestering and Transducing Hedgehog. Cell 87(3):553-563.

Cheng W, Bishop AE, Spitz L, Polak JM. 1997. Abnormalities of neuropeptides and neural markers in the esophagus of fetal rats with adriamycin-induced esophageal atresia. J Pediatr Surg 32(10):1420 - 1423.

Chiang C, Litingtung Y, Lee E, Young KE, Corden JL, Westphal H, Beachy PA. 1996. Cyclopia and defective axial patterning in mice lacking Sonic hedgehog gene function. Nature 383(6599):407-413.

Chittmittrapap S, Spitz L, Kiely EM, Brereton RJ. 1989. Oesophageal atresia and associated anomalies. Arch Dis Child 64(3):364-368.

Chuang P-T, Kawcak TN, McMahon AP. 2003. Feedback control of mammalian Hedgehog signaling by the Hedgehog-binding protein, Hip1, modulates Fgf signaling during branching morphogenesis of the lung. Genes & Development 17(3):342-347.

Clark D. 1999. Esophageal atresia and tracheoesophageal fistula. Am Fam Physician 59(4):910-916; 919-920.

Cleaver O, Krieg PA. 2001. Notochord Patterning of the Endoderm. Developmental Biology 234(1):1-12.

Clementi M, Di Gianantonio E, Pelo E, Mammi I, Basile RT, Tenconi R. 1999. Methimazole embryopathy: Delineation of the phenotype. American Journal of Medical Genetics 83(1):43-46.

Coutinho P, Parsons MJ, Thomas KA, Hirst EMA, Saúde L, Campos I, Williams PH, Stemple DL. 2004. Differential Requirements for COPI Transport during Vertebrate Early Development. Developmental Cell 7(4):547-558.

Crisera CA, Connelly PR, Marmureanu AR, Colen KL, Rose MI, Li M, Longaker MT, Gittes GK. 1999. Esophageal atresia with tracheoesophageal fistula: suggested mechanism in faulty organogenesis. J Pediatr Surg 34(1):204 - 208.

Crisera CA, Maldonado TS, Kadison AS, Li M, Longaker MT, Gittes GK. 2000a. Patterning of the "Distal Esophagus" in Esophageal Atresia with Tracheo-esophageal Fistula: Is Thyroid Transcription Factor 1 a Player? Journal of Surgical Research 92(2):245-249.

Crisera CA, Maldonado TS, Longaker MT, Gittes GK. 2000b. Defective fibroblast growth factor signaling allows for nonbranching growth of the respiratory-derived fistula tract in esophageal atresia with tracheoesophageal fistula. Journal of Pediatric Surgery 35(10):1421-1425.

Cullinane C, Cutts SM, Panousis C, Phillips DR. 2000. Interstrand cross-linking by Adriamycin in nuclear and mitochondrial DNA of MCF-7 cells. Nucleic Acids Research 28(4):1019-1025.

Cullinane C, Cutts SM, van Rosmalen A, Phillips DR. 1994. Formation of adriamycin-DNA adducts in vitro. Nucleic Acids Research 22(12):2296-2303.

Dai P, Akimaru H, Tanaka Y, Maekawa T, Nakafuku M, Ishii S. 1999. Sonic Hedgehog-induced Activation of the Gli1Promoter Is Mediated by GLI3. Journal of Biological Chemistry 274(12):8143-8152.

Danos MC, Yost HJ. 1995. Linkage of cardiac left-right asymmetry and dorsal-anterior development in Xenopus. Development 121(5):1467-1474.

Davidson BP, Kinder SJ, Steiner K, Schoenwolf GC, Tam PPL. 1999. Impact of Node Ablation on the Morphogenesis of the Body Axis and the Lateral Asymmetry of the Mouse Embryo during Early Organogenesis. Developmental Biology 211(1):11-26.

Dawrant M, Giles S, Bannigan J, Puri P. 2007a. Adriamycin mouse model: a variable but reproducible model of tracheo-oesophageal malformations. Pediatric Surgery International 23(5):469-472.

Dawrant MJ, Giles S, Bannigan J, Puri P. 2007b. Abnormal separation of the respiratory primordium in the adriamycin mouse model of tracheoesophageal malformations. Journal of Pediatric Surgery 42(2):375-380.

Dawrant MJ, Giles S, Bannigan J, Puri P. 2007c. Adriamycin produces a reproducible teratogenic model of vertebral, anal, cardiovascular, tracheal, esophageal, renal, and limb anomalies in the mouse. Journal of Pediatric Surgery 42(10):1652-1658.

De Falco F, Cainarca S, Andolfi G, Ferrentino R, Berti C, Rodríguez Criado G, Rittinger O, Dennis N, Odent S, Rastogi A, Liebelt J, Chitayat D, Winter R, Jawanda H, Ballabio A, Franco B, Meroni G. 2003. X-linked Opitz syndrome: Novel mutations in the MID1 gene and redefinition of the clinical spectrum. American Journal of Medical Genetics Part A 120A(2):222-228.

de Jong EM, Felix JF, de Klein A, Tibboel D. 2010. Etiology of esophageal atresia and tracheoesophageal fistula: "mind the gap". Curr Gastroenterol Rep 12(3):215-222.

De Langhe SP, Sala FG, Del Moral P-M, Fairbanks TJ, Yamada KM, Warburton D, Burns RC, Bellusci S. 2005. Dickkopf-1 (DKK1) reveals that fibronectin is a major target of Wnt signaling in branching morphogenesis of the mouse embryonic lung. Developmental Biology 277(2):316-331.

De Moerlooze L, Spencer-Dene B, Revest JM, Hajihosseini M, Rosewell I, Dickson C. 200. An important role for the IIIb isoform of fibroblast growth factor receptor 2 (FGFR2) in mesenchymal-epithelial signalling during mouse organogenesis. Development 127(3):483-492.

Dean CH, Miller L-AD, Smith AN, Dufort D, Lang RA, Niswander LA. 2005. Canonical Wnt signaling negatively regulates branching morphogenesis of the lung and lacrimal gland. Developmental Biology 286(1):270-286.

del Moral P-M, De Langhe SP, Sala FG, Veltmaat JM, Tefft D, Wang K, Warburton D, Bellusci S. 2006. Differential role of FGF9 on epithelium and mesenchyme in mouse embryonic lung. Developmental Biology 293(1):77-89.

Denef N, Neubüser D, Perez L, Cohen SM. 2000. Hedgehog Induces Opposite Changes in Turnover and Subcellular Localization of Patched and Smoothened. Cell 102(4):521-531.

Depaepe A, Dolk, H, Lechat M.F. 1993. The epidemiology of tracheo-oesophageal fistula and oesophageal atresia in Europe. Arch Dis Child 68(6):743-748.

Desai TJ, Chen F, Lü J, Qian J, Niederreither K, Dollé P, Chambon P, Cardoso WV. 2006. Distinct roles for retinoic acid receptors alpha and beta in early lung morphogenesis. Developmental Biology 291(1):12-24.

Desai TJ, Malpel S, Flentke GR, Smith SM, Cardoso WV. 2004. Retinoic acid selectively regulates Fgf10 expression and maintains cell identity in the prospective lung field of the developing foregut. Developmental Biology 273(2):402-415.

Dessimoz J, Bonnard C, Huelsken J, Grapin-Botton A. 2005. Pancreas-Specific Deletion of β-Catenin Reveals Wnt-Dependent and Wnt-Independent Functions during Development. Current Biology 15(18):1677-1683.

Di Gianantonio E, Schaefer C, Mastroiacovo PP, Cournot MP, Benedicenti F, Reuvers M, Occupati B, Robert E, Bellemin B, Addis A, Arnon J, Clementi M. 2001. Adverse effects of prenatal methimazole exposure. Teratology 64(5):262-266.

Dickman ED, Thaller C, Smith SM. 1997. Temporally-regulated retinoic acid depletion produces specific neural crest, ocular and nervous system defects. Development 124(16):3111-3121.

Diez-Pardo JA, Baoquan Q, Navarro C, Tovar JA. 1996. A new rodent experimental model of esophageal atresia and tracheoesophageal fistula: Preliminary report. Journal of Pediatric Surgery 31(4):498-502.

Digilio MC, Marino B, Bagolan P, Giannotti A, Dallapiccola B. 1999. Microdeletion 22q11 and oesophageal atresia. J Med Genet 36(2):137-139.

Dodd J, Jessell TM, Placzek M. 1998. The When and Where of Floor Plate Induction. Science 282(5394):1654-1657.

Dominguez M, Brunner M, Hafen E, Basler K. 1996. Sending and Receiving the Hedgehog Signal: Control by the Drosophila Gli Protein Cubitus interruptus. Science 272(5268):1621-1625.

Domyan ET, Ferretti E, Throckmorton K, Mishina Y, Nicolis SK, Sun X. 2011. Signaling through BMP receptors promotes respiratory identity in the foregut via repression of Sox2. Development 138(5):971-981.

Drees F, Pokutta S, Yamada S, Nelson WJ, Weis WI. 2005. α-Catenin Is a Molecular Switch that Binds E-Cadherin-β-Catenin and Regulates Actin-Filament Assembly. Cell 123(5):903-915.

Echelard Y, Epstein DJ, St-Jacques B, Shen L, Mohler J, McMahon JA, McMahon AP. 1993. Sonic hedgehog, a member of a family of putative signaling molecules, is implicated in the regulation of CNS polarity. Cell 75(7):1417-1430.

Felix JF, Steegers-Theunissen RPM, de Walle HEK, de Klein A, Torfs CP, Tibboel D. 2007a. Esophageal atresia and tracheoesophageal fistula in children of women exposed to diethylstilbestrol in utero. American Journal of Obstetrics and Gynecology 197(1):38.e31-38.e35.

Felix JF, Tibboel D, de Klein A. 2007b. Chromosomal anomalies in the aetiology of oesophageal atresia and tracheo-oesophageal fistula. European Journal of Medical Genetics 50(3):163-175.

Fouquet B, Weinstein BM, Serluca FC, Fishman MC. 1997. Vessel Patterning in the Embryo of the Zebrafish: Guidance by Notochord. Developmental Biology 183(1):37-48.

Furuta Y, Hogan BLM. 1998. BMP4 is essential for lens induction in the mouse embryo. Genes & Development 12(23):3764-3775.

Gilbert AM, Bursavich MG, Alon N, Bhat BM, Bex FJ, Cain M, Coleburn V, Gironda V, Green P, Hauze DB, Kharode Y, Krishnamurthy G, Kirisits M, Lam H-S, Liu Y-B, Lombardi S, Matteo J, Murrills R, Robinson JA, Selim S, Sharp M, Unwalla R, Varadarajan U, Zhao W, Yaworsky PJ. 2010. Hit to lead studies on (hetero)arylpyrimidines--Agonists of the canonical Wnt-β-catenin cellular messaging system. Bioorganic & Medicinal Chemistry Letters 20(1):366-370.

Gilbert SF. 2006. Developmental Biology. MASS S, editor. Eight Edition ed: Sinauer Associates, Inc.

Gillick J, Giles S, Bannigan S, Puri P. 2002. Midgut atresias result from abnormal development of the notochord in an Adriamycin rat model. Journal of Pediatric Surgery 37(5):719-722.

Gillick J, Mooney E, Giles S, Bannigan J, Puri P. 2003. Notochord anomalies in the adriamycin rat model: A morphologic and molecular basis for the VACTERL association. Journal of Pediatric Surgery 38(3):469-473.

Gillick J, Mortell A, Dawrant M, Giles S, Bannigan J, Puri P. 2008. The Adriamycin rat/mouse model and its importance to the paediatric surgeon. Pediatric Surgery International 24(1):113-118.

Goss AM, Tian Y, Tsukiyama T, Cohen ED, Zhou D, Lu MM, Yamaguchi TP, Morrisey EE. 2009. Wnt2/2b and [beta]-Catenin Signaling Are Necessary and Sufficient to Specify Lung Progenitors in the Foregut. Developmental Cell 17(2):290-298.

Goujard J, Rumeau-Rouquette C. 1977. First-trimester exposure to progestagen/oestrogen and congenital malformations. Lancet 26(1):482-483.

Goulding M, Lumsden A, Paquette AJ. 1994. Regulation of Pax-3 expression in the dermomyotome and its role in muscle development. Development 120(4):957-971.

Granata A, Quaderi NA. 2003. The Opitz syndrome gene MID1 is essential for establishing asymmetric gene expression in Hensen's node. Developmental Biology 258(2):397-405.

Green RP, Cohn SM, Sacchettini JC, Jackson KE, Gordon JI. 1992. The mouse intestinal fatty acid binding protein gene: nucleotide sequence, pattern of developmental and regional expression, and proposed structure of its protein product. DNA Cell Biol 11(1):31-41.

Grindstaff KK, Yeaman C, Anandasabapathy N, Hsu S-C, Rodriguez-Boulan E, Scheller RH, Nelson WJ. 1998. Sec6/8 Complex Is Recruited to Cell-Cell Contacts and Specifies Transport Vesicle Delivery to the Basal-Lateral Membrane in Epithelial Cells. Cell 93(5):731-740.

Gross RE. 1953. Atresia of the oesophagus. In: Gross RE, editor. The surgery of infancy and chilhood. Philadelphia: W. B. Saunders.

Gumbiner B, Stevenson B, Grimaldi A. 1988. The role of the cell adhesion molecule uvomorulin in the formation and maintenance of the epithelial junctional complex. The Journal of Cell Biology 107(4):1575-1587.

Hajduk P, Murphy P, Puri P. 2010a. Fgf10 gene expression is delayed in the embryonic lung mesenchyme in the adriamycin mouse model. Pediatric Surgery International 26(1):23-27.

Hajduk P, Murphy P, Puri P. 2010b. Mesenchymal expression of Tbx4 gene is not altered in Adriamycin mouse model. Pediatric Surgery International 26(4):407-411.

Hajduk P, Sato H, Puri P, Murphy P, 2011. Abnormal notochord branching is associated with foregut abnormalities in an adriamycin treated mouse model. PloS One 6(11): e27635.

Halpern ME, Ho RK, Walker C, Kimmel CB. 1993. Induction of muscle pioneers and floor plate is distinguished by the zebrafish no tail mutation. Cell 75(1):99-111.

Hamill KJ, Kligys K, Hopkinson SB, Jones JCR. 2009. Laminin deposition in the extracellular matrix: a complex picture emerges. J Cell Sci 122(24):4409-4417.

Harris-Johnson KS, Domyan ET, Vezina CM, Sun X. 2009. β-Catenin promotes respiratory progenitor identity in mouse foregut. Proceedings of the National Academy of Sciences 106(38):16287-16292.

Heasman J, Crawford A, Goldstone K, Garner-Hamrick P, Gumbiner B, McCrea P, Kintner C, Noro CY, Wylie C. 1994. Overexpression of cadherins and underexpression of [beta]-catenin inhibit dorsal mesoderm induction in early Xenopus embryos. Cell 79(5):791-803.

Hebrok M, Kim SK, Melton DA. 1998. Notochord repression of endodermal Sonic hedgehog permits pancreas development. Genes Dev 12(11):1705-1713.

Hermiston ML, Wong MH, Gordon JI. 1996. Forced expression of E-cadherin in the mouse intestinal epithelium slows cell migration and provides evidence for nonautonomous regulation of cell fate in a self-renewing system. Genes & Development 10(8):985-996.

Herrmann BG, Kispert A. 1994. The T genes in embryogenesis. Trends in Genetics 10(8):280-286.

Hinck L, Nelson W, Papkoff J. 1994. Wnt-1 modulates cell-cell adhesion in mammalian cells by stabilizing beta-catenin binding to the cell adhesion protein cadherin. The Journal of Cell Biology 124(5):729-741.

Holland AJA, Ron O, Pierro A, Drake D, Curry JI, Kiely EM, Spitz L. 2009. Surgical outcomes of esophageal atresia without fistula for 24 years at a single institution. Journal of Pediatric Surgery 44(10):1928-1932.

Hooper JE, Scott MP. 2005. Communicating with Hedgehogs. Nat Rev Mol Cell Biol 6(4):306-317.

Hösgör M, Ijzendoorn Y, Mooi WJ, Tibboel D, de Krijger RR. 2002. Thyroid transcription factor-1 expression during normal human lung development and in patients with congenital diaphragmatic hernia. Journal of Pediatric Surgery 37(9):1258-1262.

Hynes RO. 2009. The Extracellular Matrix: Not Just Pretty Fibrils. Science 326(5957):1216-1219.

Inuzuka H, Redies C, Takeichi M. 1991. Differential expression of R- and N-cadherin in neural and mesodermal tissues during early chicken development. Development 113(3):959-967.

Ioannides AS, Chaudhry B, Henderson DJ, Spitz L, Copp AJ. 2002. Dorsoventral patterning in oesophageal atresia with tracheo-oesophageal fistula: Evidence from a new mouse model. Journal of Pediatric Surgery 37(2):185-191.

Ioannides AS, Henderson DJ, Spitz L, Copp AJ. 2003. Role of Sonic hedgehog in the development of the trachea and oesophagus. Journal of Pediatric Surgery 38(1):29-36.

Ioannides AS, Massa V, Ferraro E, Cecconi F, Spitz L, Henderson DJ, Copp AJ. 2010. Foregut separation and tracheo-oesophageal malformations: The role of tracheal outgrowth, dorso-ventral patterning and programmed cell death. Developmental Biology 337(2):351-362.

Johnston JJ, Olivos-Glander I, Killoran C, Elson E, Turner JT, Peters KF, Abbott MH, Aughton DJ, Aylsworth AS, Bamshad MJ, Booth C, Curry CJ, David A, Dinulos MB, Flannery DB, Fox MA, Graham JM, Grange DK, Guttmacher AE, Hannibal MC, Henn W, Hennekam RC, Holmes LB, Hoyme HE, Leppig KA, Lin AE, Macleod P, Manchester DK, Marcelis C, Mazzanti L, McCann E, McDonald MT, Mendelsohn NJ, Moeschler JB, Moghaddam B, Neri G, Newbury-Ecob R, Pagon RA, Phillips JA, Sadler LS, Stoler JM, Tilstra D, Walsh Vockley CM, Zackai EH, Zadeh TM, Brueton L, Black GC, Biesecker LG. 2005. Molecular and clinical analyses of Greig cephalopolysyndactyly and Pallister-Hall syndromes: robust phenotype prediction from the type and position of GLI3 mutations. Am J Hum Genet 76(4):609-622.

Jurand A. 1974. Some aspects of the development of the notochord in mouse embryos. Journal of Embryology and Experimental Morphology 32(1):1-33.

Kaufman M. 1992. The atlas of mouse development. Revised edition edn.

Kaufman MH. 1999. The atlas of mouse development. Academic, London.

Kemler R. 1993. From cadherins to catenins: cytoplasmic protein interactions and regulation of cell adhesion. Trends in Genetics 9(9):317-321.

Kenney AM, Cole MD, Rowitch DH. 2003. Nmyc upregulation by sonic hedgehog signaling promotes proliferation in developing cerebellar granule neuron precursors. Development 130(1):15-28.

Kerwin J, Scott M, Sharpe J, Puelles L, Robson S, Martinez-de-la-Torre M, Ferran J, Feng G, Baldock R, Strachan T. 2004. 3 dimensional modelling of early human brain development using optical projection tomography. BMC Neurosci 5:27.

Kerwin J, Yang Y, Merchan P, Sarma S, Thompson J, Wang X, Sandoval J, Puelles L, Baldock R, Lindsay S. 2010. The HUDSEN Atlas: a three-dimensional (3D) spatial framework for studying gene expression in the developing human brain. Journal of Anatomy 217(4):289-299.

Kikuchi M, Yatabe M, Fujiwara K, Horiguchi K, Kusumoto K, Kouki T, Sakamoto A, Yashiro T. 2009. Spatio-temporal relation between cadherin switching and cytogenesis of hormone-producing cells in the developing rat adenohypophysis. Anatomical Science International 84(3):155-160.

Kim SK, Hebrok M, Melton DA. 1997. Notochord to endoderm signaling is required for pancreas development. Development 124(21):4243-4252.

Kimura S, Hara Y, Pineau T, Fernandez-Salguero P, Fox CH, Ward JM, Gonzalez FJ. 1996. The T/ebp null mouse: thyroid-specific enhancer-binding protein is essential for the organogenesis of the thyroid, lung, ventral forebrain, and pituitary. Genes & Development 10(1):60-69.

Kimura S, Ward JM, Minoo P. 1999. Thyroid-specific enhancer-binding protein/thyroid transcription factor 1 is not required for the initial specification of the thyroid and lung primordia. Biochimie 81(4):321-327.

Kluth D, Fiegel, H.,. 2003. The embryology of the foregut. Semin Pediatr Surg 12(1):3-9.

Kluth D, Steding G, Seidl W. 1987. The embryology of foregut malformations. J Pediatr Surg 22(5):389-393.

Kyyrönen P, Hemmink K. 1988. Gastro-intestinal atresias in Finland in 1970-79, indicating time-place clustering. J Epidemiol Community Health 42(3):257-265.

Larue L, Ohsugi M, Hirchenhain J, Kemler R. 1994. E-cadherin null mutant embryos fail to form a trophectoderm epithelium. Proceedings of the National Academy of Sciences 91(17):8263-8267.

Lawson KA, Meneses JJ, Pedersen RA. 1986. Cell fate and cell lineage in the endoderm of the presomite mouse embryo, studied with an intracellular tracer. Developmental Biology 115(2):325-339.

Lawson KA, Meneses JJ, Pedersen RA. 1991. Clonal analysis of epiblast fate during germ layer formation in the mouse embryo. Development 113(3):891-911.

Lawson KA, Pedersen RA. 1987. Cell fate, morphogenetic movement and population kinetics of embryonic endoderm at the time of germ layer formation in the mouse. Development 101(3):627-652.

Lazzaro D, Price M, de Felice M, Di Lauro R. 1991. The transcription factor TTF-1 is expressed at the onset of thyroid and lung morphogenesis and in restricted regions of the foetal brain. Development 113(4):1093-1104.

Lebeche D, Malpel S, Cardoso WV. 1999. Fibroblast growth factor interactions in the developing lung. Mechanisms of Development 86(1-2):125-136.

Li C, Xiao J, Hormi K, Borok Z, Minoo P. 2002. Wnt5a Participates in Distal Lung Morphogenesis. Developmental Biology 248(1):68-81.

Li M, Li C, Liu Y-h, Xing Y, Hu L, Borok Z, Kwong KY-C, Minoo P. 2008a. Mesodermal Deletion of Transforming Growth Factor-β Receptor II Disrupts Lung Epithelial Morphogenesis. Journal of Biological Chemistry 283(52):36257-36264.

Li Y, Gordon J, Manley NR, Litingtung Y, Chiang C. 2008b. Bmp4 is required for tracheal formation: A novel mouse model for tracheal agenesis. Developmental Biology 322(1):145-155.

Li Y, Litingtung Y, Ten Dijke P, Chiang C. 2007. Aberrant Bmp signaling and notochord delamination in the pathogenesis of esophageal atresia. Developmental Dynamics 236(3):746-754.

Linsenmayer TF, Gibney E, Schmid TM. 1986. Segmental appearance of type X collagen in the developing avian notochord. Developmental Biology 113(2):467-473.

Lioubinski O, Alonso MT, Alvarez Y, Vendrell V, Garrosa M, Murphy P, Schimmang T. 2006. FGF signalling controls expression of vomeronasal receptors during embryogenesis. Mechanisms of Development 123(1):17-23.

Litingtung Y, Lei L, Westphal H, Chiang C. 1998. Sonic hedgehog is essential to foregut development. Nat Genet 20(1):58-61.

Lohr JL, Danos MC, Yost HJ. 1997. Left-right asymmetry of a nodal-related gene is regulated by dorsoanterior midline structures during Xenopus development. Development 124(8):1465-1472.

Luo J, Sucov HM, Bader J-A, Evans RM, Giguère V. 1996. Compound mutants for retinoic acid receptor RARβ and RARα1 reveal developmental functions for multiple RARβ isoforms. Mechanisms of Development 55(1):33-44.

Maeda Y, Dave V, Whitsett JA. 2007. Transcriptional Control of Lung Morphogenesis. Physiol Rev 87(1):219-244.

Mahlapuu M, Enerback S, Carlsson P. 2001. Haploinsufficiency of the forkhead gene Foxf1, a target for sonic hedgehog signaling, causes lung and foregut malformations. Development 128(12):2397-2406.

Mahlapuu M, Pelto-Huikko M, Aitola M, Enerbäck S, Carlsson P. 1998. FREAC-1 Contains a Cell-Type-Specific Transcriptional Activation Domain and Is Expressed in Epithelial-Mesenchymal Interfaces. Developmental Biology 202(2):183-195.

Mailleux AA, Tefft D, Ndiaye D, Itoh N, Thiery JP, Warburton D, Bellusci S. 2001. Evidence that SPROUTY2 functions as an inhibitor of mouse embryonic lung growth and morphogenesis. Mechanisms of Development 102(1-2):81-94.

Malpel S, Mendelsohn C, Cardoso WV. 2000. Regulation of retinoic acid signaling during lung morphogenesis. Development 127(14):3057-3067.

Marigo V, Davey RA, Zuo Y, Cunningham JM, Tabin CJ. 1996. Biochemical evidence that Patched is the Hedgehog receptor. Nature 384(6605):176-179.

Massague J, Seoane J, Wotton D. 2005. Smad transcription factors. Genes & Development 19(23):2783-2810.

Matsushita S, Urase K, Komatsu A, Scotting PJ, Kuroiwa A, Yasugi S. 2008. Foregut endoderm is specified early in avian development through signal(s) emanating from Hensen's node or its derivatives. Mechanisms of Development 125(5-6):377-395.

McMahon JA, Takada S, Zimmerman LB, Fan C-M, Harland RM, McMahon AP. 1998. Noggin-mediated antagonism of BMP signaling is required for growth and patterning of the neural tube and somite. Genes & Development 12(10):1438-1452.

Mendelsohn C, Lohnes D, Decimo D, Lufkin T, LeMeur M, Chambon P, Mark M. 1994. Function of the retinoic acid receptors (RARs) during development (II). Multiple

abnormalities at various stages of organogenesis in RAR double mutants. Development 120(10):2749-2771.

Merei J, Hasthorpe S, Farmer P, Hutson JM. 1999. Visceral anomalies in prenatally adriamycin-exposed rat fetuses: a model for the VATER association. Pediatric Surgery International 15(1):11-16.

Merei J, Hutson J. 2002. Embryogenesis of tracheo esophageal anomalies: a review. Pediatric Surgery International 18(5):319-326.

Merei J, Kotsios C, Hutson JM, Hasthorpe S. 1997. Histopathologic study of esophageal atresia and tracheoesophageal fistula in an animal model. Journal of Pediatric Surgery 32(1):12-14.

Meriwether WD, Bachur NR. 1972. Inhibition of DNA and RNA Metabolism by Daunorubicin and Adriamycin in L1210 Mouse Leukemia. Cancer Res 32(6):1137-1142.

Metzger RJ, Klein OD, Martin GR, Krasnow MA. 2008. The branching programme of mouse lung development. Nature 453(7196):745-750.

Miller-Delaney SF, Lieberam I, Murphy P, Mitchell KJ. 2011. Plxdc2 is a mitogen for neural progenitors. PLoS One 6(1):e14565.

Miner JH, Yurchenco PD. 2004. Laminin functions in tissue morphogenesis. Annual Review of Cell and Developmental Biology 20(1):255-284.

Minoo P, Hamdan H, Bu D, Warburton D, Stepanik P, deLemos R. 1995. TTF-1 Regulates Lung Epithelial Morphogenesis. Developmental Biology 172(2):694-698.

Minoo P, Su G, Drum H, Bringas P, Kimura S. 1999. Defects in Tracheoesophageal and Lung Morphogenesis inNkx2.1(-/-) Mouse Embryos. Developmental Biology 209(1):60-71.

Miyazono K, Kamiya Y, Morikawa M. Bone morphogenetic protein receptors and signal transduction. Journal of Biochemistry 147(1):35-51.

Morrisey EE, Hogan BLM. 2010. Preparing for the First Breath: Genetic and Cellular Mechanisms in Lung Development. Developmental Cell 18(1):8-23.

Mortell A, Gillick J, Giles S, Bannigan J, Puri P. 2005. Notable sequential alterations in notochord volume during development in the Adriamycin rat model. Journal of Pediatric Surgery 40(2):403-406.

Motoyama J, Liu J, Mo R, Ding Q, Post M, Hui C-c. 1998. Essential function of Gli2 and Gli3 in the formation of lung, trachea and oesophagus. Nat Genet 20(1):54-57.

Mucenski ML, Wert SE, Nation JM, Loudy DE, Huelsken J, Birchmeier W, Morrisey EE, Whitsett JA. 2003. β-Catenin Is Required for Specification of Proximal/Distal Cell Fate during Lung Morphogenesis. Journal of Biological Chemistry 278(41):40231-40238.

Myers NA. 1986. The history of oesophageal atresia and tracheo-oesophageal fistula--1670-1984. Prog Pediatr Surg 20:106-177.

Naiche LA, Papaioannou VE. 2003. Loss of Tbx4 blocks hindlimb development and affects vascularization and fusion of the allantois. Development 130(12):2681-2693.

Nakamura H, Katahira T, Sato T, Watanabe Y, Funahashi J-i. 2004. Gain- and loss-of-function in chick embryos by electroporation. Mechanisms of Development 121(9):1137-1143.

Nelson WJ, Nusse R. 2004. Convergence of Wnt, β-Catenin, and Cadherin Pathways. Science 303(5663):1483-1487.

Nora JJ, Nora AH, Perinchief AG, Ingram JW, Fountain AK, Peterson MJ. 1976. Congenital abnormalities and first-trimester exposure to progestagen/oestrogen [letter]. Lancet 1:313-314.

Nose A, Takeichi M. 1986. A novel cadherin cell adhesion molecule: its expression patterns associated with implantation and organogenesis of mouse embryos. The Journal of Cell Biology 103(6):2649-2658.

Nusslein-Volhard C, Wieschaus E. 1980. Mutations affecting segment number and polarity in Drosophila. Nature 287(5785):795-801.

Oda H, Tsukita S, Takeichi M. 1998. Dynamic Behavior of the Cadherin-Based Cell-Cell Adhesion System duringDrosophilaGastrulation. Developmental Biology 203(2):435-450.

Okubo T, Hogan B. 2004. Hyperactive Wnt signaling changes the developmental potential of embryonic lung endoderm. Journal of Biology 3(3):11.

Orford J, Manglick P, Cass DT, Tam PPL. 2001. Mechanisms for the development of esophageal atresia. Journal of Pediatric Surgery 36(7):985-994.

Orford JE, Cass DT. 1999. Dose response relationship between adriamycin and birth defects in a rat model of VATER association. Journal of Pediatric Surgery 34(3):392-398.

Parsons MJ, Pollard SM, Saude L, Feldman B, Coutinho P, Hirst EMA, Stemple DL. 2002. Zebrafish mutants identify an essential role for laminins in notochord formation. Development 129(13):3137-3146.

Pepicelli CV, Lewis PM, McMahon AP. 1998. Sonic hedgehog regulates branching morphogenesis in the mammalian lung. Current Biology 8(19):1083-1086.

Perez-Moreno M, Jamora C, Fuchs E. 2003. Sticky Business: Orchestrating Cellular Signals at Adherens Junctions. Cell 112(4):535-548.

Perl A-KT, Wert SE, Nagy A, Lobe CG, Whitsett JA. 2002. Early restriction of peripheral and proximal cell lineages during formation of the lung. Proceedings of the National Academy of Sciences of the United States of America 99(16):10482-10487.

Peterson RS, Lim, L., Ye, H., Zhou, H., Overdier, D.G., Costa, R.H. 1997. The winged helix transcriptional activator HFH-8 is expressed in the mesoderm of the primitive streak stage of mouse embryos and its cellular derivatives. Mech Dev 69(1-2):53-69.

Placzek M. 1995. The role of the notochord and floor plate in inductive interactions. Curr Opin Genet Dev 5(4):499-506.

Possoegel AK, Diez-Pardo JA, Morales C, Tovar JA. 1999. Notochord involvement in experimental esophageal atresia. Pediatric Surgery International 15(3):201-205.

Possogel AK, Diez-Pardo JA, Morales C, Navarro C, Tovar JA. 1998. Embryology of esophageal atresia in the adriamycin rat model. J Pediatr Surg 33(4):606 - 612.

Puusepp H, Zilina O, Teek R, Männik K, Parkel S, Kruustük K, Kuuse K, Kurg A, Õunap K. 2009. 5.9 Mb microdeletion in chromosome band 17q22-q23.2 associated with tracheo-esophageal fistula and conductive hearing loss. European Journal of Medical Genetics 52(1):71-74.

Qi B, Diez-Pardo JA, Navarro C, Tovar JA. 1996. Narrowing the embryologic window of the adriamycin-induced fetal rat model of esophageal atresia and tracheoesophageal fistula. Pediatric Surgery International 11(7):444-447.

Qi BQ, Beasley SW. 1998. Preliminary evidence that cell death may contribute to separation of the trachea from the primitive foregut in the rat embryo. Journal of Pediatric Surgery 33(11):1660-1665.

Qi BQ, Beasley SW. 1999. Relationship of the notochord to foregut development in the fetal rat model of esophageal atresia. Journal of Pediatric Surgery 34(11):1593-1598.

Qi BQ, Beasley SW. 2000. Stages of normal tracheo-bronchial development in rat embryos: resolution of a controversy. Dev Growth Differ 42(2):145 - 153.

Qi BQ, Merei J, Farmer P, Hasthorpe S, Myers NA, Beasley SW, Hutson JM. 1997. The vagus and recurrent laryngeal nerves in the rodent experimental model of esophageal atresia. Journal of Pediatric Surgery 32(11):1580-1586.

Quan L, Smith DW. 1973. The VATER association. Vertebral defects, Anal atresia, T-E fistula with esophageal atresia, Radial and Renal dysplasia: a spectrum of associated defects. J Pediatr 82(1):104 - 107.

Que J, Choi M, Ziel JW, Klingensmith J, Hogan BLM. 2006. Morphogenesis of the trachea and esophagus: current players and new roles for noggin and Bmps. Differentiation 74(7):422-437.

Que J, Luo X, Schwartz RJ, Hogan BLM. 2009. Multiple roles for Sox2 in the developing and adult mouse trachea. Development 136(11):1899-1907.

Que J, Okubo T, Goldenring JR, Nam K-T, Kurotani R, Morrisey EE, Taranova O, Pevny LH, Hogan BLM. 2007. Multiple dose-dependent roles for Sox2 in the patterning and differentiation of anterior foregut endoderm. Development 134(13):2521-2531.

Rajagopal J, Carroll TJ, Guseh JS, Bores SA, Blank LJ, Anderson WJ, Yu J, Zhou Q, McMahon AP, Melton DA. 2008. Wnt7b stimulates embryonic lung growth by coordinately increasing the replication of epithelium and mesenchyme. Development 135(9):1625-1634.

Rajagopal R, Huang J, Dattilo LK, Kaartinen V, Mishina Y, Deng C-X, Umans L, Zwijsen A, Roberts AB, Beebe DC. 2009. The type I BMP receptors, Bmpr1a and Acvr1, activate multiple signaling pathways to regulate lens formation. Developmental Biology 335(2):305-316.

Rhinn M, Dierich A, Shawlot W, Behringer RR, Le Meur M, Ang SL. 1998. Sequential roles for Otx2 in visceral endoderm and neuroectoderm for forebrain and midbrain induction and specification. Development 125(5):845-856.

Robert E, Mutchinick O, Mastroiacovo P, Knudsen LB, Daltveit AK, Castilla EE, Lancaster P, Källén B, Cocchi G. 1993. An international collaborative study of the epidemiology of esophageal atresia or stenosis. Reprod Toxicol 7(5):405-421.

Roddy KA, Nowlan NC, Prendergast PJ, Murphy P. 2009. 3D representation of the developing chick knee joint: a novel approach integrating multiple components. Journal of Anatomy 214(3):374-387.

Rossant J, Zirngibl R, Cado D, Shago M, GiguÃ¨re V. 1991. Expression of a retinoic acid response element-hsplacZ transgene defines specific domains of transcriptional activity during mouse embryogenesis. Genes & Development 5(8):1333-1344.

Ruiz i Altaba A. 1999. Gli proteins encode context-dependent positive and negative functions: implications for development and disease. Development 126(14):3205-3216.

Sakamoto A, Murata K, Suzuki H, Yatabe M, Kikuchi M. 2008. Immunohistochemical observation of co-expression of E- and N-cadherins in rat organogenesis. Acta Histochem Cytochem 41(5):143-147.

Sakiyama J-i, Yamagishi A, Kuroiwa A. 2003. Tbx4-Fgf10 system controls lung bud formation during chicken embryonic development. Development 130(7):1225-1234.

Sanson B, White P, Vincent J-P. 1996. Uncoupling cadherin-based adhesion from wingless signalling in Drosophila. Nature 383(6601):627-630.

Sarma S, Kerwin J, Puelles L, Scott M, Strachan T, Feng G, Sharpe J, Davidson D, Baldock R, Lindsay S. 2005. 3D modelling, gene expression mapping and post-mapping image analysis in the developing human brain. Brain Research Bulletin 66(4-6):449-453.

Sasaki H, Hui C, Nakafuku M, Kondoh H. 1997. A binding site for Gli proteins is essential for HNF-3beta floor plate enhancer activity in transgenics and can respond to Shh in vitro. Development 124(7):1313-1322.

Sasaki H, Nishizaki Y, Hui C, Nakafuku M, Kondoh H. 1999. Regulation of Gli2 and Gli3 activities by an amino-terminal repression domain: implication of Gli2 and Gli3 as primary mediators of Shh signaling. Development 126(17):3915-3924.

Sasaki T, Kusafuka T, Okada A. 2001. Analysis of the Development of Normal Foregut and Tracheoesophageal Fistula in an Adriamycin Rat Model Using Three-Dimensional Image Reconstruction. Surgery Today 31(2):133-139.

Sato H, Murphy P, Giles S, Bannigan J, Takayasu H, Puri P. 2008. Visualizing expression patterns of Shh and Foxf1 genes in the foregut and lung buds by optical projection tomography. Pediatric Surgery International 24(1):3-11.

Sekine K, Ohuchi H, Fujiwara M, Yamasaki M, Yoshizawa T, Sato T, Yagishita N, Matsui D, Koga Y, Itoh N, Kato S. 1999. Fgf10 is essential for limb and lung formation. Nat Genet 21(1):138-141.

Semwogerere D, Weeks ER. 2005. Confocal Microscopy. In: G WGB, editor. Encyclopedia of Biomaterials and Biomedical Engineering. United Kingdom: Taylor & Francis. p 1-10.

Serls AE, Doherty S, Parvatiyar P, Wells JM, Deutsch GH. 2005. Different thresholds of fibroblast growth factors pattern the ventral foregut into liver and lung. Development 132(1):35-47.

Sharpe J. 2003. Optical projection tomography as a new tool for studying embryo anatomy. Journal of Anatomy 202(2):175-181.

Sharpe J, Ahlgren U, Perry P, Hill B, Ross A, Hecksher-Sorensen J, Baldock R, Davidson D. 2002. Optical Projection Tomography as a Tool for 3D Microscopy and Gene Expression Studies. Science 296(5567):541-545.

Shaw-Smith C. 2006. Oesophageal atresia, tracheo-oesophageal fistula, and the VACTERL association: review of genetics and epidemiology. Journal of Medical Genetics 43(7):545-554.

Shaw-Smith C. 2009. Genetic factors in esophageal atresia, tracheo-esophageal fistula and the VACTERL association: Roles for FOXF1 and the 16q24.1 FOX transcription factor gene cluster, and review of the literature. European Journal of Medical Genetics 53(1):6-13.

Sherwood RI, Chen T-YA, Melton DA. 2009. Transcriptional dynamics of endodermal organ formation. Developmental Dynamics 238(1):29-42.

Shu W, Guttentag S, Wang Z, Andl T, Ballard P, Lu MM, Piccolo S, Birchmeier W, Whitsett JA, Millar SE, Morrisey EE. 2005. Wnt/β-catenin signaling acts upstream of N-myc, BMP4, and FGF signaling to regulate proximal-distal patterning in the lung. Developmental Biology 283(1):226-239.

Shu W, Jiang YQ, Lu MM, Morrisey EE. 2002. Wnt7b regulates mesenchymal proliferation and vascular development in the lung. Development 129(20):4831-4842.

Small EM, Vokes SA, Garriock RJ, Li D, Krieg PA. 2000. Developmental expression of the Xenopus Nkx2-1 and Nkx2-4 genes. Mechanisms of Development 96(2):259-262.

Smits P, Lefebvre V. 2003. Sox5 and Sox6 are required for notochord extracellular matrix sheath formation, notochord cell survival and development of the nucleus pulposus of intervertebral discs. Development 130(6):1135-1148.

Speleman F, Van Roy N, Wiegant J, Verschraegen-Spae MR, Benoit Y, Govaert P, Goossens L, Leroy JG. 1992. Detection of subtle reciprocal translocations by fluorescence in situ hybridization. Clin Genet 41(4):169-174.

Spilde T, Bhatia A, Ostlie D, Marosky J, Holcomb G, Snyder C, Gittes G. 2003a. A role for sonic hedgehog signaling in the pathogenesis of human tracheoesophageal fistula. Journal of Pediatric Surgery 38(3):465-468.

Spilde TL, Bhatia AM, Mehta S, Ostlie DJ, Hembree MJ, Preuett BL, Prasadan K, Li Z, Snyder CL, Gittes GK. 2003b. Defective sonic hedgehog signaling in esophageal atresia with tracheoesophageal fistula. Surgery 134(2):345-350.

Spitz L. 2006. Esophageal atresia: Lessons I have learned in a 40-year experience. Journal of Pediatric Surgery 41(10):1635-1640.

Spitz L. 2007. Oesophageal atresia. Orphanet Journal of Rare Diseases 2(1):24.

Stankiewicz P, Sen P, Bhatt SS, Storer M, Xia Z, Bejjani BA, Ou Z, Wiszniewska J, Driscoll DJ, Maisenbacher MK, Bolivar J, Bauer M, Zackai EH, McDonald-McGinn D, Nowaczyk MM, Murray M, Hustead V, Mascotti K, Schultz R, Hallam L, McRae D, Nicholson AG, Newbury R, Durham-O'Donnell J, Knight G, Kini U, Shaikh TH, Martin V, Tyreman M, Simonic I, Willatt L, Paterson J, Mehta S, Rajan D, Fitzgerald T, Gribble S, Prigmore E, Patel A, Shaffer LG, Carter NP, Cheung SW, Langston C, Shaw-Smith C. 2009. Genomic and genic deletions of the FOX gene cluster on 16q24.1 and inactivating mutations of FOXF1 cause alveolar capillary dysplasia and other malformations. Am J Hum Genet 84(6):780-791.

Stemple DL. 2005. Structure and function of the notochord: an essential organ for chordate development. Development 132(11):2503-2512.

Stern CD. 2005. The Chick: A Great Model System Becomes Even Greater. Developmental Cell 8(1):9-17.

Stone DM, Hynes M, Armanini M, Swanson TA, Gu Q, Johnson RL, Scott MP, Pennica D, Goddard A, Phillips H, Noll M, Hooper JE, de Sauvage F, Rosenthal A. 1996. The tumour-suppressor gene patched encodes a candidate receptor for Sonic hedgehog. Nature 384(6605):129-134.

Stottmann RW, Anderson RM, Klingensmith J. 2001. The BMP Antagonists Chordin and Noggin Have Essential but Redundant Roles in Mouse Mandibular Outgrowth. Developmental Biology 240(2):457-473.

Summerhurst K, Stark M, Sharpe J, Davidson D, Murphy P. 2008. 3D representation of Wnt and Frizzled gene expression patterns in the mouse embryo at embryonic day 11.5 (Ts19). Gene Expression Patterns 8(5):331-348.

Szumska D, Pieles G, Essalmani R, Bilski M, Mesnard D, Kaur K, Franklyn A, El Omari K, Jefferis J, Bentham J, Taylor JM, Schneider JE, Arnold SJ, Johnson P, Tymowska-Lalanne Z, Stammers D, Clarke K, Neubauer S, Morris A, Brown SD, Shaw-Smith C, Cama A, Capra V, Ragoussis J, Constam D, Seidah NG, Prat A, Bhattacharya S. 2008. VACTERL/caudal regression/Currarino syndrome-like malformations in mice with mutation in the proprotein convertase Pcsk5. Genes & Development 22(11):1465-1477.

Takeichi M. 1977. Functional correlation between cell adhesive properties and some cell surface proteins. The Journal of Cell Biology 75(2):464-474.

Takeichi M. 1991. Cadherin cell adhesion receptors as a morphogenetic regulator. Science 251(5000):1451-1455.

Tarpey PS, Smith R, Pleasance E, Whibley A, Edkins S, Hardy C, O'Meara S, Latimer C, Dicks E, Menzies A, Stephens P, Blow M, Greenman C, Xue Y, Tyler-Smith C, Thompson D, Gray K, Andrews J, Barthorpe S, Buck G, Cole J, Dunmore R, Jones D, Maddison M, Mironenko T, Turner R, Turrell K, Varian J, West S, Widaa S, Wray P, Teague J, Butler A, Jenkinson A, Jia M, Richardson D, Shepherd R, Wooster R, Tejada MI, Martinez F, Carvill G, Goliath R, de Brouwer APM, van Bokhoven H, Van Esch H, Chelly J, Raynaud M, Ropers H-H, Abidi FE, Srivastava AK, Cox J, Luo Y, Mallya U, Moon J, Parnau J, Mohammed S, Tolmie JL, Shoubridge C, Corbett M, Gardner A, Haan E, Rujirabanjerd S, Shaw M, Vandeleur L, Fullston T, Easton DF, Boyle J, Partington M, Hackett A, Field M, Skinner C, Stevenson RE, Bobrow M, Turner G, Schwartz CE, Gecz J, Raymond FL, Futreal PA, Stratton MR. 2009. A systematic, large-scale resequencing screen of X-chromosome coding exons in mental retardation. Nat Genet 41(5):535-543.

Tefft D, Lee M, Smith S, Crowe DL, Bellusci S, Warburton D. 2002. mSprouty2 inhibits FGF10-activated MAP kinase by differentially binding to upstream target proteins. American Journal of Physiology - Lung Cellular and Molecular Physiology 283(4):L700-L706.

Tefft JD, Lee M, Smith S, Leinwand M, Zhao J, Bringas Jr P, Crowe DL, Warburton D. 1999. Conserved function of mSpry-2, a murine homolog of Drosophila sprouty, which negatively modulates respiratory organogenesis. Current Biology 9(4):219-222.

Temtamy SA, Miller JD. 1974. Extending the scope of the VATER association: definition of the VATER syndrome. J Pediatr 85(3):345-349.

Tepass U, Truong K, Godt D, Ikura M, Peifer M. 2000. Cadherins in embryonic and neural morphogenesis. Nat Rev Mol Cell Biol 1(2):91-100.

Theiler K. 1989. The House Mouse: Atlas of Embryonic Development. . Springer, Berlin, Heidelberg, New York.

Thomas P, Beddington R. 1996. Anterior primitive endoderm may be responsible for patterning the anterior neural plate in the mouse embryo. Current Biology 6(11):1487-1496.

Thompson DJ, Molello JA, Strebing RJ, Dyke IL. 1978. Teratogenicity of adriamycin and daunomycin in the rat and rabbit. Teratology 17(2):151-157.

Tomaselli V, Volpi M, Dell'Agnola C, Bini M, Rossi A, Indriolo A. 2003. Long-term evaluation of esophageal function in patients treated at birth for esophageal atresia. Pediatric Surgery International 19(1):40-43.

Topol L, Jiang X, Choi H, Garrett-Beal L, Carolan PJ, Yang Y. 2003. Wnt-5a inhibits the canonical Wnt pathway by promoting GSK-3-independent β-catenin degradation. The Journal of Cell Biology 162(5):899-908.

Tsao P-N, Chen F, Izvolsky KI, Walker J, Kukuruzinska MA, Lu J, Cardoso WV. 2008. γ-Secretase Activation of Notch Signaling Regulates the Balance of Proximal and Distal Fates in Progenitor Cells of the Developing Lung. Journal of Biological Chemistry 283(43):29532-29544.

Ukita K, Hirahara S, Oshima N, Imuta Y, Yoshimoto A, Jang C-W, Oginuma M, Saga Y, Behringer RR, Kondoh H, Sasaki H. 2009. Wnt signaling maintains the notochord fate for progenitor cells and supports the posterior extension of the notochord. Mechanisms of Development 126(10):791-803.

van Bokhoven H, Celli J, van Reeuwijk J, Rinne T, Glaudemans B, van Beusekom E, Rieu P, Newbury-Ecob RA, Chiang C, Brunner HG. 2005. MYCN haploinsufficiency is associated with reduced brain size and intestinal atresias in Feingold syndrome. Nat Genet 37(5):465-467.

van Straaten HW, Hekking JW, Thors, F., , Wiertz-Hoessels EL, Drukker J. 1985a. Induction of an additional floor plate in the neural tube. Acta Morphol Neerl Scand 23(2):91-97.

van Straaten HW, Hekking, J.W.,. 1991. Development of floor plate, neurons and axonal outgrowth pattern in the early spinal cord of the notochord-deficient chick embryo. Anat Embryol (Berl) 184(1):55-63.

van Straaten HWM, Hekking JWM, Wiertz-Hoessels EJLM, Thors F, Drukker J. 1988. Effect of the notochord on the differentiation of a floor plate area in the neural tube of the chick embryo. Anatomy and Embryology 177(4):317-324.

van Straaten HWM, Thors F, Wiertz-Hoessels L, Hekking J, Drukker J. 1985b. Effect of a notochordal implant on the early morphogenesis of the neural tube and neuroblasts: Histometrical and histological results. Developmental Biology 110(1):247-254.

Vendrell V, Summerhurst K, Sharpe J, Davidson D, Murphy P. 2009. Gene expression analysis of canonical Wnt pathway transcriptional regulators during early morphogenesis of the facial region in the mouse embryo. Gene Expression Patterns 9(5):296-305.

Vissers LELM, van Ravenswaaij CMA, Admiraal R, Hurst JA, de Vries BBA, Janssen IM, van der Vliet WA, Huys EHLPG, de Jong PJ, Hamel BCJ, Schoenmakers EFPM, Brunner HG, Veltman JA, van Kessel AG. 2004. Mutations in a new member of the chromodomain gene family cause CHARGE syndrome. Nat Genet 36(9):955-957.

Wallis JW, Aerts J, Groenen MAM, Crooijmans RPMA, Layman D, Graves TA, Scheer DE, Kremitzki C, Fedele MJ, Mudd NK, Cardenas M, Higginbotham J, Carter J, McGrane R, Gaige T, Mead K, Walker J, Albracht D, Davito J, Yang S-P, Leong S, Chinwalla A, Sekhon M, Wylie K, Dodgson J, Romanov MN, Cheng H, de Jong PJ, Osoegawa K, Nefedov M, Zhang H, McPherson JD, Krzywinski M, Schein J, Hillier L, Mardis

ER, Wilson RK, Warren WC. 2004. A physical map of the chicken genome. Nature 432(7018):761-764.

Walsh LE, Vance GH, Weaver DD. 2001. Distal 13q Deletion Syndrome and the VACTERL Association: Case report, literature review, and possible implications. American Journal of Medical Genetics 98(2):137-144.

Wang B, Fallon JF, Beachy PA. 2000. Hedgehog-Regulated Processing of Gli3 Produces an Anterior/Posterior Repressor Gradient in the Developing Vertebrate Limb. Cell 100(4):423-434.

Warburton D, Bellusci S, De Langhe S, Del Moral PM, Fleury V, Mailleux A, Tefft D, Unbekandt M, Wang K, Shi W. 2005. Molecular Mechanisms of Early Lung Specification and Branching Morphogenesis. Pediatric Research 57(5 Part 2):26R-37R.

Weaver M, Batts L, Hogan BLM. 2003. Tissue interactions pattern the mesenchyme of the embryonic mouse lung. Developmental Biology 258(1):169-184.

Weaver M, Dunn N, Hogan B. 2000. Bmp4 and Fgf10 play opposing roles during lung bud morphogenesis. Development 127:2695 - 2704.

Wells JM, Melton DA. 1999. Vertebrate endoderm development. Annual Review of Cell and Developmental Biology 15(1):393-410.

Wells JM, Melton DA. 2000. Early mouse endoderm is patterned by soluble factors from adjacent germ layers. Development 127(8):1563-1572.

Westfall TA, Brimeyer R, Twedt J, Gladon J, Olberding A, Furutani-Seiki M, Slusarski DC. 2003. Wnt-5/pipetail functions in vertebrate axis formation as a negative regulator of Wnt/β-catenin activity. The Journal of Cell Biology 162(5):889-898.

Willert K, Brown JD, Danenberg E, Duncan AW, Weissman IL, Reya T, Yates JR, Nusse R. 2003. Wnt proteins are lipid-modified and can act as stem cell growth factors. Nature 423(6938):448-452.

Williams AK, Qi BQ, Beasley SW. 2001. Demonstration of abnormal notochord development by three-dimensional reconstructive imaging in the rat model of esophageal atresia. Pediatric Surgery International 17(1):21-24.

Williams AK, Quan QB, Beasley SW. 2003. Three-dimensional imaging clarifies the process of tracheoesophageal separation in the rat. Journal of Pediatric Surgery 38(2):173-177.

Williamson KA, Hever AM, Rainger J, Rogers RC, Magee A, Fiedler Z, Keng WT, Sharkey FH, McGill N, Hill CJ, Schneider A, Messina M, Turnpenny PD, Fantes JA, van Heyningen V, FitzPatrick DR. 2006. Mutations in SOX2 cause anophthalmia-esophageal-genital (AEG) syndrome. Human Molecular Genetics 15(9):1413-1422.

Wilson JG, Roth CB, Warkany J. 1953. An analysis of the syndrome of malformations induced by maternal vitamin A deficiency. Effects of restoration of vitamin A at various times during gestation. Am J Anat 92(2):189-217.

Wong-Gibbons DL, Romitti PA, Sun L, Moore CA, Reefhuis J, Bell EM, Olshan AF. 2008. Maternal periconceptional exposure to cigarette smoking and alcohol and esophageal atresia ± tracheo-esophageal fistula. Birth Defects Research Part A: Clinical and Molecular Teratology 82(11):776-784.

Yang SZ, Kohno N, Kondo K, Yokoyama A, Hamada H, Hiwada K., Miyake M. 1999. Adriamycin activates E-cadherin-mediated cell-cell adhesion in human breast cancer cells. International Journal of Oncology 15(6):1109-1124.

Yonemura S, Wada Y, Watanabe T, Nagafuchi A, Shibata M. 2010. [alpha]-Catenin as a tension transducer that induces adherens junction development. Nat Cell Biol 12(6):533-542.

Zhou B, Hutson JM, Farmer PJ, Hasthorpe S, Myers NA, Liu M. 1999. Apoptosis in tracheoesophageal embryogenesis in rat embryos with or without adriamycin treatment. J Pediatr Surg 34(5):872 - 875; discussion 876.